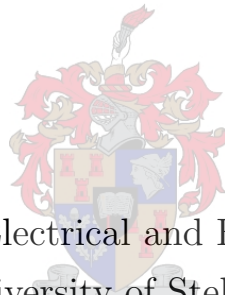


Design and Test Implementation of a Global Interconnected SQUID Geomagnetometer Network

LUCAS JACOBUS JANSE VAN VUUREN

Thesis presented in partial fulfilment of the requirements of the
degree Master in Engineering (Research) in the Faculty of
Engineering at the University of Stellenbosch



Department of Electrical and Electronic Engineering
University of Stellenbosch
Private Bag X1, Matieland 7602 , South Africa.

SUPERVISOR:
PROF. COENRAD J. FOURIE

March 2015

Declaration

By submitting this thesis electronically, I declare that the entirety of the work contained therein is my own, original work, that I am the sole author thereof (save to the extent explicitly otherwise stated), that reproduction and publication thereof by Stellenbosch University will not infringe any third party rights and that I have not previously in its entirety or in part submitted it for obtaining any qualification.

Lucas Janse van Vuuren

Copyright © 2015 Stellenbosch University
All rights reserved

Abstract

In 2012, a three-axis HTS-SQUID magnetometer project for geomagnetic measurements has been started at SANSA Space Science in Hermanus, South Africa. The goal of this project was to replicate a three-axis SQUID magnetometer for geomagnetic field measurements at LSBB at Rustrel, France. This is to allow better characterizing of faint, low frequency geomagnetic and ionospheric phenomena. To record the output signals of the SQUID magnetometers, a measurement system had to be developed. To utilise the full sensitivity of the SQUID magnetometers, the output signals have to be recorded with high accuracy. A high-speed and high-accuracy data acquisition system was installed and software was developed to record data from it. The software is capable of sending the recorded data to a web server as it is being recorded. Basic hardware control of the SQUID magnetometers has also been implemented from this data acquisition system, by monitoring conditions with its software. Timing accuracy is an important aspect of this system, in order to enable comparisons with measurements from LSBB and from different locations in the world. A GPS receiver was used to obtain the current UTC time accurately in order to timestamp measurements. A software method was devised for timestamping, to improve accuracy by triggering measurements directly from the GPS receiver. A hardware real-time clock between the GPS receiver and the rest of the system has been avoided using this method. For research purposes, this measurement data must be available on the internet for the lifetime of the system. A data server was set up and a large database of recorded data has been generated over two years of this project. Long term implementation issues have also been addressed. A web interface was developed for the data server to enable live viewing of the recorded data. This web interface also facilitates access to the raw measurements for public use. Analysis of phenomena in the recorded data has been performed by other students from Stellenbosch University.

Opsomming

In 2012 is daar by SANSA Space Science in Hermanus, Suid-Afrika begin met 'n drie-as HTS-SQUID magnetometerprojek vir die opneem van geomagnetiese metings. Die doel van hierdie projek was om die drie-as SQUID magnetometer vir geomagnetiese veldmetings by LSBB naby Rustrel in Frankryk te dupliseer. Dit sou dit moontlik maak om subtiële, laefrekwensie geomagnetiese en ionosferiese verskynsels beter te beskryf. Om die uittreeseine wat deur die SQUID magnetometers voortgebring word op te neem, moes 'n data-opnemerstelsel ontwikkel word. Ten einde die volle sensitiwiteit van die SQUID magnetometers te benut, moes die seine baie akkuraat gemeet word. 'n Hoë- en hoë-akkuraatheidsdata-opnemer is gestalleer en die nodige sagteware is ontwikkel om hierdie data op te neem. Die sagteware is in staat om die data, soos dit opgeneem word, na 'n webbediener te stuur. Basiese hardewarebeheer van die SQUID magnetometers is ook vanaf hierdie data-opnemerstelsel gecomplementeer deur toestande met die sagteware te monitor. Akkurate tydmeting is 'n belangrike aspek van hierdie sisteem, sodat metings met die van LSBB en ander soortgelyke projekte in ander posisies op die aarde vergelyk kan word. 'n GPS-ontvanger is gebruik om die UTC-tyd akkuraat te ontvang, ten einde akkurate tydstempeling by metings te voeg. 'n Sagtewaremetode vir tydstempeling is ontwikkel om akkuraatheid te bevorder deur metings direk vanaf die GPS-ontvanger te sneller. Deur hierdie metode te gebruik, is dit onnodig om 'n intydse hardewaretidhouer tussen die GPS-ontvanger en die res van die sisteem te gebruik. Vir navorsingsdoeleindes moet hierdie metingsdata op die internet beskikbaar wees vir die duur van die stelsel se leeftyd. 'n Databediener is opgestel en 'n baie groot databasis van opgeneemde data is oor die twee jaar van hierdie projek gegenereer. Langtermynimplementeringskwessies het ook aandag geniet. 'n Webblad is vir die databediener ontwikkel sodat die data onmiddellik besigtig kan word soos dit opgeneem word. Hierdie webblad fasiliteer ook toegang tot die rou data-opnames vir openbare gebruik. Verskynsels in die data-opnames is by SANSA geanaliseer deur ander studente van die Universiteit van Stellenbosch.

Acknowledgements

I would like to give humble thanks to the following people:

- The Lord God Almighty, to whom I owe my entire existence, for carrying me this far through all my successes and failures.
- My study leader, Prof Coenrad Fourie, for his advice and for having this interesting project available. Also to the staff at SANSA Space Science in Hermanus, specifically Elda Saunderson and Danie Gouws, for all their patience and friendly assistance with this project.
- My parents, who have supported me all these years. Specifically my father, who made great sacrifices to financially support my siblings and myself at university.
- My friends from campus, who also supported me through easy and hard times. I am forever grateful.

Contents

1	Introduction	1
1.1	Background	1
1.1.1	LSBB	1
1.1.2	SANSA	2
1.1.3	Kanazawa Institute of Technology	2
1.1.4	Tokyo Metropolitan University and others	2
1.2	Purpose	2
1.3	Benefits	3
2	Overview of the SQUID Geomagnetometer System	4
2.1	Overview of DC SQUID magnetometer	4
2.1.1	Overview of superconductivity	6
2.1.2	Flux quantisation	10
2.1.3	The Josephson junction	10
2.1.4	Flux-locked loop	12
2.2	Typical geomagnetometers	14
2.2.1	Hall-effect sensor	14
2.2.2	Magnetoresistive devices	14
2.2.3	Fluxgates	14
2.3	Other relevant magnetometers	15
2.3.1	Spin-exchange relaxation-free magnetometer (SERF)	15

2.3.2	Digital SQUID	16
2.4	LSBB SQUID ² System	16
2.4.1	Overview of unique bunker facility	16
2.4.2	Effects of mountain and capsule armour	17
2.4.3	Effects of vibration and seismic waves	20
2.4.4	LTS SQUID advantages and disadvantages	20
3	Requirements and design for Global Interconnected SQUID Geomagnetometer System	22
3.1	Facility overview of SANSA SQUID geomagnetometer	23
3.1.1	Buildings	23
3.1.2	System diagram	24
3.2	Data acquisition system functions and requirements	25
3.3	Centralised data storage system functions and requirements	27
4	Electromagnetic considerations	30
4.1	Common sources of interference	31
4.2	Accounting for noise sources	33
4.2.1	Signal transmission lines	33
4.2.2	USB connections	33
4.2.3	PCI-1000 SQUID controller	35
4.3	Local magnetic field interference	35
4.3.1	Distortion of magnetic field	35
4.4	Shielding of AC magnetic fields around sensor	37
4.4.1	Active cancellation	38
4.4.2	Passive shielding with plates	39
5	Software-interrupt based precision-timed data acquisition system	41
5.1	Timing source	41

5.1.1	GPS time	42
5.1.2	FPGA timer	42
5.1.3	Real-time Operating System	43
5.1.4	u-blox LEA-6T Timing GPS	44
5.2	Signal conditioning filter	45
5.2.1	Theoretical calculations	46
5.2.2	Active filter	47
5.2.3	Passive filter and issues thereof	47
5.3	Data Acquisition Unit	48
5.4	Software	48
5.4.1	Principle behind GPS time stamping with software	49
5.4.2	Functions of data capture software	49
5.4.3	Automatic reset of SQUID magnetometers	50
5.5	Mitigating implementation issues	50
5.5.1	Memory overflows in software	50
5.5.2	False trigger	51
6	Implementation of a robust data-storage and post-processing system	58
6.1	MySQL implementation for data storage	58
6.2	Web interface for transferring data	60
6.2.1	dbadd.php	61
6.2.2	dbread.php	61
6.3	Web interface for viewing data	62
6.4	Preprocessing	62
6.4.1	Averaging to reduce data (Downsampling)	63
6.4.2	Discrete Fourier Transforms (DFTs)	63
6.4.3	Band pass filtered data	64
6.5	Data integrity	64

6.5.1	Sample by sample	64
6.5.2	Verifying number of samples in dataset	65
6.6	Reliability concerns	67
6.6.1	Hard drive wear	67
6.6.2	Slow file systems	67
6.6.3	Incomplete data transmissions	68
7	System Tests	69
7.1	Database size	69
7.2	Spectrum comparison between +- 1 V and +- 10 V sampling	69
7.3	Power Spectra	70
7.3.1	Zero signal power spectrum	73
7.3.2	Zero signal power spectrum with internal filter	73
7.3.3	SQUID magnetometer power spectrum	74
8	Conclusions	81
8.1	Results of software-interrupt based precision-timed data acquisition system	81
8.2	Results of the implementation of a robust data-storage and post-processing system	82
8.3	Recommendations	82
8.3.1	Data capture software	82
8.3.2	Preprocessing of data at the web server	83
8.3.3	World Data System	83
8.3.4	Server stability: automatic shut down on UPS	83
8.3.5	Mobile SQUID geomagnetometer	83
8.3.6	Using a well for measurements	84

List of Figures

2.1	Wafer level photomicrograph of SQUID input coil (a) and Josephson junctions (b). A diagram of the fundamental SQUID structure is in (c). [1] . . .	5
2.2	Circuit diagrams of magnetometer (a) and gradiometer (b) configuration of a SQUID. [1]	6
2.3	Critical surface plot of popular superconducting materials with relation to temperature, current density and magnetic field. [2]	8
2.4	Critical field vs critical temperature for type 1 (a) and type 2 (b) superconductors, illustrating the Meissner state region in type 2 superconductors. [3]	10
2.5	Circuit diagram of a DC SQUID (a), voltage versus bias current hysteresis (b) and enclosed multiples of magnetic flux quanta versus output voltage (using a constant biasing current), showing the voltage modulation caused by changing magnetic flux (c). [1]	11
2.6	Possible flux modulation schemes for a SQUID magnetometer in (a) and (b) and flux to voltage transfer characteristic of the lock-in amplifier in (c). [1]	12
2.7	Circuit diagram of a SQUID with Flux Locked Loop (FLL) configuration. [1]	13
2.8	Diagram of the working principle behind the Hall-effect sensor [4].	15
2.9	Liquid helium dewar with the LSBB LTS SQUID geomagnetometer.	17
2.10	Map of static magnetic field inside the LSBB cabin. Magnetic field intensity values are in nT. [5].	19
2.11	Diagram of LSBB capsule [6].	21
3.1	3D floorplan of the SQUID hut as designed in [7].	24

3.2	The magnetically neutral SQUID hut at SANSA, Hermanus (a), with a close-up of the mechanical construction (b) and a close-up of the Programmable Feedback Loop (PFL) controllers [8].	28
3.3	Overall system diagram as implemented.	29
4.1	Diagram of signal flow in the system with key interference sources indicated.	33
4.2	Undistorted (a) and hard iron distorted (b) fields rotated through 360 degrees, showing measured field strength on the x and y axes. [9]	36
4.3	Combined hard and soft iron distortion for two axis fields (a) and for three axis fields (b). [9]	37
4.4	Illustration of soft iron distortion in flux lines [10].	38
4.5	Shielding effectiveness of certain materials [11] versus frequency in kilocycles (KC).	39
4.6	Setup for practical shielding efficiency test of certain materials [11].	40
5.1	Block diagram of a possible FPGA implementation of a real-time clock. . .	43
5.2	Block diagram of the u-blox LEA-6T GPS receiver [12, 7].	45
5.3	An illustration of aliasing, or an image frequency, in recorded samples when sampling a signal at a rate slower than the Nyquist frequency. The dots represent the sample acquisition points, and the long wave is reconstructed from it even though a much shorter wave was present. [13]	46
5.4	Respective phase shift versus frequency graphs of third order Bessel-Thompson, Butterworth and Chebyshev low pass filters with cut-off frequency at 50 Hz.	52
5.5	Respective delay versus frequency graphs of third order Bessel-Thompson, Butterworth and Chebyshev low pass filters with cut-off frequency at 50 Hz.	53
5.6	Respective step responses of third order Bessel-Thompson, Butterworth and Chebyshev low pass filters with cut-off frequency at 50 Hz.	54
5.7	Circuit diagram of an active third order Bessel-Thompson low pass filter. [14]	55
5.8	Measured attenuation characteristics of the filter constructed.	55

5.9	Circuit diagram for a passive third order Bessel-Thompson low pass filter [15].	56
5.10	Diagram of the threads in the software with the order in which they are triggered.	56
5.11	User interface of the data capture software.	57
6.1	Screenshot of live graph implementation.	62
6.2	Illustration of a short binary search [16].	66
7.1	Spectrum of a 45 minute period of the X-axis SQUID at +- 1 V sampling, with linear (top) and logarithmic (bottom) frequency axes.	70
7.2	Spectrum of a 45 minute period of the Z-axis SQUID at +- 1 V sampling, with linear (top) and logarithmic (bottom) frequency axes.	71
7.3	Spectrum of a 45 minute period of the X-axis SQUID at +- 10 V sampling, with linear (top) and logarithmic (bottom) frequency axes.	72
7.4	Spectrum of a 45 minute period of the Z-axis SQUID at +- 10 V sampling, with linear (top) and logarithmic (bottom) frequency axes.	73
7.5	Oscillogram of a differential channel on the data acquisition unit at 500kHz sample rate.	74
7.6	Power spectral density of a differential channel on the data acquisition unit, with linear (top) and logarithmic (bottom) frequency.	75
7.7	Power spectral density of a differential channel on the data acquisition unit, with the internal 40 kHz filter switched on.	76
7.8	Power spectral density of channel 1 M2700 SQUID magnetometer, with linear (top) and logarithmic (bottom) frequency axes.	77
7.9	Power spectral density of channel 2 M2700 SQUID magnetometer, with linear (top) and logarithmic (bottom) frequency axes.	78
7.10	Power spectral density of channel 1 M2700 SQUID magnetometer, with linear (top) and logarithmic (bottom) frequency axes. Measured simultaneously with spectrum in Figure 7.11.	79
7.11	Power spectral density of channel 2 M2700 SQUID magnetometer, with linear (top) and logarithmic (bottom) frequency axes. Measured simultaneously with spectrum in Figure 7.10.	80

List of Tables

2.1	Specifications of LSBB SQUID ² System [17], [18], [19].	18
2.2	Layers of material surrounding the LSBB SQUID magnetometer [6], [20].	20
3.1	Specifications of initial M2700 SQUID magnetometers.	26
3.2	Specifications of three axis M1000 SQUID magnetometers.	26
3.3	Specifications for measurements.	26
3.4	Specifications for data storage at a sample rate of 125 Hz.	27
5.1	Specifications for measurements.	42
5.2	Timepulse specifications of LEA-6T [12], [21].	44
5.3	NMEA sentence codes for the LEA-6T GPS receiver [22].	44
5.4	Specifications of NI USB-6281 Data Acquisition Unit [23].	48
6.1	Set of fields used for each record in the database [24], [25], [26], [27]	59
6.2	Number of three-channel measurement entries into database and their associated sizes over different time periods, for a sample rate of 125 Hz is used.	59
6.3	Number of three-channel measurement entries into database and their associated sizes over different time periods, for a sample rate of 1 000 Hz.	59
6.4	Number of six-channel measurement entries into database and their associated sizes over different time periods, for a sample rate 125 Hz.	60

Chapter 1

Introduction

Making a SQUID geomagnetometer is no simple task. SQUIDs are highly sensitive measurement devices, which are usually too difficult to implement as geomagnetometers due to precautions required. Shielding requirements to operate SQUID magnetometers are very strict in order to maintain the measured magnetic field within its own measurement limits. However, it has become desirable to implement SQUIDs for geomagnetic measurements to improve understanding of geophysical and ionospheric phenomena. Shielding would either remove or disturb the geomagnetic field, therefore it is required to use an unshielded SQUID magnetometer for this project. This requires careful consideration of the electromagnetic environment when designing such a system.

1.1 Background

1.1.1 LSBB

The Laboratoire Souterrain à Bas Bruit (LSBB) in France started operating a SQUID magnetometer in a unique low noise bunker environment in 2001. This magnetometer has been successful at measuring the geomagnetic field for long terms with very high accuracy [8]. The interaction between earthquakes and the ionosphere became of particular interest from the results of this system. However, for full characterisation of Ultra Low Frequency (ULF) magnetic field signatures, data from more locations are required [28]. This project has been established to aid this need.

At the time this project was started, LSBB was the only reference design available. However, replicating a shielded bunker for measuring the geomagnetic field is not practical. Other difficulties are also present, such as finding a cost-effective way to record data accurately and using HTS SQUID magnetometers. From this, it is clear that the design

of the system developed in this project is considerably different from the LSBB system. The design is discussed in Chapter 3.

1.1.2 SANSA

The South African National Space Agency (SANSA) Space Science Center, formerly known as the Hermanus Magnetic Observatory, has been established in a magnetically clean environment and has been conducting geomagnetic measurements since 1941. The facility is a favourable location for a SQUID geomagnetometer due to their expertise and has collaborated on a joint project to establish a SQUID geomagnetometer system at their facility. A fluxgate magnetometer is permanently logging the absolute geomagnetic field at the (SANSA) Space Science Center. This data is available, together with that of a global network of geomagnetometers, on the INTERMAGNET network.

1.1.3 Kanazawa Institute of Technology

A successful experimental setup of an LTS SQUID geomagnetometer has been operated by a research group from the Kanazawa Institute of Technology in Japan. This has been documented in 1999 [29], however it could only be operated at night due to daytime activity at its location. Research on it was halted until 2011, when it was restarted in response to a devastating earthquake and tsunami. It is now being operated in a rural area near Kanazawa [30].

1.1.4 Tokyo Metropolitan University and others

Another research group collaboration between Tokyo Metropolitan University, the International Superconductivity Technology Center (ISTEC), TIERRA TECNICA, Fukushima National College of Technology and Tohoku University in Japan also successfully developed a SQUID geomagnetometer in 2012. A HTS SQUID geomagnetometer is being operated in Iwaki, Fukushima prefecture, Japan, sampling at 50 Hz with GPS synchronisation. Their aim is to correlate variations in the geomagnetic field with fault movements. Seismographic data is also being recorded. [31]

1.2 Purpose

The purpose of this Master's project was to develop and implement the data acquisition and online data storage system for the SQUID geomagnetometer. The software imple-

mentation for the GPS-timestamped data acquisition system and the online data storage system is the primary outputs. A substantial portion of background information was considered for the hardware design and is also reported.

1.3 Benefits

Global interconnection of SQUID geomagnetometers will allow full space events to be characterised more easily. By monitoring data recorded at different locations, it is possible to analyse the way effects on the geomagnetic field propagate around the earth. It is required that the timing of measurements are synchronised with high accuracy to be able to follow these effects as it travels around the globe.

Data analysis will be an important aspect of this project. A large amount of data must be collected and processed to characterise the events recorded by this system. Storing the recorded data of multiple nodes of a geomagnetometer network at a centralised server and in a single format will speed up analysis, with regard to data transfer and processing time.

Chapter 2

Overview of the SQUID Geomagnetometer System

2.1 Overview of DC SQUID magnetometer

The DC SQUID magnetometer is amongst the most sensitive magnetometers available. It is able to measure magnetic field changes accurate to fractions of the magnetic flux quanta, Φ_0 . Applications include magnetoencephalography (MEG) for mapping out brain activity, mineral prospecting and other geophysical measurements, radio frequency (RF) amplifiers, highly accurate voltmeters and magnetic microscopes. It can also be adapted for many other uses.

A brief overview of the DC SQUID is presented here. The principles required to understand a SQUID magnetometer cannot be discussed in full detail here, however the reader can be referred to [1], [32] and [3] for full details. The parts necessary for a basic understanding of operation and its influence on the rest of the system will be covered.

A SQUID is made up by placing two identical Josephson junctions in parallel and biasing it with a current, shown in Figure 2.1. The current should divide equally between the two junctions, however an imbalance can be created in this current division. The imbalance can be created by increasing or decreasing magnetic flux through the loop created by the two parallel junctions. As an effect, a modulated voltage is presented over the junctions by the imbalance. This voltage is dependent on fractions of flux quanta passing through the loop and is periodic, with a period of one flux quanta. It is illustrated in Figure 2.5. By monitoring this voltage, changes in the magnetic field can be measured. In the SQUID used in this project, the aforementioned voltage is monitored to maintain a constant field through the SQUID. More detail on this is discussed in Section 2.1.4.

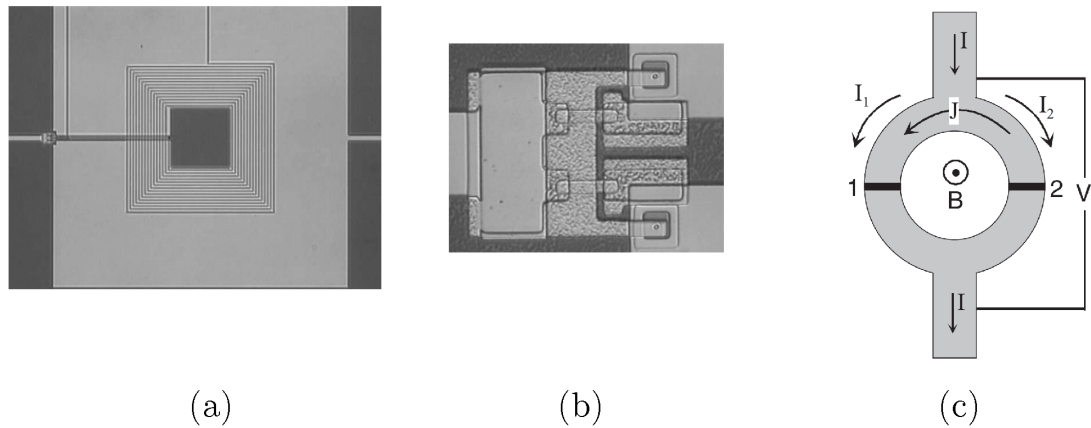


Figure 2.1: Wafer level photomicrograph of SQUID input coil (a) and Josephson junctions (b). A diagram of the fundamental SQUID structure is in (c). [1]

Wire-wound pick-up loops or thin film pick-up loops manufactured with lithographic processes are common, which is used to couple the magnetic field to be measured into the SQUID loop. This pick-up loop is referred to as a flux transformer and it can be designed to increase or decrease the magnetic field that is coupled into the SQUID loop. This can be seen in Figure 2.1.

SQUID Gradiometer

Many of the aforementioned applications of SQUIDs are used in this configuration, since the measurements are mostly done on smaller or moving objects. The measurements are typically of a non-destructive kind, such as biomedical measurements. Another application is small and large scale geophysical prospecting [1]. It is an easier application of SQUIDs to use, since distant noise sources do not affect it as much. Geomagnetic field variation as a function of position can be measured with gradiometers, and is used for geological surveys [1]. The geomagnetic field locally approaches a uniform field, and as a consequence gradiometers are not applicable to measure variations thereof over time, as desired in this project. However, gradiometers will be described briefly, in order to differentiate.

SQUID gradiometers are a configuration of SQUIDs which can ignore uniform magnetic fields that may be present. Uniform magnetic fields can be explained as a large volume where the direction and magnitude of the magnetic field is consistent. Uniform magnetic fields can be static or fluctuating, and usually originates from the geomagnetic field or distant interference sources. Since gradiometers are immune to uniform magnetic fields, it can strongly reject distant sources and exclude it from measurements. The rate

of change of a magnetic field with a relatively sharp change in direction can be measured with high sensitivity. More specifically, non-uniform magnetic fields with relatively high gradients, or magnetic fields with a flux loop limited to a small area or volume, can be measured.

An example of the pick-up loop configuration of a SQUID gradiometer is shown in Figure 2.2. Using this type of pick-up loop, little or no flux is coupled into the SQUID by uniform fields. Second order gradiometers can be realised by connecting two gradiometers of opposite polarity. A third order gradiometer can also be realised by connecting two second order gradiometers of opposite polarity.

SQUID magnetometer

For measuring a geomagnetic field, the SQUID has to be configured as a magnetometer, since it will be measuring a uniform field. Careful consideration of the environmental magnetic field is required for this configuration. Due to the high sensitivity, even small sources of magnetic fluctuations or noise can saturate the control electronics. This is discussed further in Chapter 4.

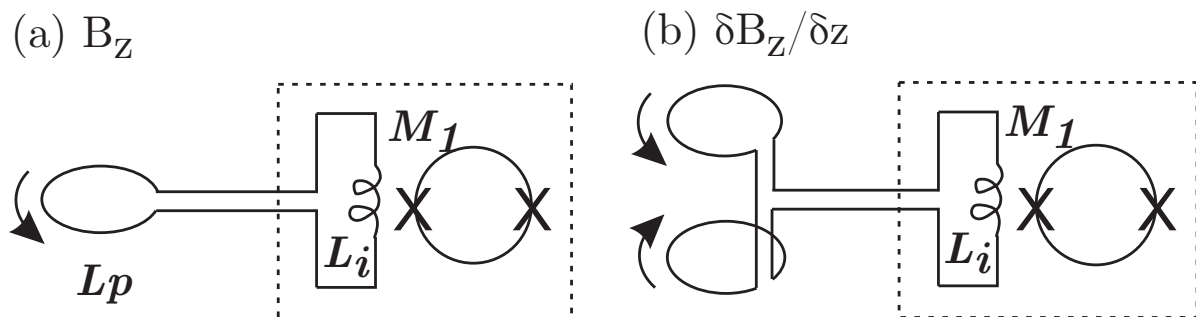


Figure 2.2: Circuit diagrams of magnetometer (a) and gradiometer (b) configuration of a SQUID. [1]

2.1.1 Overview of superconductivity

Brief history

The earliest superconductors were discovered when the first methods of cooling helium into liquid state became available. Heike Kamerlingh Onnes constructed a plant for liquefying helium in 1908. In 1911, he cooled mercury with liquid helium as an experiment. Mercury

unexpectedly lost all resistivity at a temperature close to the boiling point of liquid helium, 4.2 K, instead of gradually decreasing as he predicted. [33]

About a century of development has passed since the discovery of superconductivity, and a large field of research has developed around it. Many applications for superconductors have been developed, ranging from highly efficient transmission lines, very powerful magnets, perfect electromagnetic shields, sensors accurate to smallest measurable quanta, low noise and accurate analog signal processing and ultra high speed digital electronics. However, many underlying principles of superconductivity are not fully understood yet.

Basic principles of superconductivity

Superconductivity is often simply understood as a material with no resistance to electrical current. However, this does not translate to a conductor capable of carrying an infinitely large electrical current. The following parameters are required to be low enough for a material to be in the superconducting state:

- Electrical current density.
- Magnetic field intensity around the conductor.
- Temperature of the material.

A critical surface (or phase space) can be plotted in order to visualise the requirements for superconductivity. The critical surface of some popular superconductors is shown in Figure 2.3. From this it is clear that a specific operating temperature will define the limits of the magnetic field intensity present as well as the maximum current density. If these limits are exceeded, the material will again become resistive.

The following parameters of a superconducting material can be defined:

- Critical current: the maximum current which a specific superconducting object can carry while remaining in the superconducting state.
- Critical current density: the maximum current density flowing into a cross-section of a specific superconducting object, while remaining in the superconducting state.
- Critical magnetic field strength H_{c2} : the maximum magnetic field intensity a superconductor can be exposed to before losing superconductivity.
- Critical magnetic field strength H_{c1} : the maximum magnetic field intensity a superconductor can be exposed to before losing the Meissner or diamagnetic state, as discussed in Section 2.1.1.

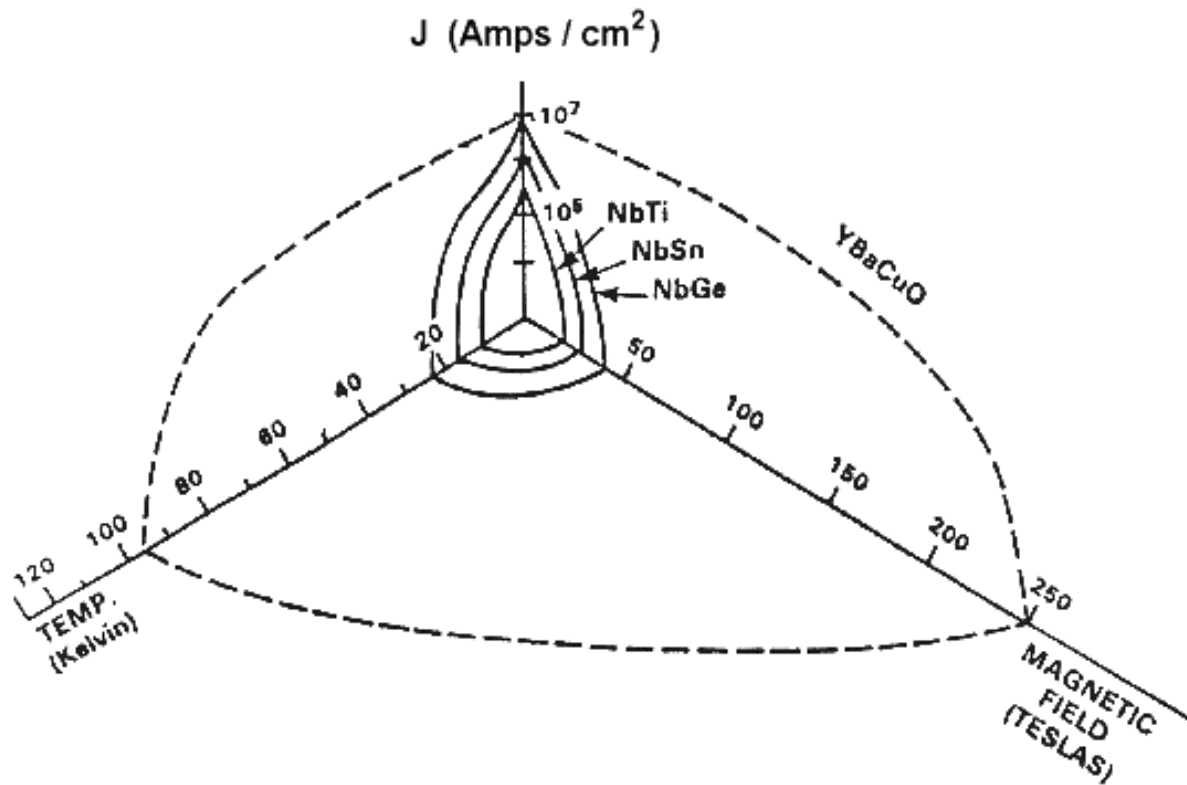


Figure 2.3: Critical surface plot of popular superconducting materials with relation to temperature, current density and magnetic field. [2]

- Transition temperature: temperature threshold below which a material becomes superconducting.

Low temperature and high temperature superconductors

Since its discovery, superconductors became a field of continual research. Higher transition temperatures are always desired. It is a major goal of research in superconductivity to find a superconductor which is superconductive at room temperature. The complexity of operating cryogenics in using superconducting devices currently places it beyond the reach of all but specialist users. Initially, liquid helium could only be produced in a small number of laboratories, which limited research and development to small groups.

Major advances have been achieved with cryogenics and superconducting materials, mainly in achieving superconductivity with liquid nitrogen as a cryogen. Research eventually led to the discovery of $YBa_2Cu_3O_{7-x}$ (YBCO) in 1987, the first superconductor discovered with a transition temperature above the boiling point of liquid nitrogen. Liquid nitrogen is more freely available and an easier cryogen to use than liquid helium,

due to its higher boiling point (77 K compared to 4.2 K). This has enabled wider use of superconducting devices.

Superconductors are split into the categories of low temperature superconductors (LTS) and high temperature superconductors (HTS). LTS electronics almost exclusively use niobium as a superconductor. YBCO is popular for HTS electronics. Development of fabrication technology present many obstacles to manufacture thin film superconducting circuits reliably, which is a major obstacle for developing electronics with different superconductors. [1]

Meissner state and types 1 and 2 superconductivity

If a low magnetic field is present when a superconductor is cooled down, different superconductors present different types of behaviour at the transition temperature. Some superconductors will enter the Meissner or diamagnetic state, where all magnetic flux passing through the superconductor is expelled. Currents opposing the external magnetic field will then be flowing in the superconductor. These superconductors are known as type 1 superconductors, and their critical temperature is below 9 K. No high temperature superconductors (HTS) are type 1 superconductors.

Type 2 superconductors can achieve superconductivity without expelling the field originally passing through it. When it is cooled down further, there is another transition temperature where it will also enter the Meissner state as shown in Figure 2.4. There are advantages and disadvantages to this. In a superconducting transmission line, this will allow it to remain superconducting when large magnetic fields are present. However, the critical current density of the superconductor is dependent on the amount of magnetic field passing through it. The functioning of components based on Josephson junctions will be influenced by this, since their parameters are a function of the critical current density. In a SQUID, this manifests as $1/f$ noise [1].

A type 2 superconductor outside the Meissner state will have magnetic flux passing through it. Small current vortices are present in the superconductor around the path of each fluxon passing through it. The area required for these vortices are then unavailable for current conducted by the superconductor, which affects the critical current density. When the field passing through the superconductor is increased, the density of fluxons passing through the superconductor will also increase. This further increases the density of the vortices and reduces the critical current density further.

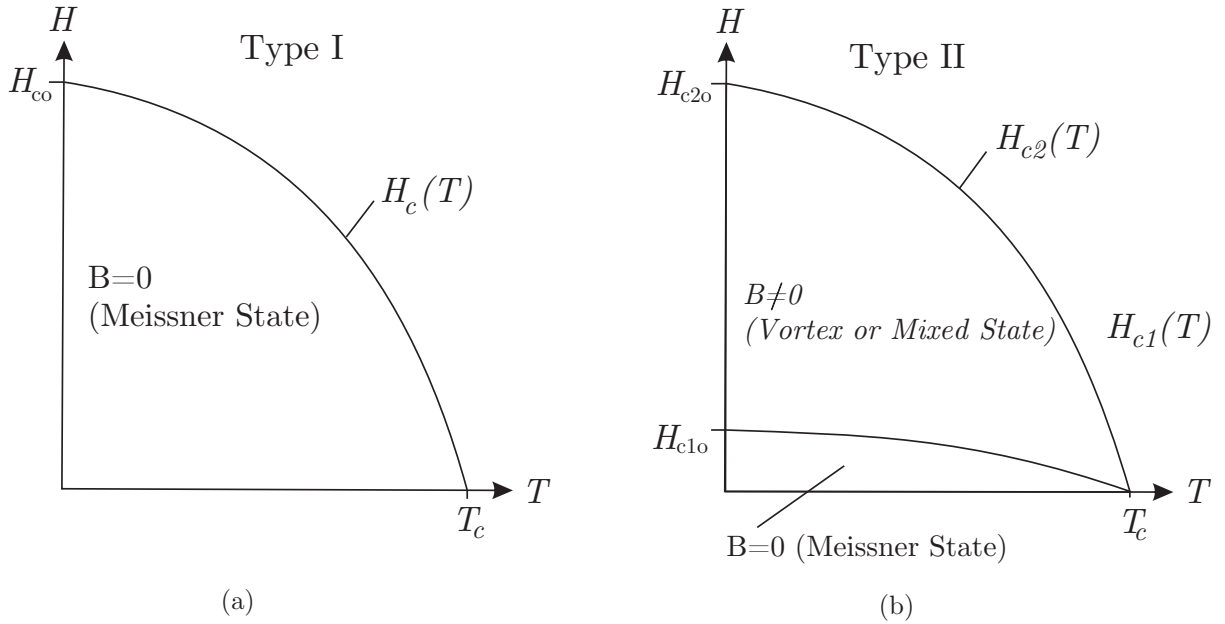


Figure 2.4: Critical field vs critical temperature for type 1 (a) and type 2 (b) superconductors, illustrating the Meissner state region in type 2 superconductors. [3]

2.1.2 Flux quantisation

The phenomenon of flux quantisation was discovered in 1961 [34]. It is in principle similar to the charge of a single electron, eV . It was found that the magnetic flux through a superconducting ring carrying a constant current only increases with multiples of Φ_0 . Magnetic field lines always form a closed loop, and to continue from this concept a fluxon was defined as a single circulating particle of magnetic flux. The magnetic field intensity of a fluxon has a fixed value, $\frac{h}{2e} = \Phi_0 \approx 2.067833 \times 10^{-15} \text{ Wb (T} \cdot \text{m}^2)$. Superconducting electronics have developed to a state where it is possible to work with single flux quanta in analog measurements as well as digital applications. In the case of a SQUID magnetometer, flux quantisation effects are used to measure changes in magnetic field intensity.

2.1.3 The Josephson junction

The Tunnel junction

When a thin, insulating layer exists between two conductors, a probability exists that the matter waves of electrons can tunnel across this insulating layer. The probability increases as the thickness of the insulator is decreased, and at the order of several Angströms and at

a specific voltage threshold it will start to conduct current across the insulator [3]. This is referred to as normal electron tunnelling. A variation of normal electron tunnelling is used to inject charge into the gate of a Field Effect Transistor (FET) covered with a similar thin insulator, for use as a memory element in flash memory. [35]

Tunnel junction using superconductors

The electrons of superconductors are available in Cooper pairs. When two superconductors are separated with a similar insulating layer, these Cooper pairs can tunnel across the junction without applying the aforementioned voltage threshold. This is referred to as Cooper pair tunnelling, and when a specific critical current is exceeded, normal electron tunnelling start conducting the rest of the current. Normal electron tunnelling then presents a voltage drop across the link. This feature makes the Josephson junction a useful basic circuit element in superconducting electronics. The Josephson junction is named after Brian Josephson, a Nobel laureate who originally predicted the Cooper pair tunnelling behaviour a year before it was confirmed in 1963. [3]

The way a Josephson junction is constructed can affect its voltage and current characteristics. All the details cannot be discussed here, but the reader can be referred to [1] and [3] for detailed discussions.

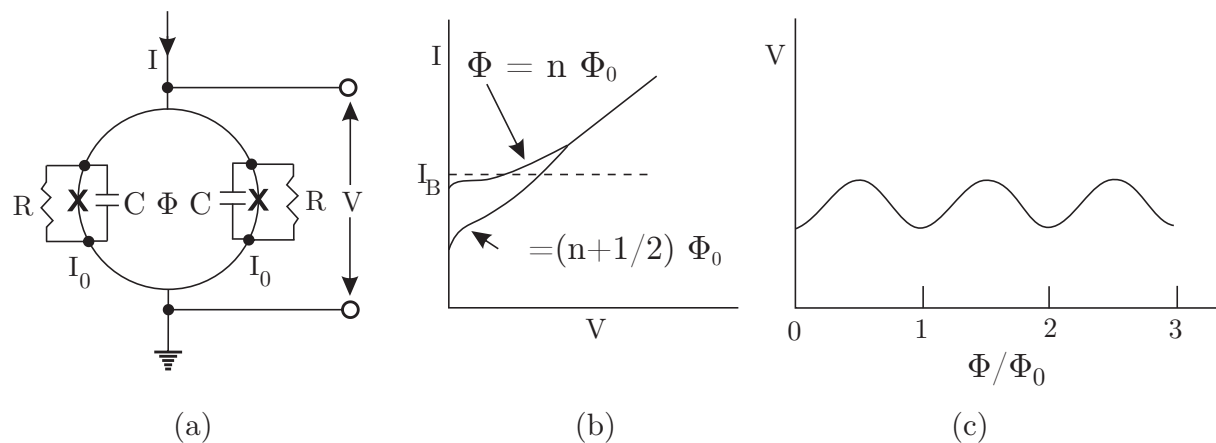


Figure 2.5: Circuit diagram of a DC SQUID (a), voltage versus bias current hysteresis (b) and enclosed multiples of magnetic flux quanta versus output voltage (using a constant biasing current), showing the voltage modulation caused by changing magnetic flux (c). [1]

2.1.4 Flux-locked loop

The SQUID magnetometers at LSBB and SANSA were obtained from Star Cryoelectronics. These SQUID magnetometers are built around a flux locked loop, which is technically an indirect method of measuring magnetic field. A small feedback coil is present at each SQUID loop and attempts to maintain a constant magnetic flux, usually an integer multiple of Φ_0 , through the SQUID loop. An analog negative feedback circuit is used to facilitate this. A flux-locked loop circuit is shown in Figure 2.7. Its working can be described as follows:

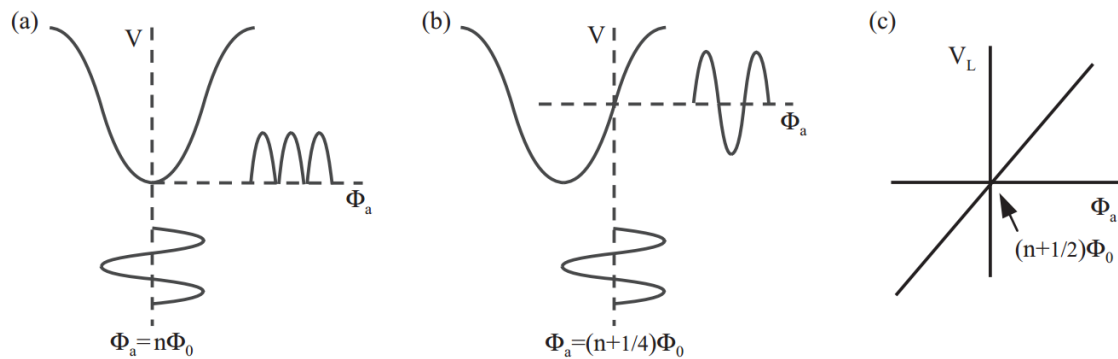


Figure 2.6: Possible flux modulation schemes for a SQUID magnetometer in (a) and (b) and flux to voltage transfer characteristic of the lock-in amplifier in (c). [1]

Oscillator

The oscillator is used to add an AC bias to the current in the feedback coil. This AC bias can also be referred to as flux modulation. Different modulation schemes are possible (see Figure 2.6) and depends on the enclosed flux to voltage characteristic of a SQUID, as illustrated in Figure 2.5. The voltage output of the SQUID will then also have an AC bias of the same frequency, if the amplitude of the AC bias is configured as in Figure 2.6(b). The SQUID magnetometers used in this project have a bias frequency of about 125 kHz.

Lock-in amplifier

A lock-in amplifier is used when it is needed to extract a very faint signal from noise, however it requires the carrier frequency as input. The carrier frequency is obtained from the oscillator. The output of this lock-in amplifier is proportional to the phase

shift between the modulated voltage from the SQUID and the carrier frequency from the oscillator. A phase shift indicates the offset between the average magnetic flux through the SQUID loop and an integer multiple of Φ_0 . The transfer characteristic of the lock-in amplifier is shown in Figure 2.6.

Integrator

When the output of the lock-in amplifier is non-zero, it will indicate that the average flux through the SQUID loop is above or below an integer multiple of Φ_0 . The output of the integrator will then respectively increase or decrease until the input becomes zero.

Output voltage and magnetic cancellation

The output of the integrator is then fed to the feedback coil via a resistor, which completes the negative feedback. The voltage over the aforementioned resistor is proportional to the external magnetic field. This voltage is the output of the SQUID magnetometer.

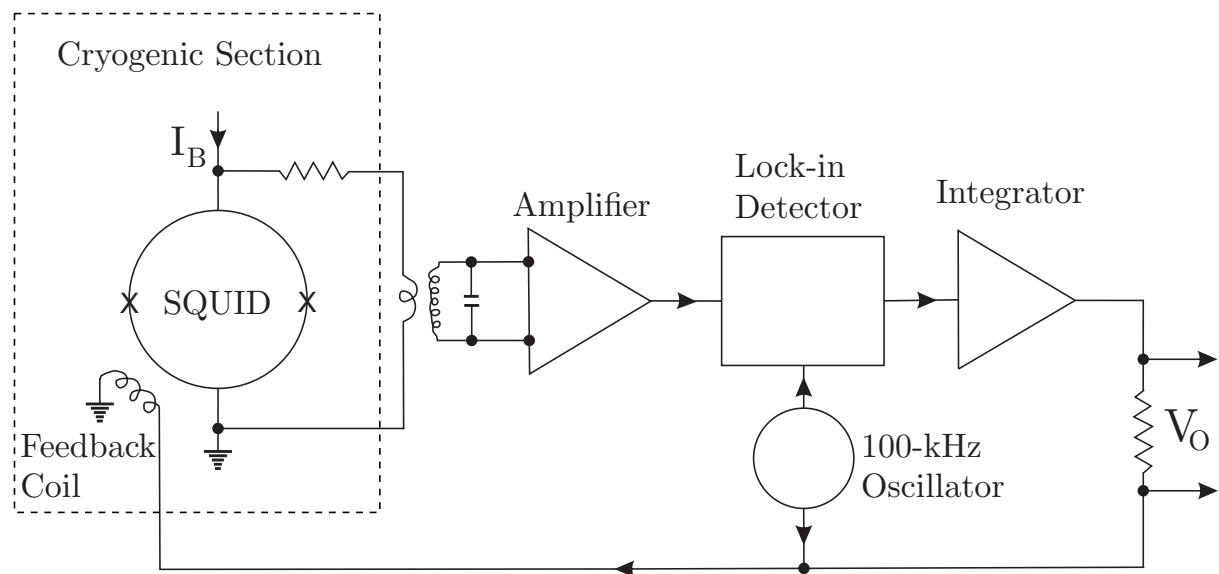


Figure 2.7: Circuit diagram of a SQUID with Flux Locked Loop (FLL) configuration. [1]

2.2 Typical geomagnetometers

2.2.1 Hall-effect sensor

A Hall effect sensor operates on the Lorentz force induced on charge carriers by a magnetic field. The distribution of current over the length of a rectangular resistive plate will be affected by a perpendicular magnetic field passing through it. The current will be pushed towards one side of the width of the plate, and this will cause a voltage distribution over the surface of the plate. The voltage distribution is typically measured at several points on the edges of this plate, which can then be processed to calculate the magnetic field strength passing through the plate. Figure 2.8 illustrates this effect. [36, 175]

This kind of magnetometer is usually better suited for measuring strong magnetic fields in the millitesla range, and are not used for geomagnetic measurements. However, higher accuracy is possible using a magnetic flux concentrator technique. An example of this is the Asahi Kasei range of three-axis magnetometer integrated circuits, which are available in many high-end smartphones today, and can be accurate to 0.15 microteslas [37]. These magnetometers are used as a compass, and also in combination with accelerometers and gyroscopes in order to record movement, determine orientation, or assist GPS navigation.

2.2.2 Magnetoresistive devices

Magnetoresistive devices are based on materials of which the resistance is a function of the applied magnetic field. It is applied as industrial sensors, read-heads for magnetic storage media, position sensors, detecting large or nearby metal objects and analysing magnetic properties. It can also be used for geomagnetic sensing, however more sensitive instruments are usually desired for scientific measurements. [36]

2.2.3 Fluxgates

Fluxgates work by having a cylindrical bar of low-hysteresis magnetically conductive material such as ferrite, with two coils wound around it. The first (driving) coil is excited with an oscillating current, which has a large enough amplitude to saturate the bar. A current will be induced in the second (sensing) coil. If there is a magnetic field along the axis of the bar, more time is required to saturate the bar in one direction than in the other, due to the magnetic field that is present. The time asymmetry can be measured, which is used to determine the magnetic field. Relatively small changes in magnetic fields can be detected, which allows it to be used for measuring magnetic properties in materials

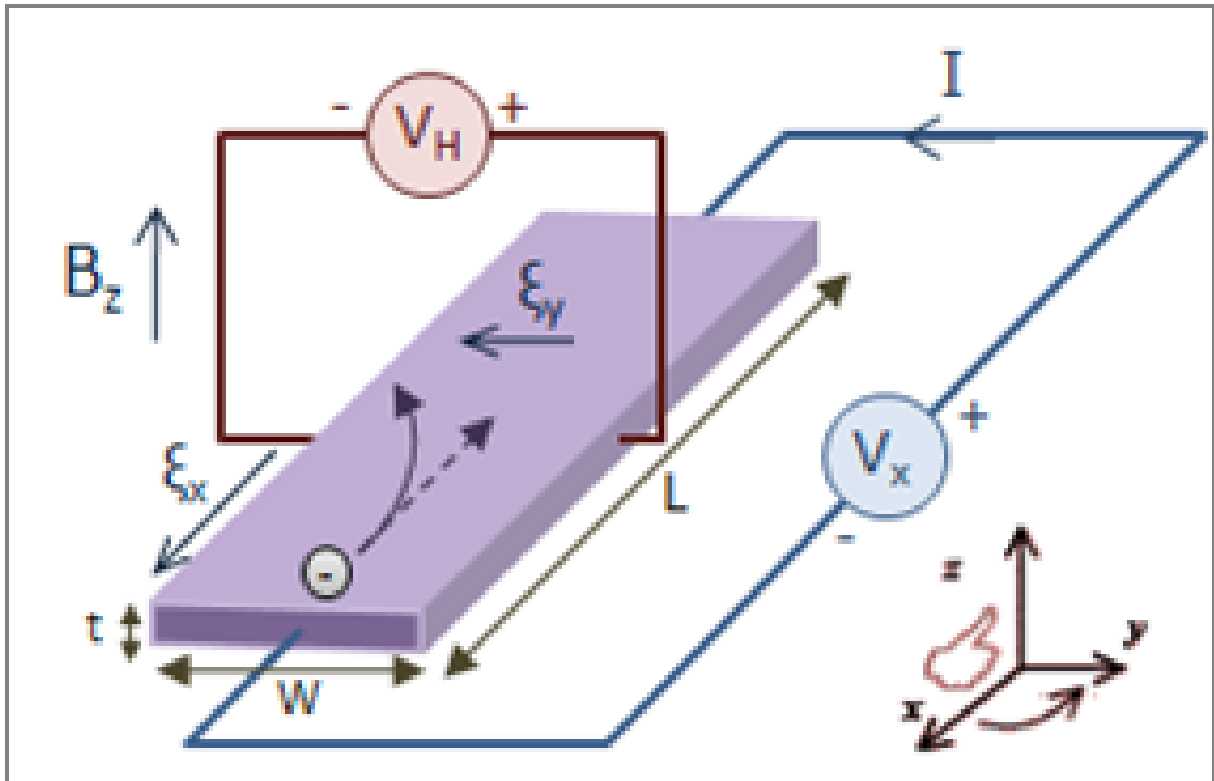


Figure 2.8: Diagram of the working principle behind the Hall-effect sensor [4].

or for measuring absolute magnetic field. It has been used to measure variations in the geomagnetic field since its discovery, and are accurate to about 0.1 nT in commercial devices. [36]

2.3 Other relevant magnetometers

2.3.1 Spin-exchange relaxation-free magnetometer (SERF)

Also known as an optically pumped atomic magnetometer, it was developed in 2003 at Princeton University and is not widely used yet. This type of magnetometer works by measuring deviations in the spin of electrons (precession) of a specific vapour, using a laser. The deviations are caused when a magnetic field passes through it. This magnetometer is more sensitive than a SQUID magnetometer, with initial reported noise floor of 0.54 fT per root Hertz and theoretical optimum at less than 0.01 fT per root Hertz [38]. It can only operate in very small magnetic fields of less than 500 nT or less, depending on how it was manufactured. This makes it unsuitable to use as a unshielded magnetometer for geomagnetic measurements at this time. It has the advantage of operating at room

temperature. It is possible to replace shielded SQUIDs with this magnetometer in relevant applications, such as biomagnetic measurements.

2.3.2 Digital SQUID

A digital SQUID magnetometer works by tracking changes of flux in a SQUID loop with Rapid Single-Flux-Quantum (RSFQ) digital electronics. The analog SQUIDs used in this project works with flux cancellation, which is an indirect method of measuring the flux through a SQUID loop. A digital SQUID will avoid using an external analog to digital converter and thus circumvent many sources of noise. Digital superconducting electronics can detect much faster changes in magnetic field than a flux-locked loop configuration. One such device is under development by a research group at the University of Savoie. This type of SQUID can only be produced with low temperature superconductors. [39]

Digital superconducting electronics are difficult to interface with and will be a challenge with this device. Using an external clock for GPS timestamping might thus be difficult, but sampling a digital output with an externally clocked device could be an easier method.

2.4 LSBB SQUID² System

2.4.1 Overview of unique bunker facility

Laboratoire Souterrain à Bas Bruit (LSBB) is a low noise research facility in the southeast of France at Rustrel, Vaucluse, Provence. The facility was created in a decommissioned nuclear bunker situated in a mountain, which served as a launch control facility until 1997. A 28 m by 8 m cylindrical concrete room with a steel armor plated interior was created 500 m underground. A 20 m by 6 m spring-suspended capsule was built inside, which served as a container for the launch control station and was supposed to be able to function after a nuclear bomb detonation had happened outside. The cylindrical room was also required to function as a Faraday cage to shield against the electromagnetic pulse that is caused by a nuclear explosion. The 14 mm thick interior steel armor plating was created to achieve this shielding. The continuity of the shielding in the seams of the capsule door is ensured by bronze-beryllium leaf springs, which creates a conductive seal. After decommissioning of the bunker, the capsule became a favourable location for low noise measurements. A diagram of the shielded capsule is shown in Figure 2.11. [40], [20]

A Low-temperature Superconductor (LTS) SQUID magnetometer was installed in-

side this capsule to measure the geomagnetic field, shown in Figure 2.9. An Agecodagis Kephren Data Logger is used to record the outputs of the SQUID. It is currently the most sensitive geomagnetometer functioning, and its specifications is given in Table 2.1.



Figure 2.9: Liquid helium dewar with the LSBB LTS SQUID geomagnetometer.

2.4.2 Effects of mountain and capsule armour

In [11] it is noted that static magnetic field and varying magnetic fields are attenuated when passing through steel plate. The armour plating completely surrounds the room, which means that it may conduct some magnetic flux around the room instead of allowing it to pass through the room. It is also not clear whether the armour plating was degaussed, so it may have a static field of its own, which could add an offset to the magnetic field inside the room. However, electromagnetic noise are shielded to values below the noise floor of the SQUID magnetometer at low frequency.

A comparison of LSBB's SQUID geomagnetic measurements with geomagnetic measurements from the Chambon-La-Forêt (CLF) observatory showed that the geomagnetic variation is 1.5 times larger inside LSBB's capsule between 0.2 and 2 millihertz (mHz). Between 3 and 20 mHz the field variation was 0.5 times the magnitude of the CLF measurements. [6] The geomagnetic field inside the capsule at LSBB measured 5 microtesla (μT), compared to 47 μT at CLF [40]. Quasistatic field variations correlated well between LSBB and CLF [6].

The geomagnetic field as well as any variations thereof is not measured in an undis-

Specification	Value	Units
ADC Temperature Coefficient	<10	Microvolts per degree Celcius
Delta Sigma ADC resolution	24	Bits
ADC input range	4.5	Volt
ADC input impedance	25	$k\Omega$
ADC dynamic range (at at 1000Hz sample rate)	117	dB
ADC THD	<105	dB
ADC crosstalk	<120	dB
ADC CMR	<120	dB
Low pass filter cutoff frequency	<2	kHz
Low pass filter signal to noise ratio	<72	dB
Low pass filter type	Butterworth	-
Low pass filter number of poles	<4	poles
SQUID operating temperature	4.2	Kelvin
Sampling rates	1, 125, 250	Hz
Timing resolution/accuracy with GPS locked	<5	us
Maximum dynamic range	+166	nT
Sensitivity in low sensitivity mode	5	pT
Sensitivity in high sensitivity mode	50	fT
Noise floor above 40 Hz (SQUID intrinsic noise, [20])	2	fT per root Hz
Noise floor above 600 Hz (SQUID intrinsic noise, [20])	3	fT per root Hz
Volume of shielded capsule	1250	m^3
Approximate magnetic field strength in capsule [40]	5000	nT
Approximate ambient magnetic field strength outside capsule [40]	47	Microtesla
Noise at 0.5 Hz at door of LSBB	20	nT per root Hz
Noise at 0.5 Hz under 500m limestone	1	nT per root Hz

Table 2.1: Specifications of LSBB SQUID² System [17], [18], [19].

turbed form, because some scaling and changes of direction may be involved. However, it is important to note that any variation outside the room that is large enough will still cause a variation inside, and the measurement data obtained has already yielded notable results [20]. A report of a mapping of magnetic field was performed with a fluxgate magnetometer inside the LSBB capsule, and it indicates some non-uniformities [5]. Figure shows a mapping of the static magnetic field inside the capsule.

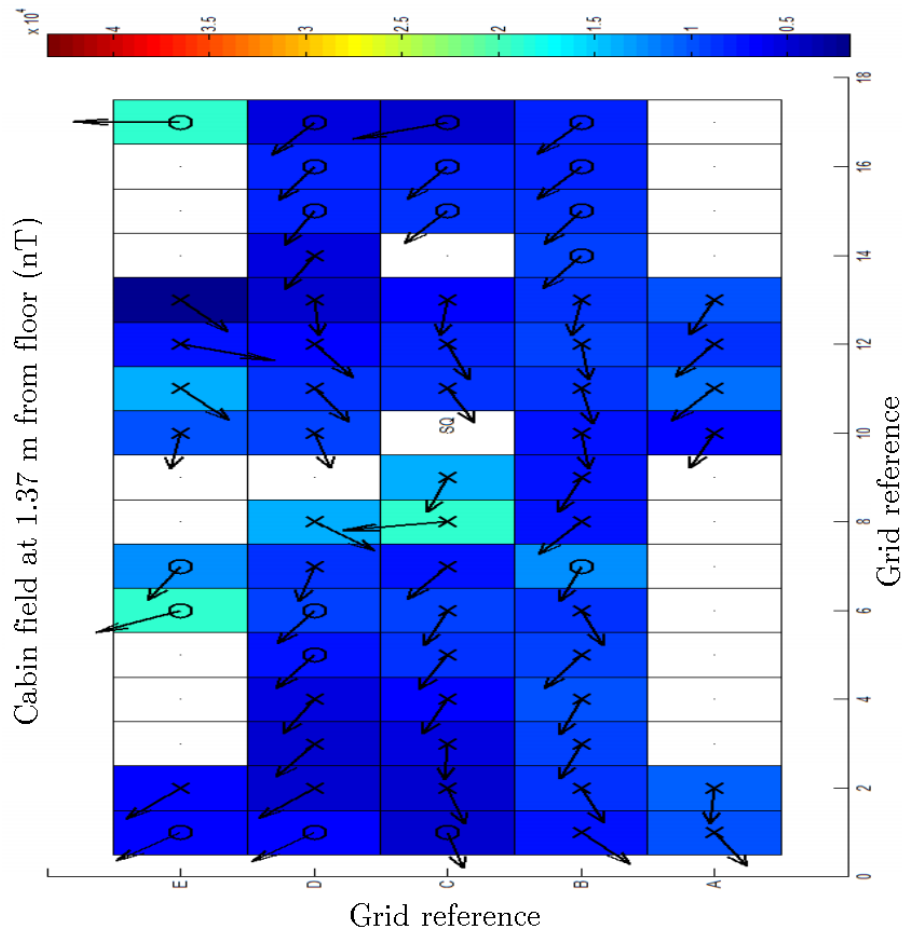


Figure 2.10: Map of static magnetic field inside the LSBB cabin. Magnetic field intensity values are in nT. [5].

At the door of LSBB, noise level of 20 nT per root Hertz was measured. Under 550m of limestone, this reduces to 1 nT per root Hertz. The intrinsic noise of the SQUID magnetometers are 2fT per root Hertz above 10 Hz. Above 600 Hz, the intrinsic noise level of the SQUIDS is reached at 3 fT per root Hertz. [20], [6]

Material	Depth	Cut-off frequency
Limestone	500 m	200 Hz
Reinforced concrete	2 m	10 Hz
Semi-mild steel armor plating	14 mm	10 Hz

Table 2.2: Layers of material surrounding the LSBB SQUID magnetometer [6], [20].

2.4.3 Effects of vibration and seismic waves

To measure the geomagnetic field accurately, it is very important to ensure that vibration sources are either not present or mitigated by a vibration damping method. Vibrations of the sensor itself will influence its measurements, which could include very faint vibrations when a SQUID magnetometer is used. It has been proposed that a strong stacking procedure could be used to improve signal to noise ratio. [41]

The cabin inside the capsule of LSBB is mounted on springs. There are some resonances visible in the swaying of the cabin at 300 to 370 mHz on the length axis, and 370 to 470 mHz in the transverse axis. This swaying can also be caused by very faint seismic waves. The RMS spectral amplitude of these vibrations were 40 microtesla per second per root hertz during the documented Indian earthquake. No vertical movement was induced by this earthquake. [6]

It has been noted that motion of groundwater and electrolyte particle acceleration due to seismic waves can cause effects that would be visible in the magnetic field measurements. This would also combine with any other magneto-seismic effects from seismic waves. [6]

A magnitude 6.1 earthquake in India, around 6250 km from LSBB, caused a magneto-hydro-seismic response of magnitude order of 10 pT [20].

2.4.4 LTS SQUID advantages and disadvantages

HTS SQUIDs generate more internal noise due to thermal noise and flux trapping which happens in high temperature superconductors. Flux motion is a major source of noise in HTS SQUIDs, however it is not a large concern in LTS SQUIDs due to lower operating temperature. Consequently, the noise floor of an LTS SQUID is lower than that of a HTS SQUID, which allows an LTS SQUID to be a more sensitive instrument [1].

Liquid helium is required to operate a LTS SQUID at 4.2K in a low noise environment. Using liquid helium brings about a few difficulties, including high cost at around US\$22 per liter in 2013 [42]. Careful considerations are required to prevent excessive loss of liquid helium by thermal conduction.

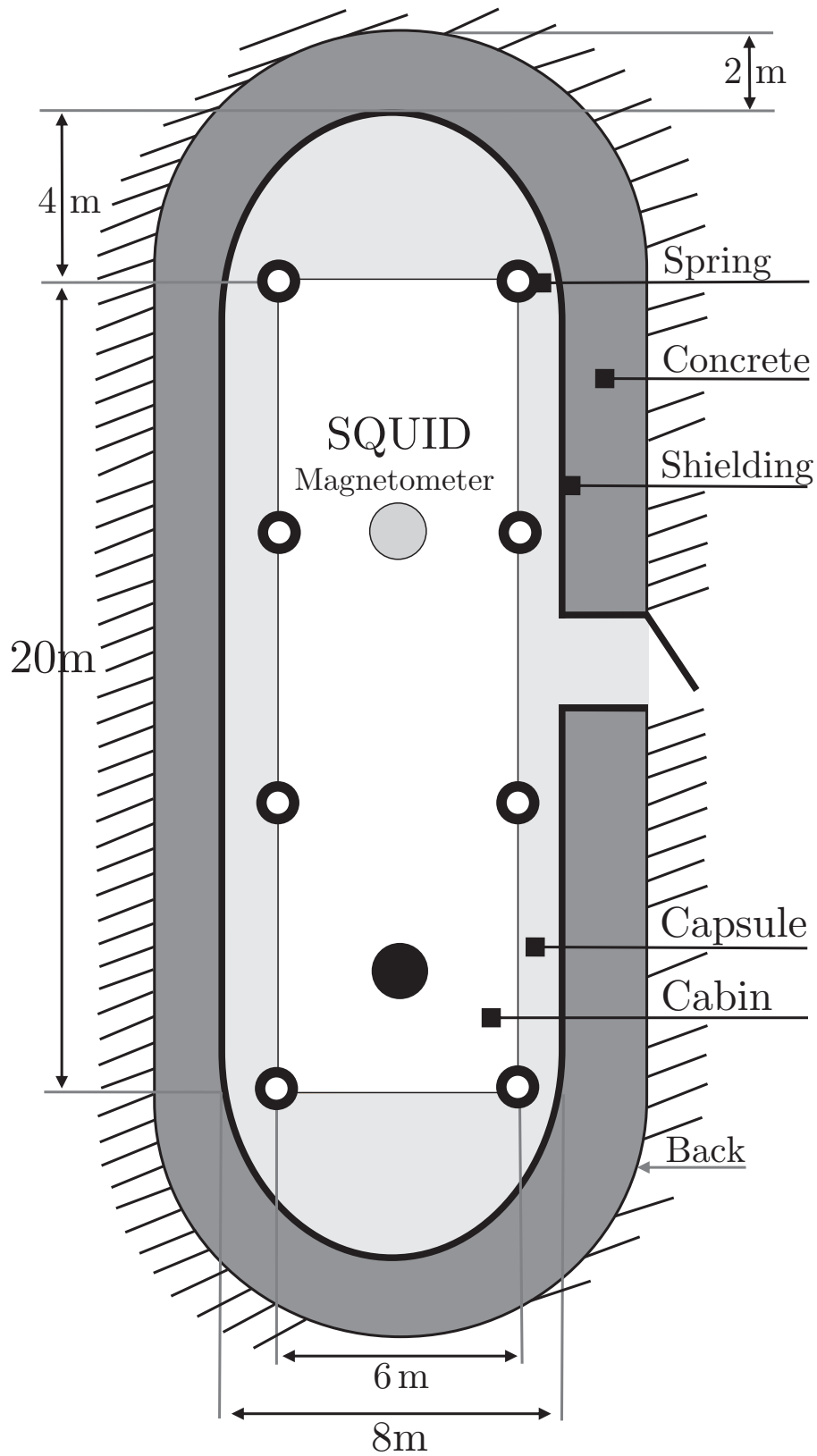


Figure 2.11: Diagram of LSBB capsule [6].

Chapter 3

Requirements and design for Global Interconnected SQUID Geomagnetometer System

In the interest of easily obtaining geomagnetic data from more locations, it is desired to design a SQUID geomagnetometer station which is easy to reproduce. Financial constraints as well as operational aspects are to be considered.

Financial constraints

Reproducing the SQUID² system from LSBB is not entirely feasible under financial constraints. Components of concern would be:

- The underground bunker with EMP shielded capsule: large construction project to reproduce, and over-specified.
- Low temperature SQUID magnetometer: requires liquid helium to operate, which requires expertise and has high operating costs.
- Data acquisition system: commercially available data acquisition systems with GPS timestamping are expensive.

Operational aspects

It is optimal for this project to centralise data storage by uploading data as it is recorded. It does require a constant internet connection to operate well, but it does remove the manual labour required to upload locally recorded data, which could introduce delays. In

the course of this project it became necessary to allow local storage of some data during interruptions of the internet connection, which is discussed in 5.5.1.

A high temperature superconductor (HTS) SQUID magnetometer was used in this project, which involves a higher up-front cost. However, liquid helium has a high risk of excessive loss during transport and by thermal conductivity of the equipment involved, and would increase the running cost by about 2000% when considering the evaporation rate involved. There is also a trade-off between sensitivity and ease of operation: the electromagnetic environment at SANSA Space Science in Hermanus is too noisy to operate an unshielded LTS SQUID.

3.1 Facility overview of SANSA SQUID geomagnetometer

The SANSA Space Science Center is a very suitable location for a SQUID geomagnetometer when considering the favourable magnetic environment and expertise available. Verification and calibration of the measurements produced by a SQUID geomagnetometer would also be possible here since recorded geomagnetic data of the location is available. This would serve well in proving the SQUID as a viable instrument for recording the geomagnetic field. A detailed analysis for viability of the LSBB SQUID² system has been done, and also of the initial operation of the SANSA SQUID Geomagnetometer [43], [8].

3.1.1 Buildings

SQUID hut

A specialised hut was constructed for the SQUID geomagnetometer. No magnetic materials are present in the hut itself, and it is surrounded by a 20 m magnetically neutral radius. Two pillars have been cast in the center of the hut, reaching down to the bedrock. The purpose of these pillars are to prevent any vibration in the surrounding soil from influencing the measurements. The pillars are also mechanically isolated from each other with styrofoam. One of the pillars serves as a stable platform for the dewar, while a jig is mounted on the other to hold the SQUID probes.

Control room

The control room is 20 m away from the SQUID hut, and houses the control electronics of the SQUID as well as the data acquisition system and its associated computer. There is a network connection at this computer.

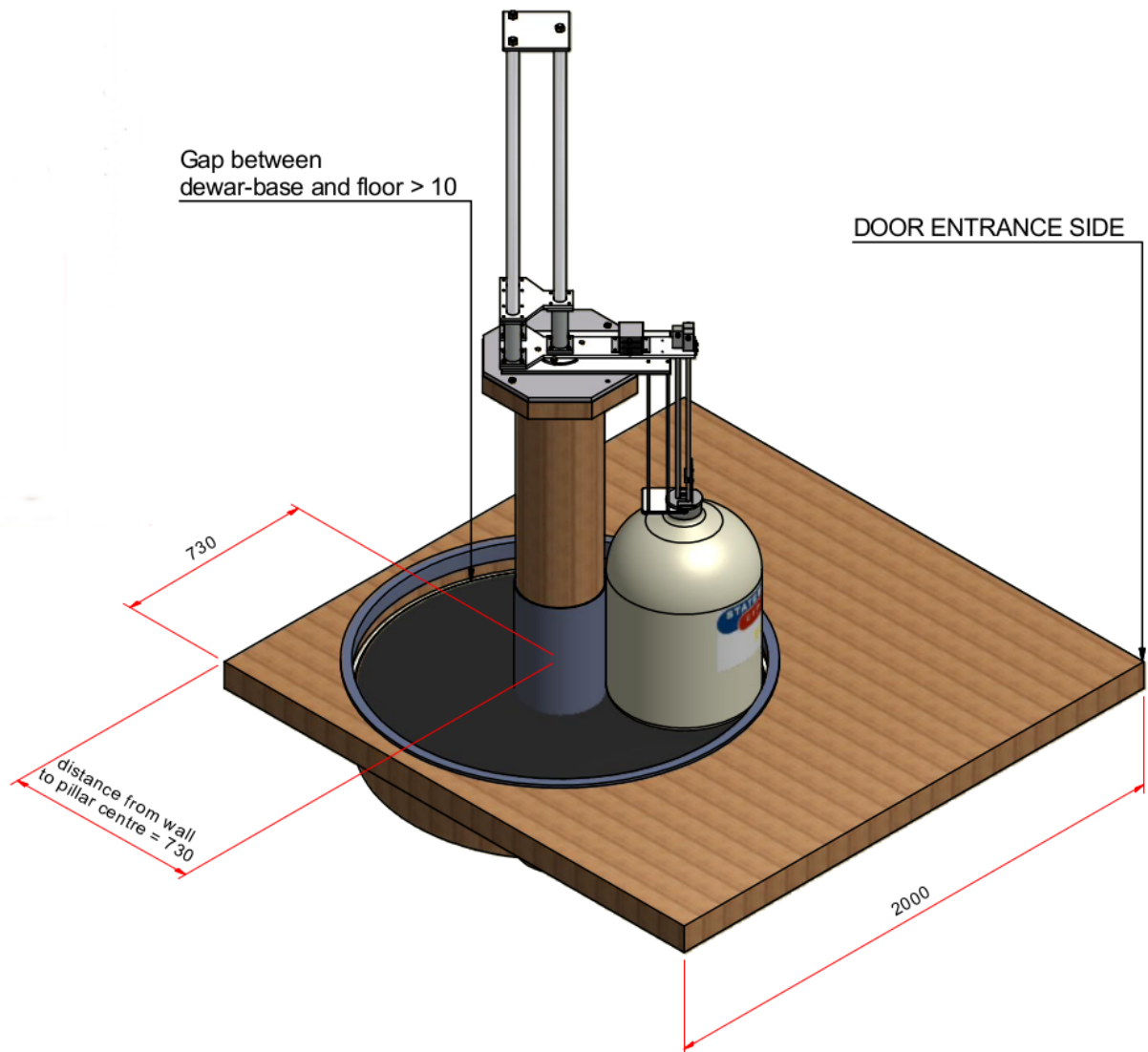


Figure 3.1: 3D floorplan of the SQUID hut as designed in [7].

3.1.2 System diagram

A diagram of the full system is shown in Figure 3.3.

3.2 Data acquisition system functions and requirements

The signal output of the SQUID magnetometer used in this project ranges between -10 V and 10 V. A scaling factor of 3.196 nT/V was originally used to calculate the required sensitivity of the data acquisition unit. The number of quantisation levels required was calculated as follows:

$$\begin{aligned}
 L &= \frac{A}{\Delta v} & (3.1) \\
 &= \frac{(10V - (-10V)) \times 3.196nT/V}{1 \times 10^{-3}nT} \\
 &= 63920
 \end{aligned}$$

where L is the amount of quantisation levels, A is the dynamic range of the signal to be quantised, and Δv is the size of a quantisation level.

The required resolution was determined as 16 bits. An engineering margin of two bits was added, therefore an 18 bit data acquisition unit was specified. The size of the quantisation levels Δv can also be specified in volts, and can be calculated as follows:

$$\begin{aligned}
 \Delta v &= \frac{A}{L} & (3.2) \\
 &= \frac{(10V - (-10V))}{2^{16}} \\
 &= 305,175 \times 10^{-6}
 \end{aligned}$$

(3.3)

The specifications of the Star-Cryo M2700 SQUID magnetometers that were initially used at SANSA is given in Table 3.1. The SQUID magnetometer was later replaced with three Star-Cryo M1000 SQUID magnetometers that were built into a three-axis enclosure. At the time of writing, thorough testing of the M1000 magnetometers was not yet completed. The specifications thereof, as seen in Table 3.2, indicate that significantly higher sensitivity in measurements can be achieved.

The sensitivity of the geomagnetic measurements could allow new insights into the characteristics of the geomagnetic field and how it is affected. It is therefore desired to have the measurements as accurate as possible, ideally with no electromagnetic interference

Specification	Value	Units
Pick-up loop area	2.7 x 2.7	mm
Current lock	13.2	$\frac{\mu A}{\Phi_0}$
Noise above 10 Hz	168	fT per root Hertz
Noise above 1000 Hz	149	fT per root Hertz
Sensitivity	25	nT per Φ_0
Feedback loop calibration	25.39	nT per Volt

Table 3.1: Specifications of initial M2700 SQUID magnetometers.

Specification	X-Axis	Y-Axis	Z-Axis	Units
Pick-up loop area	9.3 x 8.5	9.3 x 8.5	9.3 x 8.5	mm
Current lock	55.6	55.0	56.2	$\frac{\mu A}{\Phi_0}$
Noise above 10 Hz	84	110	98	fT per root Hertz
Noise above 1000 Hz	73	62	48	fT per root Hertz
Sensitivity	10.5	10.5	10.5	nT per Φ_0
Feedback loop calibration	1.89	1.91	1.87	nT per Volt

Table 3.2: Specifications of three axis M1000 SQUID magnetometers.

Constraint	Specification	Units
Measurable voltage range	-10 to +10	Volts
Amount of voltages to be measured	3	Channels
Voltage accuracy	300	Microvolts
Sample rate	125	Hertz
Sample timing accuracy	100	Nanoseconds

Table 3.3: Specifications for measurements.

Constraint	Specification	Units
Sample rate	125	Hertz
Data rate per second	4625	Bytes per second
Measured data rate per second	7000	Bytes per second
Calculated storage required per day	288.39	Megabytes
Measured storage required per day	394	Megabytes
Predicted storage required per year	140.8	Gigabytes

Table 3.4: Specifications for data storage at a sample rate of 125 Hz.

present. Sources of interference are explored in Chapter 4.

The data acquisition system that is required needs a few specific features:

- Simultaneous sampling of multiple channels.
- Differentially sampled channels.
- High accuracy on measurements as well as high accuracy on timing.
- External clocking of sample acquisitions, or built in GPS timestamping.

3.3 Centralised data storage system functions and requirements

It is required to have an online storage system for the data recorded to aid analysis thereof. The storage system is to be based at Stellenbosch University. The size requirements for the database is shown in Table 3.4. Data will be transmitted to it over an internet connection from SANSA Space Science in Hermanus. However, it could in theory be expanded to receive measurements from multiple locations to allow a globally interconnected geomagnetometer network.

For informational purposes, a website for live viewing of measured data is also required. Data must also have open access to it to allow any interested party to use it.



Figure 3.2: The magnetically neutral SQUID hut at SANSA, Hermanus (a), with a close-up of the mechanical construction (b) and a close-up of the Programmable Feedback Loop (PFL) controllers [8].

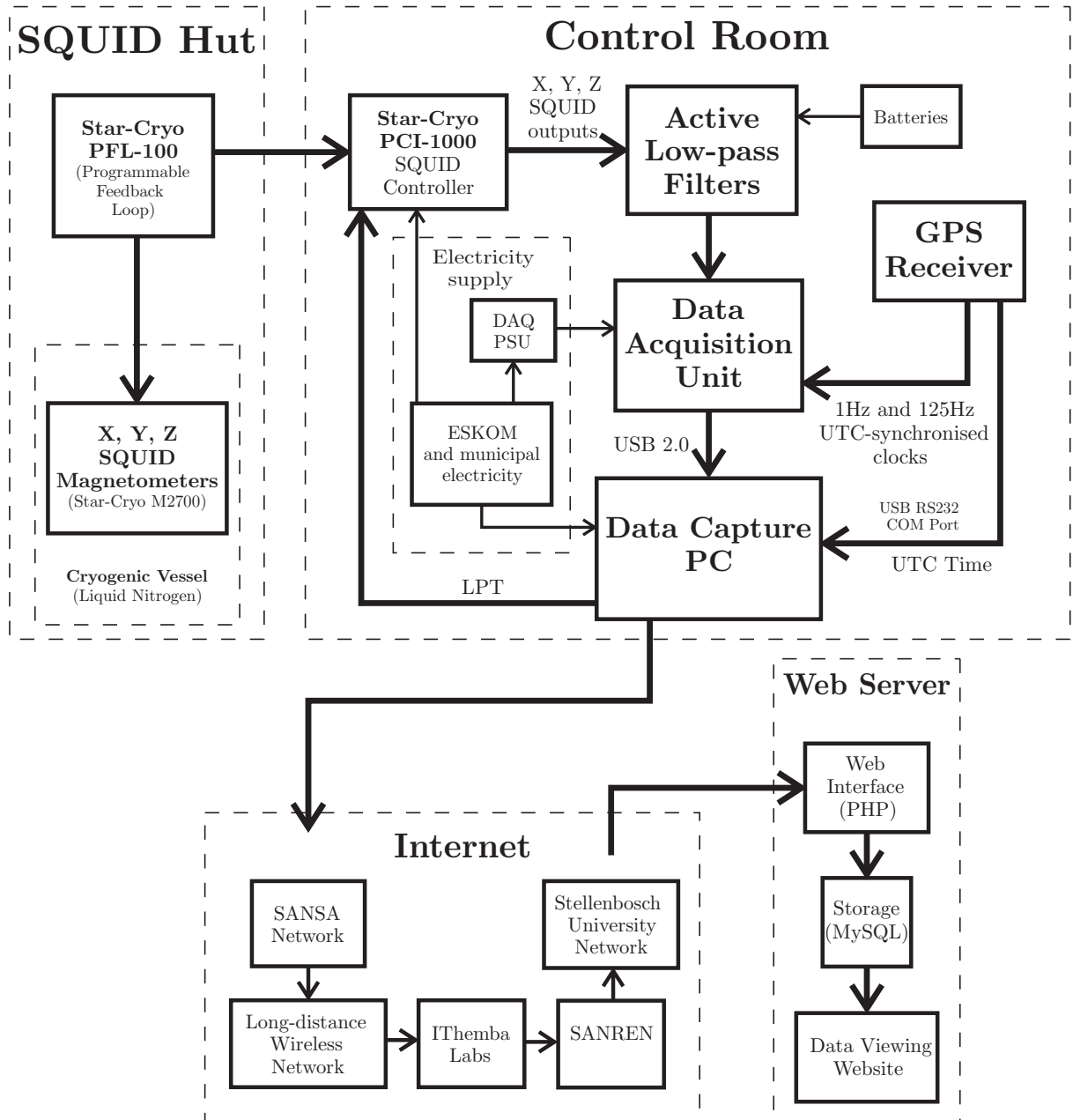


Figure 3.3: Overall system diagram as implemented.

Chapter 4

Electromagnetic considerations

Interference is usually caused by having noise coupling channels available in a system. Noise sources can be categorised into radiating sources and conducted sources, which couple into systems through different channels. All electronic circuit elements radiate noise when charge is moved, but with proper design the effects thereof can be mitigated. [44]

Coupling channels are usually different aspects of cables. A single cable can couple both radiated and conducted noise into a system. Proper use of grounding and cabling can remove most interference. A brief overview is given below:

Conducted coupling

Common conductors shared by electronic devices are coupling channels for conducted sources of noise. A common impedance is shared by two devices when common conductors are present. Currents drawn by one device may cause a drop in the supply voltage to another, or may cause a ground to be at a voltage higher than 0 V. [44]

Radiated coupling

Radiated coupling often manifest as capacitive or inductive coupling. The magnitude of noise received from these coupling mechanisms are proportional to: the length of the cables involved, and to the frequency of the noise involved.

Inductive (or magnetic) coupling requires a loop formed by a conductor and a ground. Alternating currents, moving magnets or magnetic materials, direct currents switching on or off, or rapidly increasing or decreasing direct current can induce a voltage into the aforementioned loop. Mutual inductances to other conductors allow noise to be received

through inductive coupling. Inductive coupling is specifically increased by increasing the size of a loop (or cable length). It can also be increased by increasing the magnetic field intensity or magnitude of currents at the radiating sources. [44]

Capacitive (or electric field) coupling are caused by stray capacitances between conductors. Increasing the length of a conductor will increase the stray capacitances it has to other conductors in the surrounding area. Noise from capacitively coupled sources can be increased by increasing the voltage of the noise source, and by increasing the conductor's resistance to ground. [44]

Considering the aforementioned, it is clear that an unshielded SQUID magnetometer and data acquisition instruments requires careful consideration of the environment where it will be used. All transmission lines and all electric and electronic equipment can be considered. Magnetic interference in the magnetic field measured by the SQUID magnetometers and interference caused in the electronics involved will be discussed separately.

4.1 Common sources of interference

The sensitivity of the DAQ and SQUID magnetometers is higher than that of common measurement instruments. This creates the need to consider even faint noise sources in the environment of the system in this project.

AC electricity supply

AC electricity supply transmission lines are common in most developed areas, and range from large overhead transmission lines to distribution wiring in buildings. These are sources of time-varying electric and magnetic fields. In South Africa, the electricity is standardised at 50 Hz AC and is synchronised across all power stations. Due to pressure on the local electricity supply, this frequency fluctuates to a very small degree and has been seen in measurements. Other harmonic frequency components may also be present in AC interference, depending on the quality of the local network and loads nearby. It is also possible that devices are present on the premises that do not conform to industry standards, which could introduce interference.

Interference due to AC electricity is problematic in multiple aspects of measuring the geomagnetic field accurately. The magnetic field generated by electricity transmission lines and by ground currents has been measured in the geomagnetic field itself. Electric and magnetic fields generated by transmission lines can also induce interference on signal transmission lines used in the measurements.

Grounding

Multiple ground paths are often present in electronic systems. The impedance of grounding cables are not always ideal, and can introduce noise into a system in a number of ways. The impedance of ground cables may cause multiple return paths of currents, and cause the ground point of a circuit to be at a voltage other than 0 V. Multiple ground paths may also form a loop, where inductive coupling can occur.

Switching power supplies

Switching power supplies, which are used on most electronic equipment, are often problematic with regards to interference. Resistive losses in the transistors of switching power supplies are proportional to the rise and fall times of the current through it. To decrease losses, rise and fall times of transistors in switching power supplies are constantly improved, which increases the frequency spectrum of the noise generated by it.

Pulses caused by transistors in these power supplies can travel over transmission lines and introduce noise in other devices. Electromagnetic fields generated by a switching power supply can also be of concern if it is not properly contained in its enclosure.

Magnetic field of DC currents

Large DC currents can also contribute to an offset in the magnetic field measured by a SQUID magnetometer. Direct current cause a constant magnetic field around the aforementioned transmission lines. This can cause an offset in the surrounding geomagnetic field. South Africa uses the less common standard of DC current on the majority of its electric railways, which caused problems with geomagnetic measurements in Cape Town as the railways expanded. HMO was originally established in Hermanus because no DC electric railways are nearby. However, small DC currents which are switched on and off close to the SQUID could also be registered in the measurements. Unexpected sources could be considered, ranging from the starter motor of an engine to nearby electronics.

Magnetic distortion

In magnetometers, interference is not limited to magnetic fields associated by currents. Good conductors of magnetic field can distort the ambient magnetic field around the SQUID magnetometer. Materials used in the environment around the SQUID magnetometer requires careful consideration to avoid this. An example is steel, a commonly used material which is also a good magnetic conductor. This may require the materials

used in a large number of components of the system to be considered.

4.2 Accounting for noise sources

For optimal sensitivity and accuracy, it is necessary to consider all factors that could influence the noise floor. There are ultimately two noise floors in the system that would be affected: The noise floor of the SQUID magnetometers and the noise floor of the DAQ. Optimum sensitivity will be achieved if all factors which could increase the aforementioned noise floors, can be dealt with.

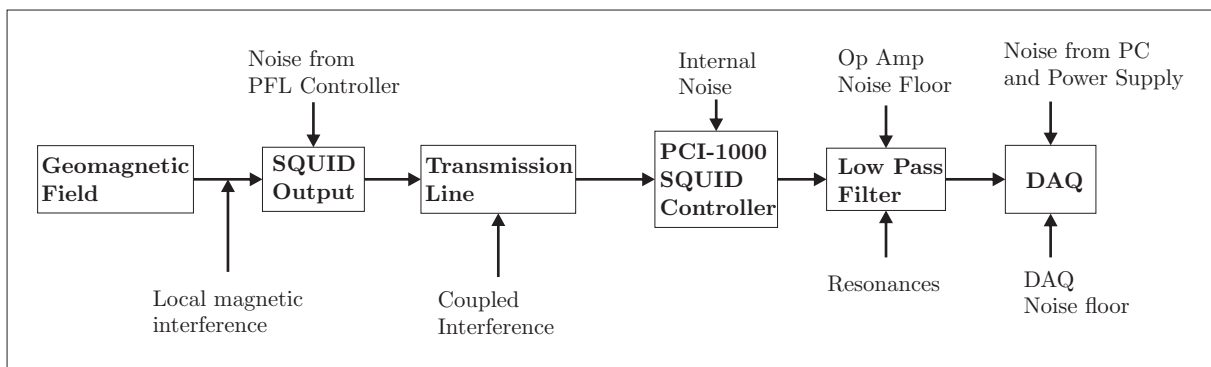


Figure 4.1: Diagram of signal flow in the system with key interference sources indicated.

4.2.1 Signal transmission lines

In the configuration of this system, the SQUID hut has been placed approximately 20 m from the control electronics. Long transmission lines are required, which have many characteristics that can degrade signals. Coupling with noise sources, transmission line resonances and resistive losses can degrade the noise floor. This also introduces signal delays which influences timing accuracy. If possible, long transmission lines should be avoided.

4.2.2 USB connections

Noise may be introduced into the system through the USB connection to the data acquisition unit and the GPS receiver. The +5V line is of interest here, since they may introduce noise from switching power supplies present in the system. The +5V line can be disconnected and replaced with a battery to supply power to where it may be needed.

However, electrical noise from the ground line and data lines can not be avoided in this way.

Triaxial signal cables

Triaxial signal cables are similar to coaxial cables, except that there is an extra cylindrical conductor between the outer and inner conductor. This extra conductor can be used as a driven shield. A unity gain amplifier can be placed at the signal source, to produce a duplicate of the center conductor signal on the shield conductor. This will help prevent any capacitive interference and displacement currents from reaching the signal on the inner conductor. [45]

If the DAQ is placed close to the SQUID outputs, triaxial signal cables should not be needed.

Battery power

It is possible to avoid using switching power supplies through most of the system, by replacing it with batteries or with less noisy power supplies. Recharging of batteries is a disadvantage since it causes downtime, however, it adds very little noise to the system and is a practical way of eliminating power supply noise. The following positions could be considered to supply power with batteries:

- The location where power is supplied to the circuit board of the PCI-1000 SQUID controller.
- The power input of the data acquisition unit.
- If the data recording computer is not electrically or optically isolated from the system by other means, it could also be provided with battery power.

Moving DAQ to SQUID hut

A number of the above-mentioned affects on signal quality can be avoided by placing the DAQ at the SQUIDS and sampling the SQUID magnetometer output directly at the PFL-100s. The signal transmission line between the SQUID hut and the control electronics can be avoided in this way. However, to prevent interference on the measured magnetic field from the DAQ's electronics, The DAQ should be built into a magnetically neutral electromagnetically sealed enclosure.

Fibre Optic / Opto-isolated data connections

USB connections can be linked with a fibre optic connection. These fibre optic connections are usually intended to extend range, but has the advantage of electrically isolating the systems involved. The device end of the fibre optic connection still requires a power supply, and a battery should be used. In this way electrical noise of a computer's USB connection can be avoided. The DAQ used in this project would require a more expensive USB 2.0 fibre optic connection, in order to to achieve full speed. Quick tests with a fibre optic connection indicated that the RMS amplitude of the DAQ's noise floor could be lowered.

4.2.3 PCI-1000 SQUID controller

The PCI-1000 SQUID controller requires a LPT connection to the computer. With this connection the ground of the computer, PCI-1000 SQUID controller and PFL-100 programmable feedback loops are shared [46].

The LPT connection can also be opto-isolated indirectly, using a USB-LPT converter and an opto-isolated USB connection. Another option could be to build opto-isolation for the serial control code signals which are required to control the PFL-100 programmable feedback loops. Power can be provided separately. The output signals of the SQUID magnetometers can then be obtained directly from the PFL-100 programmable feedback loops, bypassing the PCI-1000 SQUID controller.

4.3 Local magnetic field interference

4.3.1 Distortion of magnetic field

It is desirable that there would be no possibility of distortion of the geomagnetic field in the vicinity of a magnetometer. However, there are applications of magnetometers where this has to be compensated for. Distortion compensation algorithms are well established for magnetometers in smartphone applications. Magnetic field distortions can be subdivided into hard and soft iron distortions. [9]

Figures 4.2 and 4.3 show each of these distortions. A constant field is applied to the device and the field is rotated through 360 degrees in 10 degree intervals. The x and y axes show the measured field strength, which shows noticeable offset and scaling of the magnetic field when comparing to Figure 4.2(a).

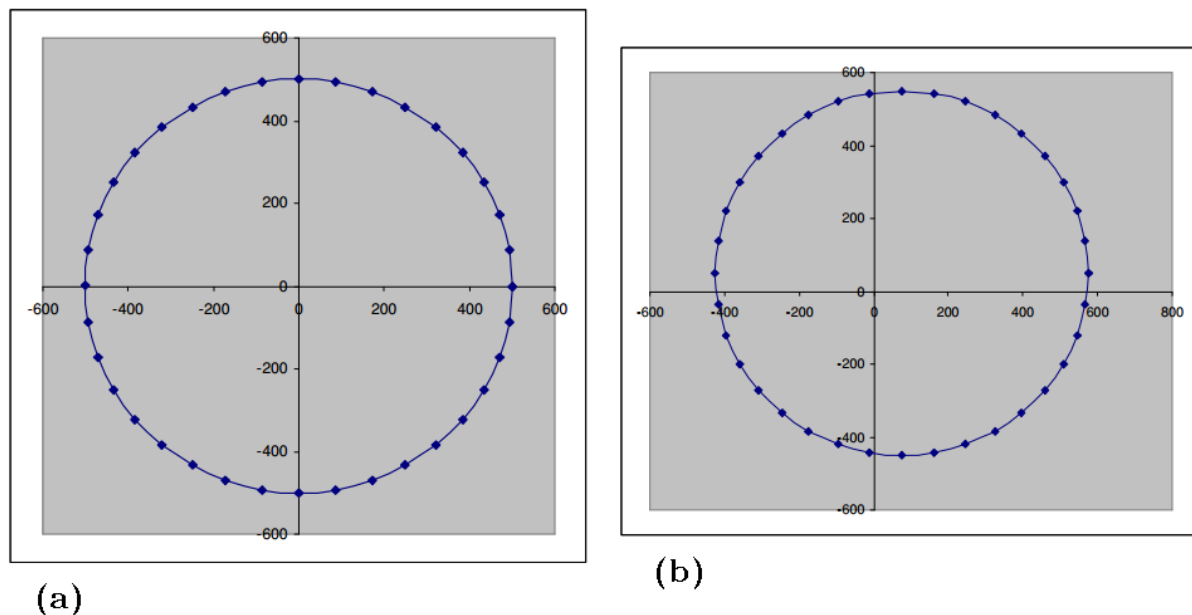


Figure 4.2: Undistorted (a) and hard iron distorted (b) fields rotated through 360 degrees, showing measured field strength on the x and y axes. [9]

Hard iron distortions

Hard iron distortions refers to permanent magnets that may be in the proximity of the magnetometer, shown in Figure 4.2. The offset caused by hard iron distortions is clear in Figure 4.2(b). These are usually compensated for by adding an offset to each axis of the magnetometer. This can also be done in software, and the software created for this project provides for this already.

Soft iron distortions

Conductors of magnetic field in the vicinity, with or without a permanent magnetic field, will create distortions called soft iron distortion as illustrated in Figure 4.3. Compensation for these distortions can become very complex. The saturation field strength of these materials may cause non-linearities in the nature of the distortion. The magnetic conductivity of the material is also not necessarily constant versus frequency or versus the magnetic field strength.

A combined hard and soft iron distortion for two axis fields is shown in Figure 4.3(a). For a three axis magnetometer, it is represented by the ellipsoid in Figure 4.3(b). The undistorted three axis field in (b) is represented by the sphere, after a compensation

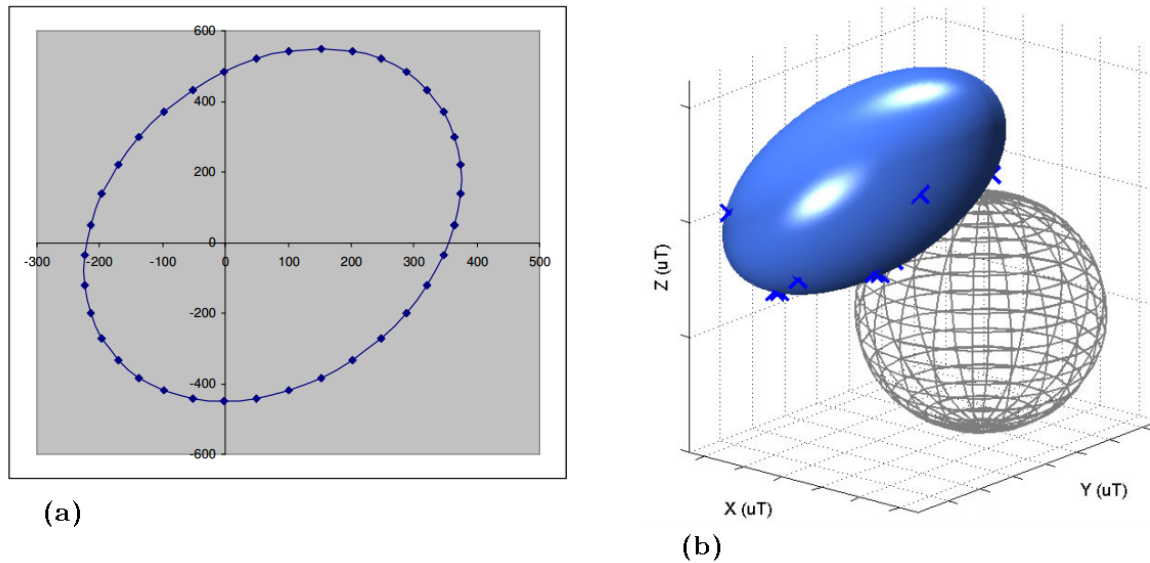


Figure 4.3: Combined hard and soft iron distortion for two axis fields (a) and for three axis fields (b). [9]

algorithm has been applied.

Compensation for these can be a project of its own, but should fortunately not be a problem for the SANSA SQUID magnetometer. However, it is an option for the measurements of the magnetic field in the LSBB capsule.

4.4 Shielding of AC magnetic fields around sensor

SQUID magnetometers are generally used in a magnetically shielded environment. One of the requirements when using a SQUID magnetometer is that the variations in the present magnetic field does not exceed the dynamic range of the instrument. This dynamic range is generally very small compared to varying magnetic fields generated by common electric, electronic or mechanical equipment. However, when measuring the magnetic field from a specific source, magnetic fields from other sources can be excluded by creating a magnetic shielded volume where the SQUID magnetometer and the specific source can be placed. [1]

When using a SQUID magnetometer as a geomagnetometer, effects from unwanted field sources have to be minimised by other means to avoid excluding the geomagnetic field. One strategy to do this is to avoid having magnetic fields with variations greater than the dynamic range of the SQUID magnetometer near the instrument. This can be

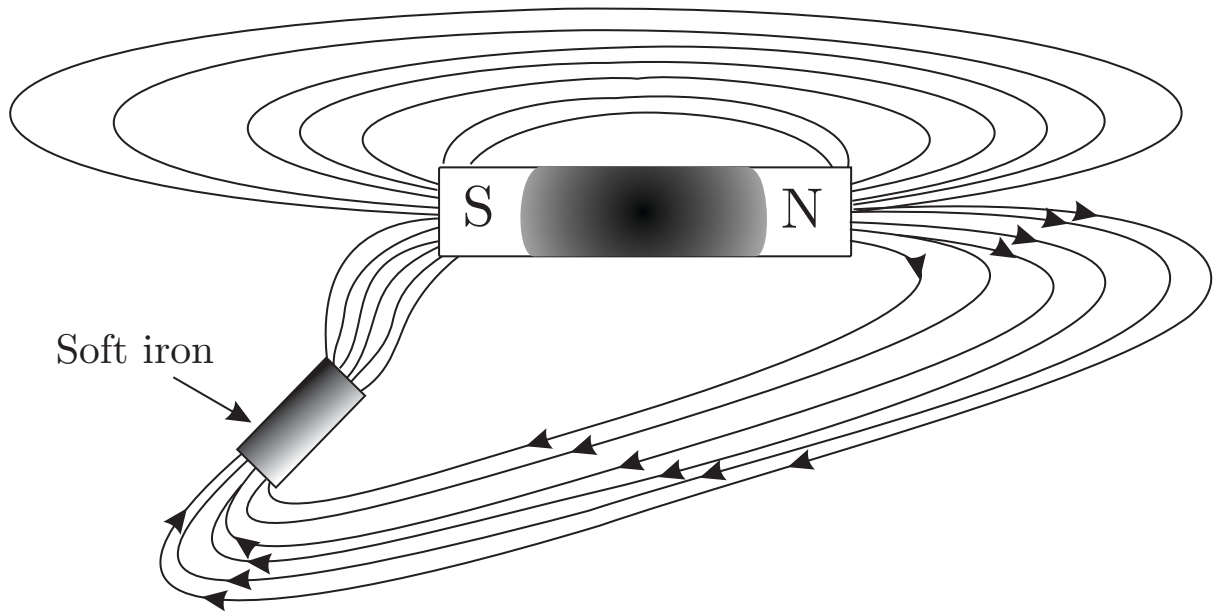


Figure 4.4: Illustration of soft iron distortion in flux lines [10].

achieved by carefully planning controlling how close any sources of magnetic fields are to the SQUID magnetometer, as well as by shielding sources of alternating magnetic fields. It is also possible to use plate shielding which shield alternating magnetic fields above a certain frequency from the SQUID, as discussed in Section 4.4.2. Both these strategies are present in the setup of the SQUID magnetometers used in this project.

A small investigation was performed to determine what shielding is possible without affecting the geomagnetic field. Finding a method to shield 50 Hz magnetic interference without affecting the geomagnetic field would make it easier to operate SQUID magnetometers. It was expected that magnetic interference from AC electricity might cause the SQUID magnetometers to saturate.

4.4.1 Active cancellation

Active cancellation of magnetic interference is performed on some measuring instruments, such as electron microscopes. Commercial systems are available which work with cancellation coils, which can cancel constant and alternating magnetic fields [47], [48], [49]. However, SQUIDs have a very high bandwidth, which will require extremely careful design of the cancellation controllers to maintain stability over wide bandwidths and to prevent introducing noise of its own. For this reason, using plates for passive shielding of interference from alternating magnetic fields is a more attractive option, since the

shielding efficiency increases with frequency.

4.4.2 Passive shielding with plates

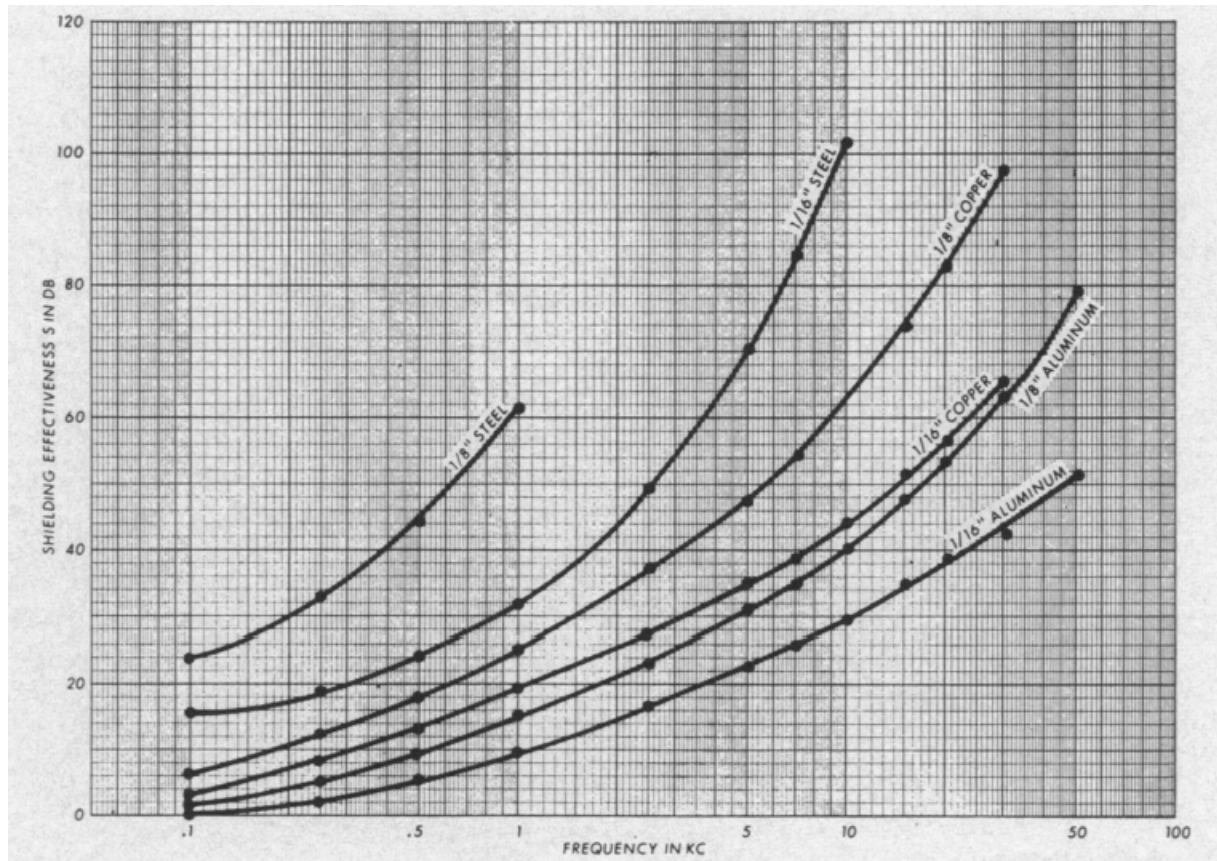


Figure 4.5: Shielding effectiveness of certain materials [11] versus frequency in kilocycles (KC).

Practical tests

Some tests were done with different kinds of non-magnetic plate shielding. To determine how effective it may be to shield 50 Hz power frequency was of particular interest, because it is present in most areas with electricity and was believed to be the strongest magnetic interference present. It was determined that several plates would not attenuate fluctuating magnetic fields better than a single plate with the same combined thickness. At 100 Hz, about 6 dB attenuation could be achieved with two 1 mm thick aluminium plates. At 50 Hz with 1 mm thick plates, only about 3 dB attenuation was possible. From this it can be concluded that plate shielding could be effective, but only if a sufficient thickness is

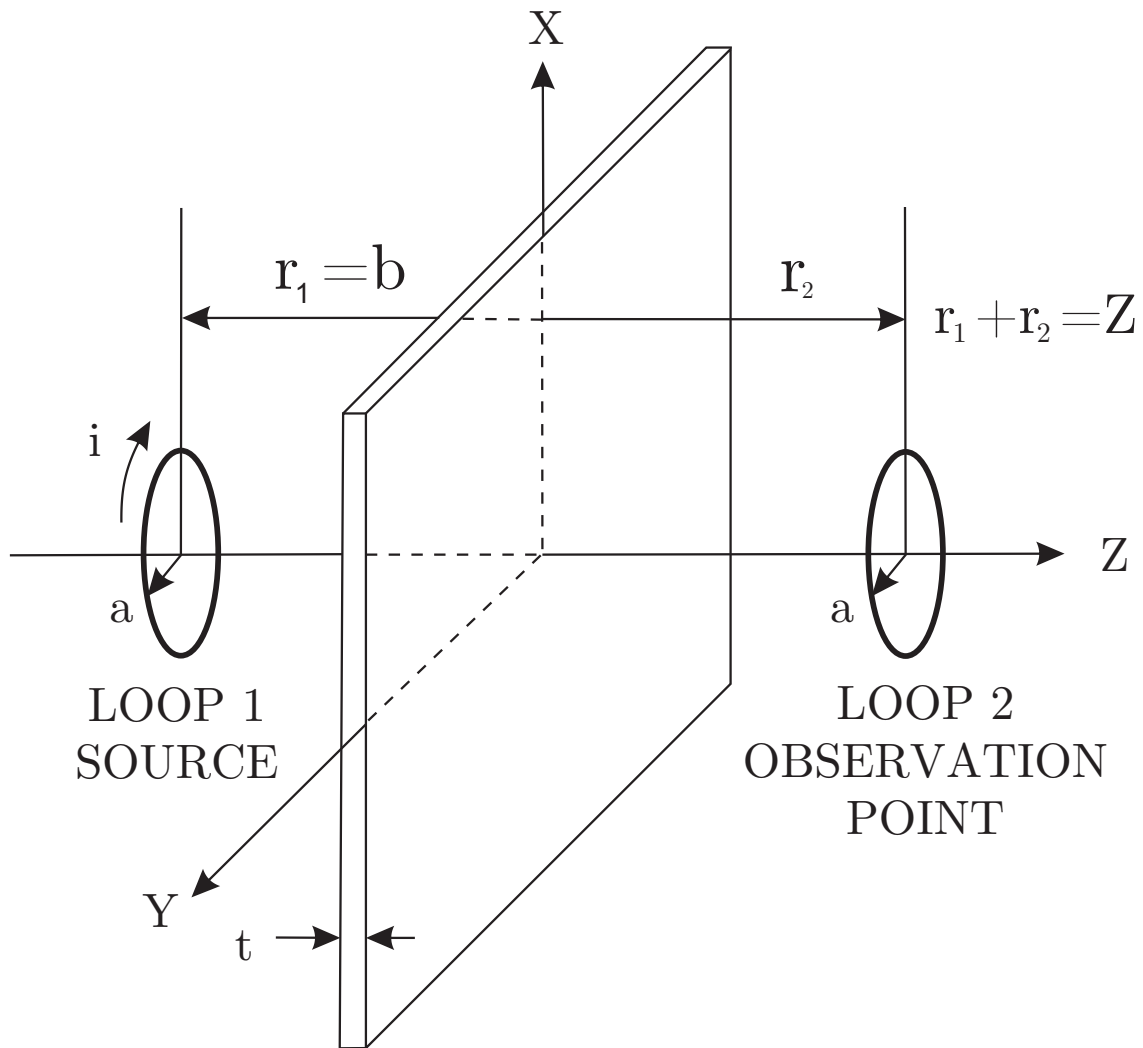


Figure 4.6: Setup for practical shielding efficiency test of certain materials [11].

used. A diagram for the setup of this test is in figure 4.6.

Shielding provided by aluminium dewar

A 34 litre aluminium dewar is used to contain the liquid nitrogen for the SQUID magnetometers. The construction is a double walled cylindrical vacuum vessel, which means the SQUID is surrounded by two sheets of approximately 1 mm thick aluminium. Considering Figure 4.5, some shielding from alternating magnetic fields should be provided without attenuating the geomagnetic field.

Chapter 5

Software-interrupt based precision-timed data acquisition system

For this project, a system was developed to measure the outputs of the SQUID magnetometers and time stamp the data accurately [50]. This system can be divided into a few components, and each component will be discussed in separate subsections:

- Timing source.
- Signal conditioning.
- Data acquisition unit.
- Data capturing software.

Part of this project was implementing the aforementioned system. There has been several implementation issues, that required some mitigation measures to be implemented as discussed in Section 5.5.

The original specifications for the system are repeated in Table 5.1.

5.1 Timing source

The requirement for the project was to have each sample timestamped with UTC time accurate to 100 ns. This is more accurate than the typical clock in a computer, and also faster than the reaction time of most non-real-time operating systems. The Linux kernel

Constraint	Specification	Units
Measurable voltage range	-10 to +10	Volts
Amount of voltages to be measured	3	Channels
Voltage accuracy	1	Microvolts
Sample rate	125	Hertz
Sample timing accuracy	100	Nanoseconds

Table 5.1: Specifications for measurements.

has shown latencies in the order of microseconds in studies [51, 24]. Microsoft Windows supports 300 to 1000 context switches per second [52]. Reaction time to an interrupt is not guaranteed officially but can range from 60 to 3000 microseconds and slower reactions are possible, depending on system load [53]. The instability in typical crystal oscillators used in personal computers are in the order of several microseconds [54, 10], which would also make them unsuitable as a frequency source for a clock.

5.1.1 GPS time

For accurate timestamping, GPS can be used as a direct or indirect time source. GPS receivers usually provide a timepulse output which are synchronised to the beginning of each second in UTC time, and can be used to set the watch. GPS satellites transmit timing and orbital information from highly accurate on-board caesium atomic clocks, which are periodically updated from atomic clocks on earth [55]. GPS receivers use the transmissions from several GPS satellites to calculate signal travel time of each transmission, from which it then determines its position on earth and also the current time. The time in GPS receivers can be accurate to 80 ns RMS on commercial models. A long term timing offset distribution is recorded by comparing it with a more stable clock source to determine this. The timing offset is usually a Gaussian distribution, and the timing specifications are determined from it [21]. See Table 5.2 for the timing specifications of the u-blox LEA-6T timing GPS used for this project.

5.1.2 FPGA timer

A timing source could thus be implemented by making an externally clocked real-time clock (RTC) in a Field Programmable Gate Array (FPGA) with a very accurate external frequency source as a clock signal. Commercially available RTC integrated circuits may also be applicable but will provide less customisability. Oven-controlled crystal oscillators are available with an accuracy of 0.1 to 0.0008 PPM (parts per million) and would be accurate enough as a frequency source [56], [57]. However, more accurate oscillators are

available and could also be considered. Several counters can be implemented to make a RTC. It will count the number of elapsed clock cycles after specific events, and activate one or more trigger output pins or reset one or more counters when certain criteria are fulfilled.

This RTC would then be configured to output trigger signals for triggering of sample acquisitions. Time information can also be provided directly from a register using a parallel output bus or using a serial transmission protocol. The timepulse output of a GPS receiver can be used to set the RTC. This timepulse can also be used to determine whether the frequency source has any drift in frequency to compensate for it. The NMEA data packet of a GPS receiver would provide the time the RTC is set to. A microcontroller can be used to process the packet first, and to communicate with the RTC.

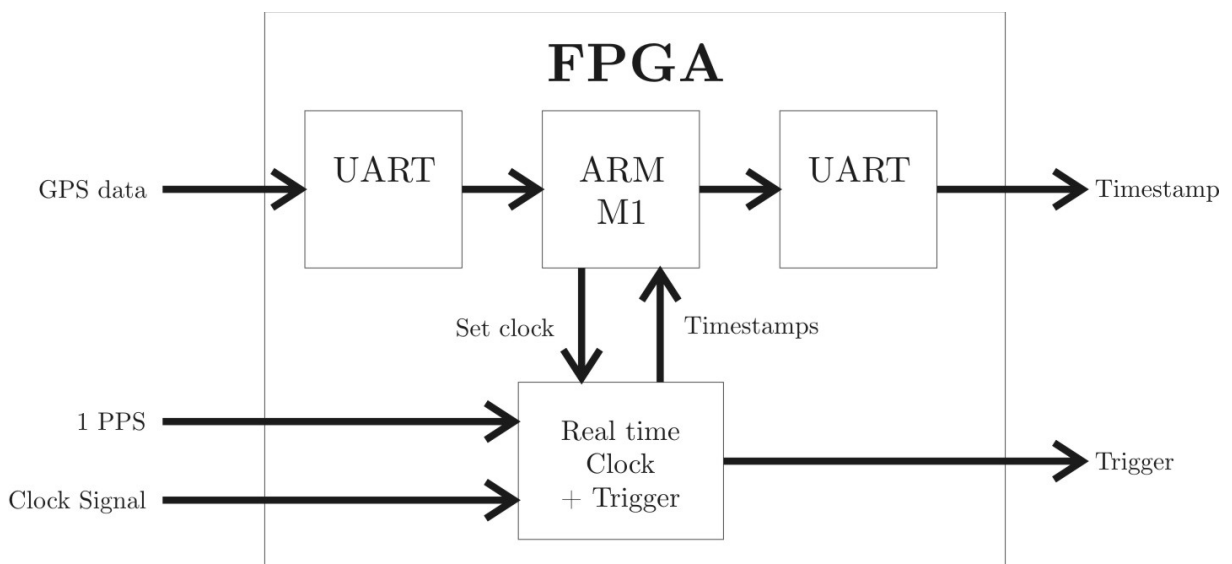


Figure 5.1: Block diagram of a possible FPGA implementation of a real-time clock.

5.1.3 Real-time Operating System

Real-time operating system (RTOS) can refer to the microcontroller firmware required for the configuration in Section 5.1.2. RTOSs which can be used with a personal computer (PC) do exist, and are designed to handle interrupts within specific time constraints. Design principles for RTOS applications are applicable to microcontrollers and PCs, and also include the application's functions. Therefore an implementation can be made where a PC is used to trigger sample acquisitions and keep an accurate clock. Industry standards are available for testing code in applications where reliability is critical, such as aircraft. When looking at how critical interrupts are, they can be classified as the following:

Specification	Value	Units
Configurable frequency range	$\frac{1}{60}$ to 10×10^6	Hertz
Frequency stability	62	Parts per trillion
Root mean square (RMS) timing accuracy	30	Nanoseconds
99% Timing accuracy	less than 60	Nanoseconds

Table 5.2: Timepulse specifications of LEA-6T [12], [21].

\$GPRMC	Position and time
\$GPGGA	Data about current fix
\$GPGLL	Position
\$GPGSA	Active satellites
\$GPZDA	UTC date and time

Table 5.3: NMEA sentence codes for the LEA-6T GPS receiver [22].

- Hard interrupt: catastrophic failure if not serviced in time.
- Soft interrupt: results become less useful if not serviced in time and may degrade performance.

Worst-case RTOS response time is difficult to determine, but some references quote as low as 1.3 microseconds on a 300 MHz processor [58]. Much faster processors are available, which could theoretically have faster response times. Thus, in theory, a RTOS could be considered for this level of precision timing. RTLinux is an open source RTOS, and the NI-DAQmx drivers are also available for Linux. However, operating and designing software requires lower level programming languages and is more complex than the configuration used in this project. An accurate oscillator or hardware clock would still be required and must be able to trigger interrupts on the PC.

5.1.4 u-blox LEA-6T Timing GPS

For this project, a u-blox LEA-6T timing GPS was provided beforehand. This GPS unit has two timepulse outputs, which are configurable with custom frequencies. The timepulse outputs can be synchronised with UTC time, and offsets can be added to correct signal delays with nanosecond accuracy. This makes it possible to do accurate triggering of sample acquisitions and also simultaneously sample a 1 Hz timepulse as a marker pulse together with the analog outputs. This marker pulse is used to indicate where in the data the beginning of each second is. It is possible to calculate an accurate timestamp for each sample using the marker pulse, the NMEA packet provided by the timing GPS for each second, and software interrupts provided by the GPS and data acquisition unit.

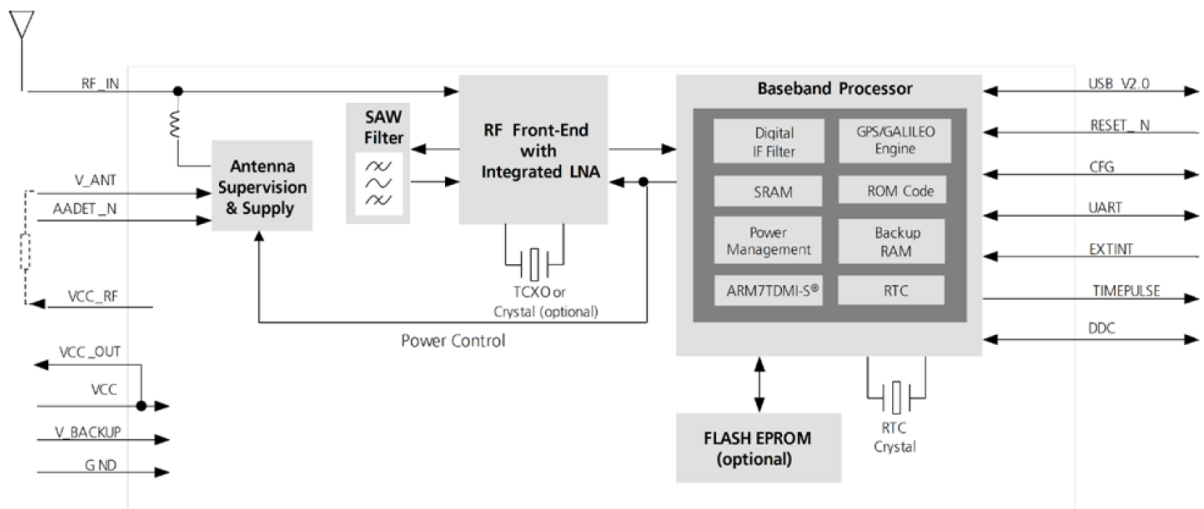


Figure 5.2: Block diagram of the u-blox LEA-6T GPS receiver [12, 7].

An example of the data transmitted by the LEA-6T is shown below.

```
$GPRMC,213939.000,V,3355.8968,S,01852.2915,E,0.33,,121011,,N*7A
$GPGGA,213939.000,3355.8968,S,01852.2915,E,0,05,3.4,127.4,M,31.3,M,,0000*4E
$GPGSA,M,1,19,11,08,28,26,,,,,,4.6,3.4,3.0*34
$GPGLL,3355.8968,S,01852.2915,E,213939.000,V,N*51
$GPZDA,213939.000,12,10,2011,,*55
```

5.2 Signal conditioning filter

When a signal is recorded with an analog to digital converter, it is necessary to ensure that there are no frequency components at a higher frequency than the Nyquist frequency (half the frequency) of the sample rate used. If not, it may cause image frequencies (also called aliasing). The image frequency will appear as a frequency lower than the Nyquist frequency, which is undesired as it does not represent what is happening in the physical analog signal accurately. This effect is demonstrated in Figure 5.3.

To prevent image frequencies, it is necessary to filter the signal with a low pass filter, which can eliminate the high frequency components. There are several types of low pass filters to consider, each with different attenuation and time delay (phase shift) characteristics. The time delay characteristics are frequency dependent, and causes a delay on each frequency component which is not necessarily a constant amount of time. This will have an effect on the time stamping of the recorded data, because this delay has to be accounted for to ensure that the time stamps on the data actually corresponds with the sensor output at that specific time.

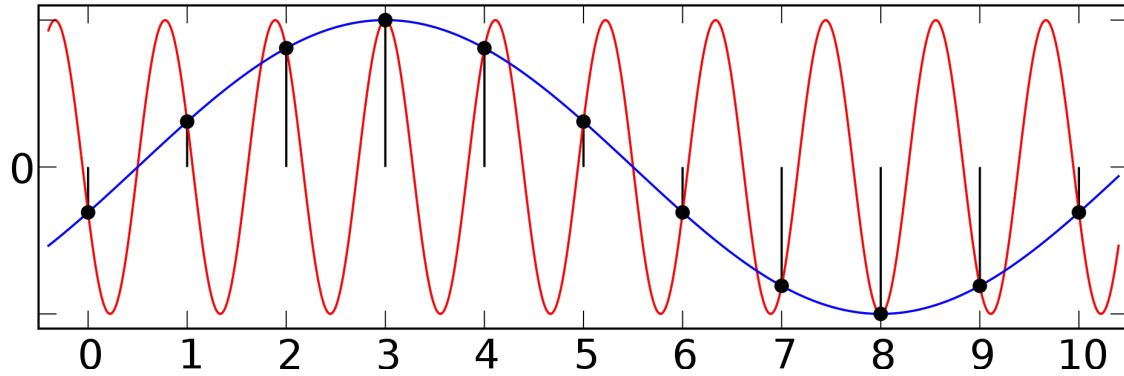


Figure 5.3: An illustration of aliasing, or an image frequency, in recorded samples when sampling a signal at a rate slower than the Nyquist frequency. The dots represent the sample acquisition points, and the long wave is reconstructed from it even though a much shorter wave was present. [13]

There are several popular filter types in use today, and several types are optimised for different characteristics. Butterworth filters are optimised for constant gain in passband, and Chebyshev filters are optimised for maximum slope at the cut-off frequency [14]. In this application a filter which is optimised for a maximally constant time delay over all frequencies in the passband is desired. This characteristic is also called a constant group delay. A Bessel-Thompson filter approximates this closely in the passband. This minimises the distortion of the original signal, which is compared with other Butterworth and Chebyshev filters in Figure 5.6. For the low frequency design required for the low pass filter in this application, the amount of distortion and the amount of time delay caused on the signal becomes relevant to respectively ensure measurement and timing accuracy.

5.2.1 Theoretical calculations

The transfer function of a third order filter is given by the following equation: [14]

$$H(s) = \frac{b_0}{s^3 + b_2s^2 + b_1s + b_0}$$

The coefficients b_0 , b_1 , and b_2 are determined by the cut-off frequency and, in this case, the Bessel function. For other filter types the function necessary for the required filter type is used instead of the Bessel function. The component values of C_1 , C_2 , C_3 , R_1 , R_2 , and R_3 of the filter circuit are then solved from the coefficients.

5.2.2 Active filter

In this application it is also required not to attenuate the signal by the filter, to prevent loss of DAQ sensitivity. Active filters which utilise operational amplifiers can achieve no loss of signal amplitude in the passband, where passive filters can not always achieve this.

A third order active Bessel-Thompson low pass filter with cut-off frequency at 50 Hz was designed and built for this application. For reliability and uniform frequency transfer characteristics, ceramic capacitors were used. The circuit diagram is given in Figure 5.7. A bode plot of the filter's measured transfer function is given in Figure 5.8. The filter's delay is constant below 14 Hz at 5.3 ms.

The theoretical calculation of the component values for the filter design as given in Figure 5.7 is as follows: [14]

$$b_0 = \frac{1}{(C_1 C_2 C_3 \times R_1 R_2 R_3)}$$

$$b_1 = (C_3 R_3 + C_2(R_2 + R_3) + (C_2 R_1)) \times b_0$$

$$b_2 = (C_2 R_2 C_3 R_3 + C_2 C_3 R_1 R_3 + C_1 C_2 R_1 (R_2 + R_3)) \times b_0$$

5.2.3 Passive filter and issues thereof

A passive Bessel-Thompson filter as shown in Figure 5.9 has an advantage of not using active components such as an operational amplifier and external power supply or battery. Active components can affect the noise floor and also affect the reliability of the filter over the the span of several years. However, there are several disadvantages:

- The filter must be matched for input and output impedance. Very large components are required because of the high output impedance of the input source in this application.
- The very large inductance required is difficult to obtain or manufacture, and will also include a large resistance component due to number of windings required.
- Components are difficult to match between identical filters at such large values.
- Thermal variations will have an influence on filter characteristics, specifically signal delay.

ADC resolution	18 bits
Number of analog input channels	8 differential or 16 single
Maximum total sampling rate	500 Kilosamples per second
Timing resolution	50 ns
Maximum analog input range	-10 V to 10 V
Input sensitivity at 10V to -10V scale	28 microvolts
Noise uncertainty	21 microvolts
Random noise (sigma)	60 microvolts RMS
Digital input minimum high voltage	2.2 Volts
Digital input maximum low voltage	0.8 Volts
External triggering	Yes

Table 5.4: Specifications of NI USB-6281 Data Acquisition Unit [23].

5.3 Data Acquisition Unit

In the aforementioned earlier project a National Instruments Data Acquisition Unit (NI-DAQ) was implemented into the system. National Instruments is a well-established provider of data acquisition units together with support for operation and data analysis, which is advantageous for future expansion of the system. The specifications for the USB-6281 data acquisition unit (DAQ) is given in Table 5.4. It is to some extent over-specified for this project, but it is the smallest model available with differential channels, simultaneous sampling and external triggering.

NI-DAQmx is a set of drivers and development tools for the Microsoft .NET environments and was used to develop the data acquisition software discussed in 5.4. LabVIEW is a software package developed by National Instruments for their range of products, including their data acquisition units [23] which enables a variety of measurements, but was not used due to cost sensitivity. Both of these software packages are to some extent independent of the NI-DAQ model used, as long as the same capabilities are present on either DAQs used [59]. More sensitive SQUID magnetometers may require a DAQ with better accuracy, which could enable a simple swap out upgrade.

5.4 Software

The NI-DAQmx API has been used to create software to control the DAQ, receive the measured samples from the SQUID outputs and to do the timestamping thereof. This software also record the data to a local hard drive and send it to a remote web server for storage, processing and viewing. The remote web server is described in chapter 6.

5.4.1 Principle behind GPS time stamping with software

Using multiple threads, interrupts and the position of the 1PPS pulse of a GPS receiver in the simultaneously measured samples, it is possible to timestamp samples accurately from just the NMEA packet received from the GPS. The accuracy would depend on the sample clock. In this case, the sample clock could be provided by the GPS using its second timepulse output. Since both timepulse outputs can be synchronised with UTC time very accurately, the timestamp accuracy is very precise. Avoiding a separate real-time clock removes timing latencies it may introduce, which makes this method very attractive. This principle is illustrated in Figure 5.10.

5.4.2 Functions of data capture software

A screenshot of the data capture software is shown in Figure 5.11.

A UTC synchronised 1 pulse per second signal, referred to as Marker Pulse in Figure 5.11, is sampled along with the SQUID outputs to indicate where the beginning of the second was during the samples received. Samples are delivered each second. The position of this pulse is determined as all the received data is entered into a table, along with the corresponding Pythagorean value.

The timestamp is initialised using the GPS packet received from the GPS unit. When the program starts operation, the GPS packet is always received at the beginning of the second, and the data at the end. It is possible to accurately timestamp all the data from just the first GPS packet received, but currently the timestamp is initialised from the GPS packet every second.

For debugging purposes, it is verified if the amount of samples received is equal to the sample rate. To date, it was always equal.

The data can optionally be recorded on hard drive, in comma separated value (CSV) format. A Last-In First-Out (LIFO) buffer initially stores the data, which is where data waits to be written to the local hard drive by a separate thread. Data is automatically organised into instrument ID, year and month folders from the GPS time. A mutex variable prevents more than one of these threads running simultaneously.

Another LIFO buffer is used to store data that has to be sent to the web server for online access. The dbadd.php web interface is used for this, which is discussed in Section 6.2. Another separate thread is used to transfer data, with a mutex variable to prevent more than one of these threads running simultaneously. Data can only be removed from this LIFO buffer if the web server returns a matching hash key.

5.4.3 Automatic reset of SQUID magnetometers

During daily operation, the geomagnetic field may vary beyond the capabilities of the SQUID magnetometers. Only a limited magnitude of change in the present magnetic field ($\Delta\Phi$) can be measured. When the offset becomes too large, the output of the PFL-100 flux locked loop saturates and does not measure further magnetic field offset. To resume measurements, the saturated SQUID magnetometer can be reset. The output of that SQUID will then revert to 0 V.

Automatic reset of the SQUID magnetometers is useful since To enable long term stability, it was necessary to implement an automatic reset function. The DAQ used in this project has TTL digital outputs available which can be used with the external reset input of the PCI-1000 SQUID controller. By monitoring upper and lower limits, a reset can be triggered from the software. Manual reset of the SQUID magnetometers may require continuous monitoring, otherwise interruptions in measurements may occur.

If necessary, the software can add the offset which was present before the reset back automatically. The offset can also be added manually, using the user interface of the software not visible in Figure 5.11.

5.5 Mitigating implementation issues

5.5.1 Memory overflows in software

Loss of internet connection

A memory buffer was implemented to keep any data if the transfer was not possible for a period of time. Initially, this was effective, but there has been longer than expected connection problems. This caused the buffer to become too large and the operating system started paging the buffer to the hard drive. This caused too much demand on the computer and it could not react to the interrupts from the data acquisition unit quickly enough. The buffer was replaced with a hard drive backup, which could then be read back and sent to the server if needed.

Memory leaks in local graphing implementation

Four graphs were also implemented to visualise the data as it was received from the data acquisition unit. Averaging was implemented to help reduce data, so that a few hours of data can be viewed without requiring a large amount of memory. However, the graphs

also had an issue with memory overflow. The .NET implementation of graphs that were used in the software did not clear the memory it used when data was removed from it, and it suspected to be a bug with the .NET implementation itself. To ensure stability of the software, the graphs were first removed until they could be implemented without causing memory problems.

5.5.2 False trigger

It was found that sample acquisitions were triggered by an unknown source during the operation of the data acquisition unit. This only affected the accuracy of timestamps during the second where the extra sample was acquired. It is suspected that interference of unknown origin on the cable of the sample clock may be the cause. The input impedance of the trigger input used on the data acquisition unit is $10\text{ M}\Omega$, and capacitive interference was suspected. To alleviate this, the leads of the cable was twisted tightly to attempt to cancel some interference, and a resistor to ground was added at the trigger input to lower the input impedance .

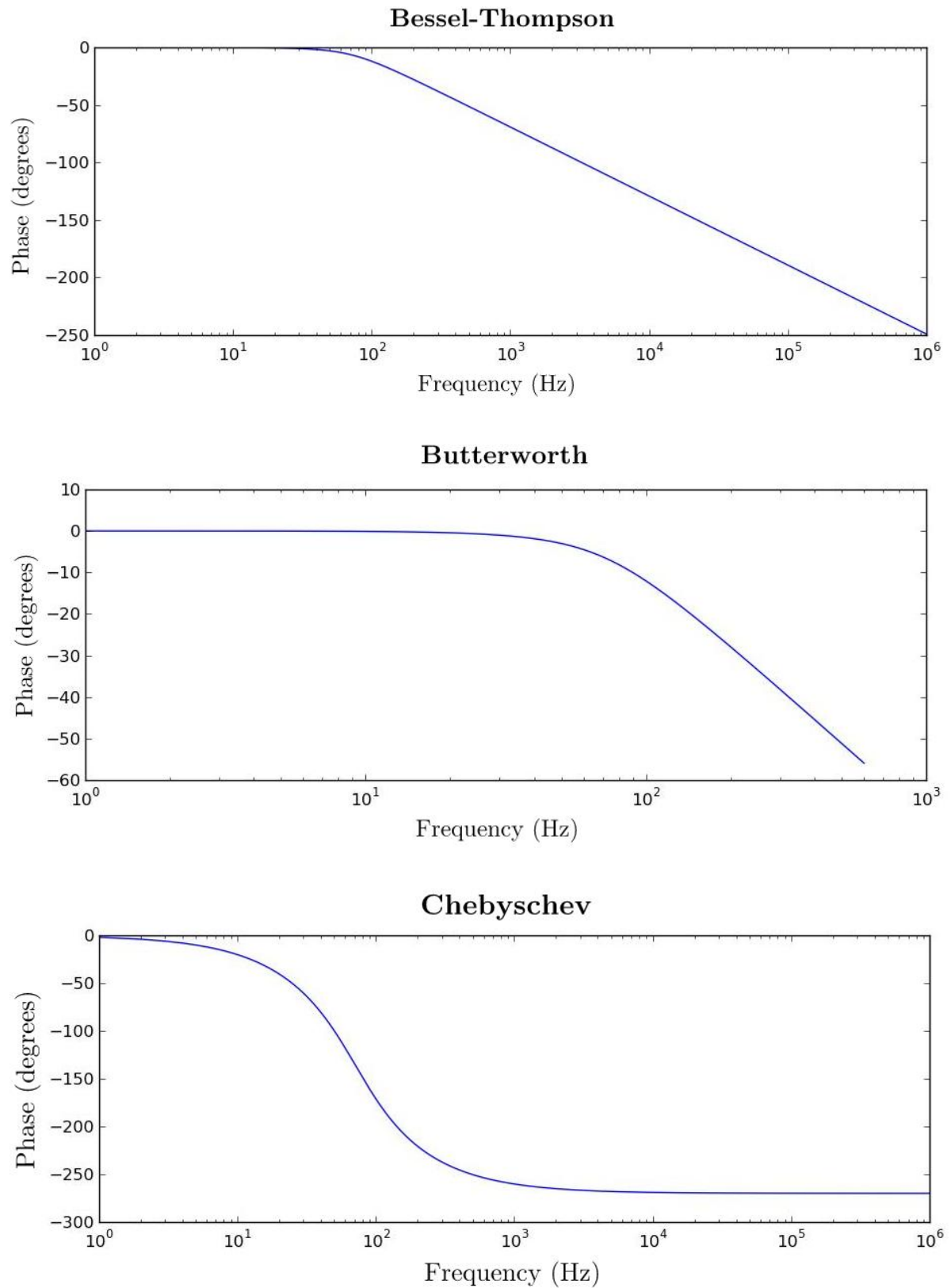


Figure 5.4: Respective phase shift versus frequency graphs of third order Bessel-Thompson, Butterworth and Chebyshev low pass filters with cut-off frequency at 50 Hz.

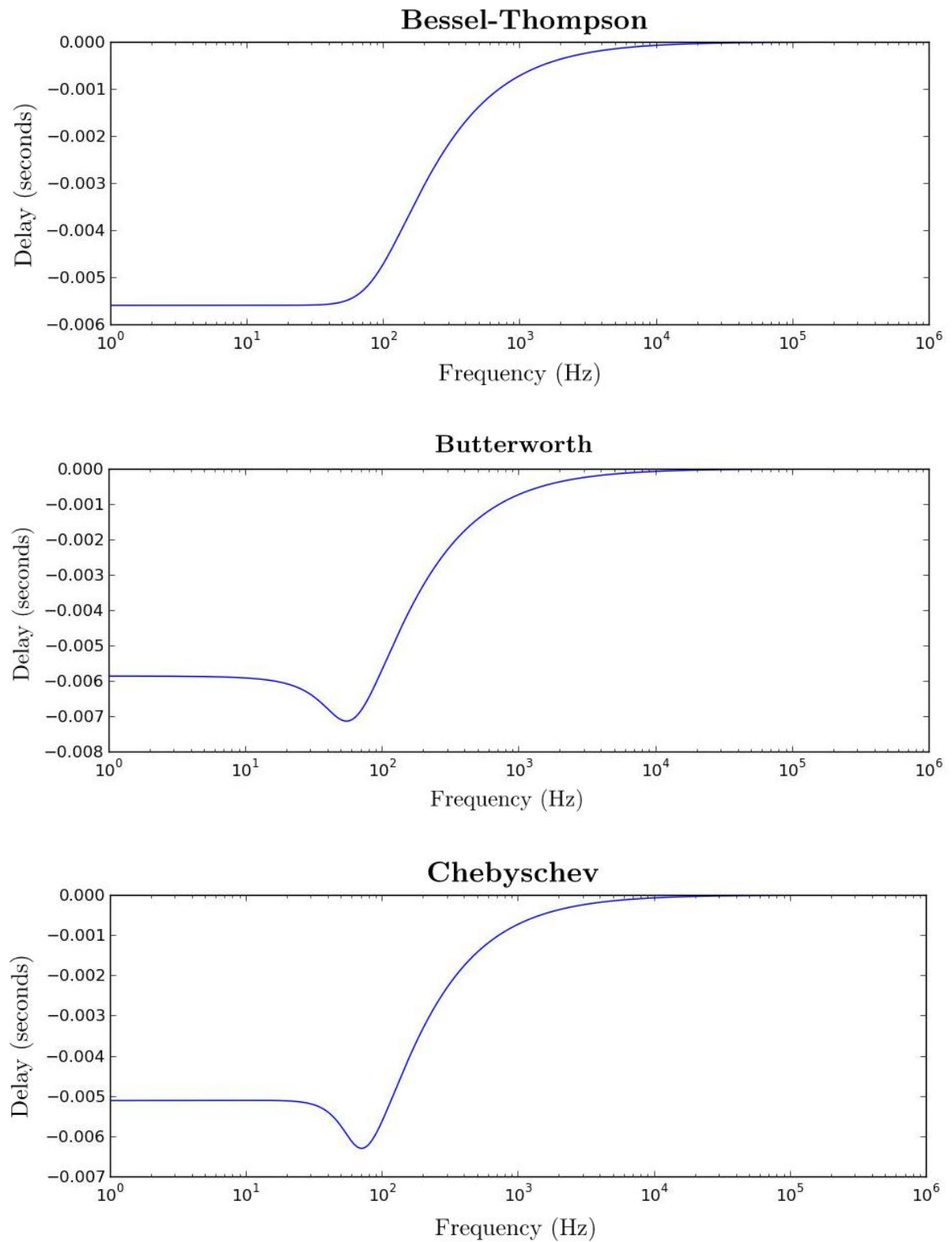


Figure 5.5: Respective delay versus frequency graphs of third order Bessel-Thompson, Butterworth and Chebyshev low pass filters with cut-off frequency at 50 Hz.

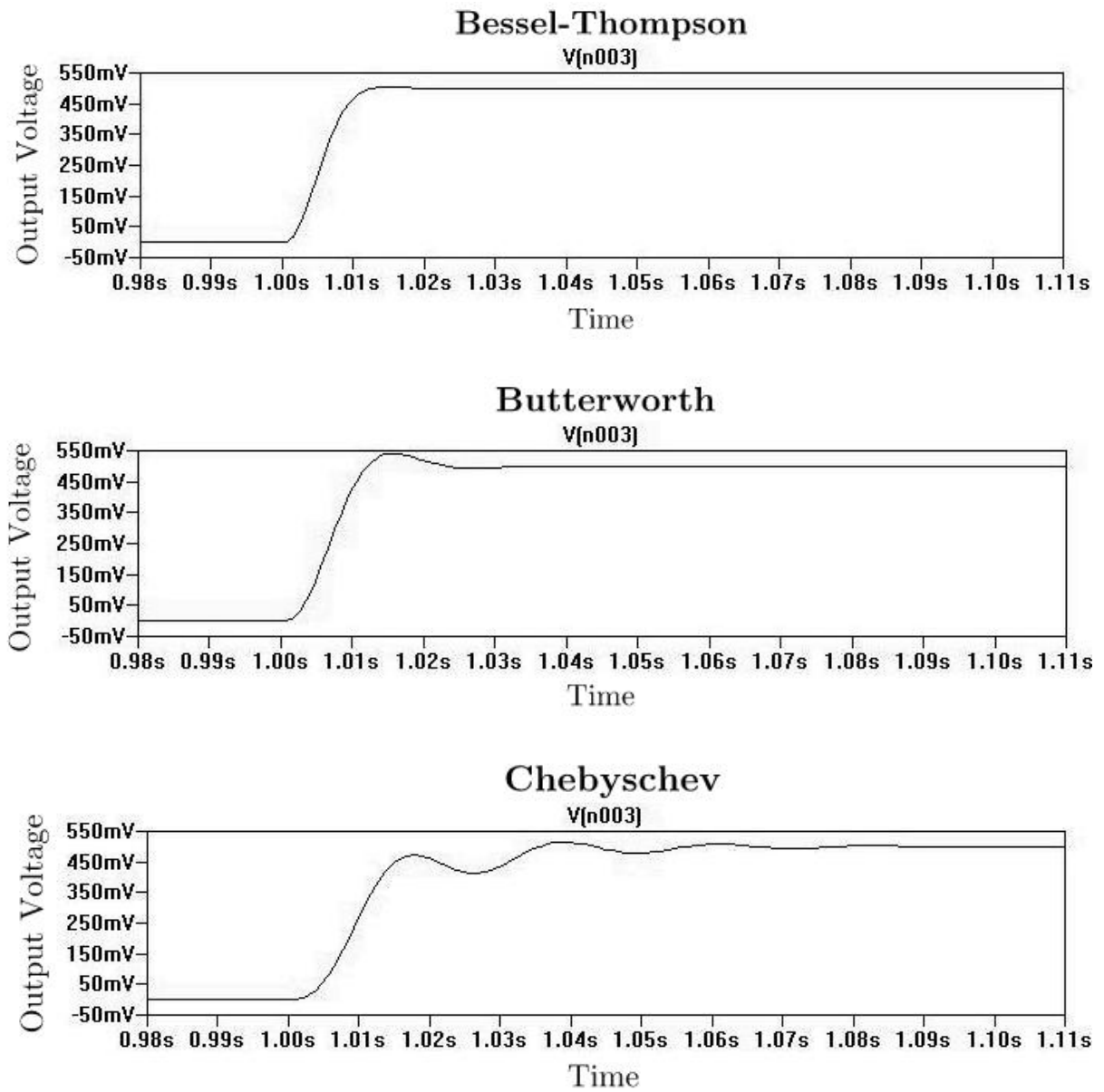


Figure 5.6: Respective step responses of third order Bessel-Thompson, Butterworth and Chebyshev low pass filters with cut-off frequency at 50 Hz.

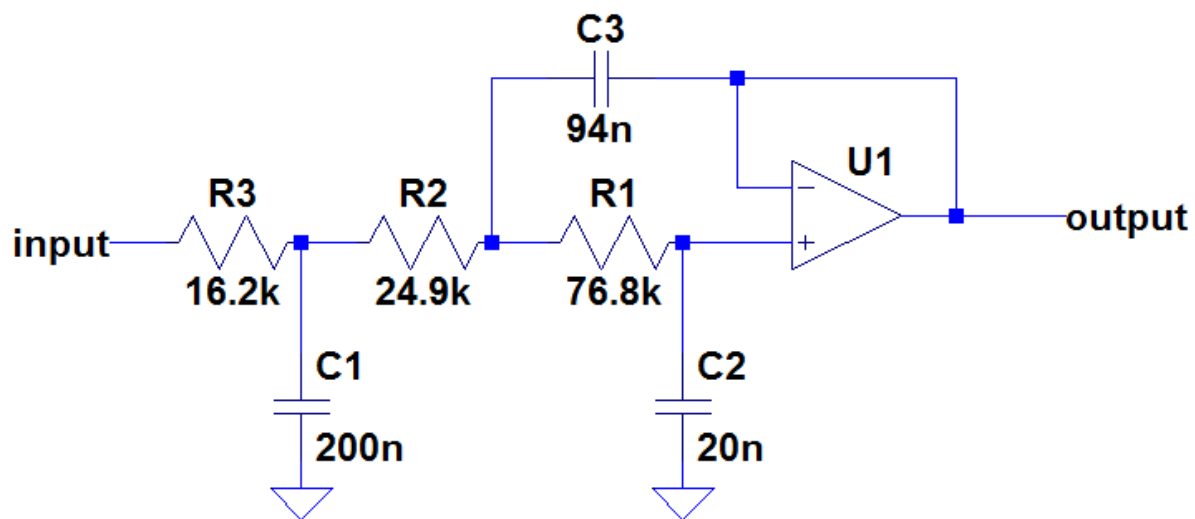


Figure 5.7: Circuit diagram of an active third order Bessel-Thompson low pass filter. [14]

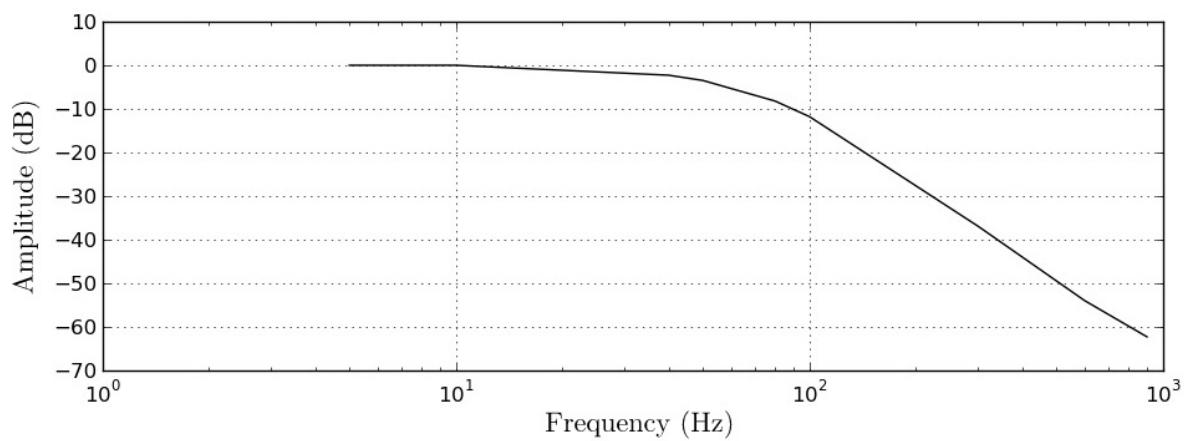


Figure 5.8: Measured attenuation characteristics of the filter constructed.

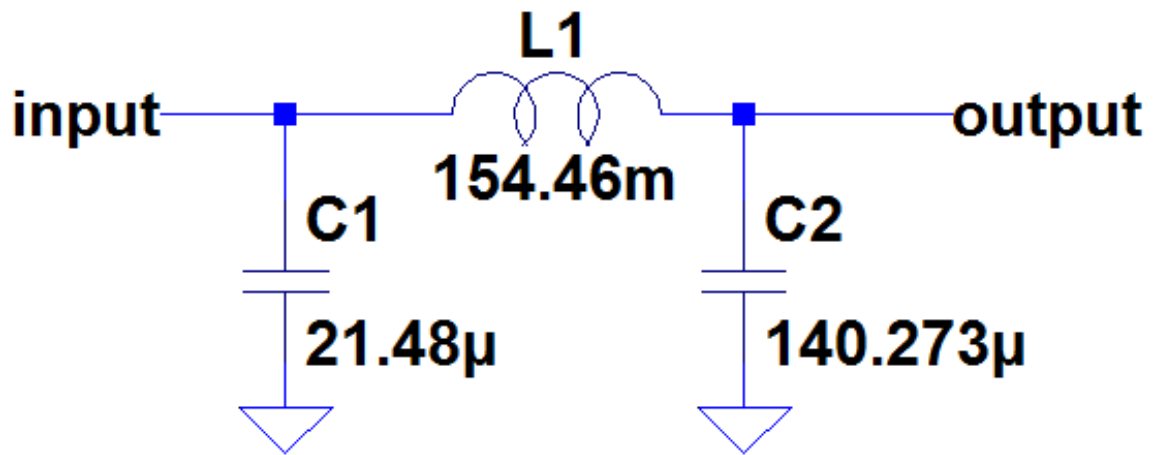


Figure 5.9: Circuit diagram for a passive third order Bessel-Thompson low pass filter [15].

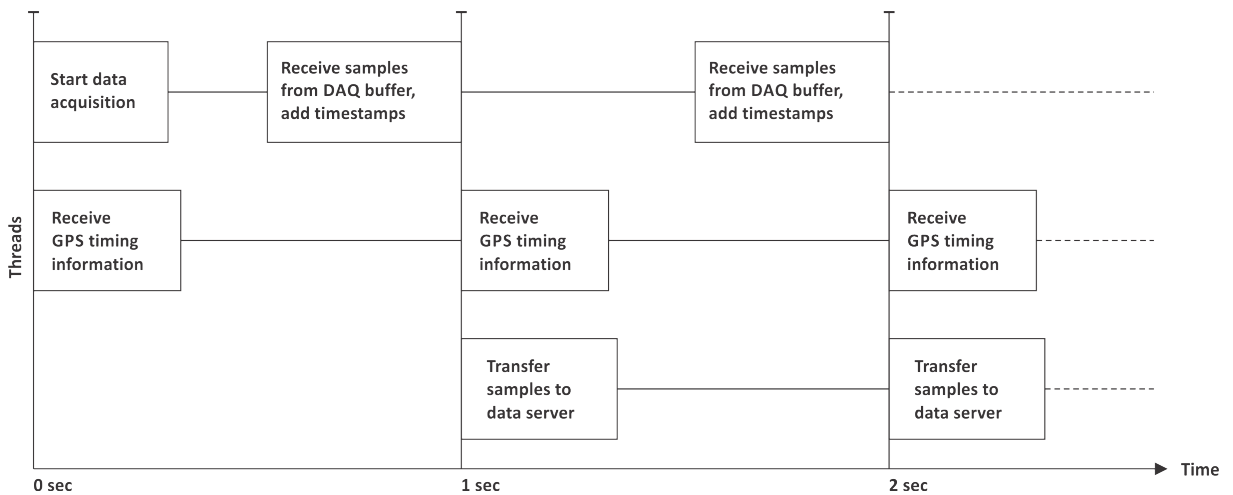


Figure 5.10: Diagram of the threads in the software with the order in which they are triggered.

The screenshot displays the user interface of a data capture software. It is divided into several sections:

- Acquisition Results:** A table showing data points with columns for X, Y, Z, filtered Dev, Z filtered Dev, Bedrag, and Marker Dev. The table contains 20 rows of numerical data.
- Additional Information:** A section with various status indicators and settings, including 'uart_count_max' (285), 'last timestamp' (144155), and 'Current UTC time' (2014-11-30).
- X Channel Parameters:** Settings for the X channel, including 'Physical Channel' (Dev1/a10), 'Minimum Value (V)' (-10.00), and 'Maximum Value (V)' (10.00).
- Y Channel Parameters:** Settings for the Y channel, including 'Physical Channel' (Dev1/a11), 'Minimum Value (V)' (-10.00), and 'Maximum Value (V)' (10.00).
- Z Channel Parameters:** Settings for the Z channel, including 'Physical Channel' (Dev1/a12), 'Minimum Value (V)' (-10.00), and 'Maximum Value (V)' (10.00).
- Automatic Reset:** A section with 'Reset X', 'Reset Y', and 'Reset Z' buttons, and various offset and scaling parameters.
- GPS Packet Data:** A section displaying GPS coordinates and other data, such as 'COM Port: COM10', 'Baud rate: 921600', and 'Disconnect' button.
- Success, duration = 2.6772220134735 Hash 1: 96572f205440b5742af668877 Hash server: 96572f205440b5742af668877**

Figure 5.11: User interface of the data capture software.

Chapter 6

Implementation of a robust data-storage and post-processing system

A very large amount of data is generated by this project compared to other geomagnetometers. This is due to a much higher sample rate involved. To store the data, an Ubuntu Linux Server with a MySQL database was implemented. MySQL is a free database which can store large amounts of data efficiently and with fast access times. The phpMyAdmin package was used to set up the database. phpMyAdmin also provides a web server and a web interface to manage the database and access data.

6.1 MySQL implementation for data storage

A MySQL table was set up with variables listed in Table 6.1, to store the data using the InnoDB engine. Minimal datatypes were chosen for the variables, in order to minimise the storage space required. The table was designed to record samples of three channels on the data acquisition unit, with an extra entry to calculate the total magnetic field from the three axis. However, during the majority of this project, only two SQUID magnetometers were in use.

Original estimates for the size of recorded data is listed in Tables 6.2 and 6.3 . Expanding the MySQL table and web interface to support up to six channels is possible with the current data recording software, and size estimates thereof are displayed in Table 6.4.

Field	Size (bytes)	Type	Range
ID	4	INT	0 to 4294967295
timestamp	4	TIMESTAMP	1970-01-01 00:00:01 to 2038-01-19 03:14:07
usec	3	MEDIUMINT	0 to 8388607
x	4	FLOAT	$\pm 3.40823466E+38$ to $\pm 1.175494351E-38$, 0
y	4	FLOAT	$\pm 3.40823466E+38$ to $\pm 1.175494351E-38$, 0
z	4	FLOAT	$\pm 3.40823466E+38$ to $\pm 1.175494351E-38$, 0
total	4	FLOAT	$\pm 3.40823466E+38$ to $\pm 1.175494351E-38$, 0
info	1 + length	TINYTEXT	ASCII characters, length 32 characters

Table 6.1: Set of fields used for each record in the database [24], [25], [26], [27]

Time period	Amount of entries	Approximate size
Per sample	1	28 bytes
Per second	125	3500 bytes
Per minute	7 500	205.1 Kilobytes
Per hour	450 000	12.02 Megabytes
Per day	10 800 000	288.39 Megabytes
Per month	324 000 000	8.4490 Gigabytes
Per year	3 942 000 000	102.80 Gigabytes

Table 6.2: Number of three-channel measurement entries into database and their associated sizes over different time periods, for a sample rate of 125 Hz is used.

Time period	Amount of entries	Approximate size
Per sample	1	28 bytes
Per second	1 000	28 000 bytes
Per minute	60 000	1.602 Megabytes
Per hour	450 000	96.13 Megabytes
Per day	10 800 000	2.253 Gigabytes
Per month	324 000 000	67.592 Gigabytes
Per year	3 942 000 000	822.37 Gigabytes

Table 6.3: Number of three-channel measurement entries into database and their associated sizes over different time periods, for a sample rate of 1 000 Hz.

Time period	Amount of entries	Approximate size
Per sample	1	40 bytes
Per second	125	5 000 bytes
Per minute	7 500	292.97 Kilobytes
Per hour	450 000	17.17 Megabytes
Per day	10 800 000	411.99 Megabytes
Per month	324 000 000	12.070 Gigabytes
Per year	3 942 000 000	146.85 Gigabytes

Table 6.4: Number of six-channel measurement entries into database and their associated sizes over different time periods, for a sample rate 125 Hz.

Notes on the chosen variables: [24], [25], [26]

- MySQL does not have fields available to store a date and time with microsecond accuracy. For this reason, a separate field, `usec`, is used to store the microsecond value of a timestamp.
- The ID field will be used for indexing as an auto-increment field and will limit the maximum amount of entries into the table. This will give the table a capacity for measurements of about 456 days (or 1.249 years), then the variable will overflow.
- A field of type FLOAT is precise to 24 digits, which is adequate for the range of values that will be handled with in this project.

6.2 Web interface for transferring data

Web interfaces were made to insert data into the database and to retrieve it. These were implemented as PHP pages on the web server provided with phpMyAdmin. Only HTTP internet access is used with this interfaces, which simplifies the design and does not require extra access through typical firewalls. Several firewalls are involved in the SANSa SQUID system.

Two PHP websites were created to provide the interfaces for inserting and retrieving data. These were named `dbadd.php` and `dbread.php`, and HTTP POST parameters about the data are to be provided when using them. `dbadd.php` and `dbread.php` are discussed in Section 6.2.1 and Section 6.2.2 respectively.

6.2.1 dbadd.php

The design of this website was kept simple, to increase reliability and speed. Data is received through an HTTP POST request. The algorithm used in this website then executes the following steps:

- Connect to the database.
- Verify that hash key of the data received matches the hash key from the sender (see Section 6.6.3).
- Add the data to the database.
- Add latest minute-average and second-average data.
- Close the connection to the database.
- Reply with a message which indicates if the data was added successfully to the database or not.

Up to 4000 samples can be received per request. An example of the string sent with the HTTP POST request is as follows,

```
timestamp#=2014-01-01 00:12:34&usec#=8000&x#=1.234&y#=5.678901  
&z#=0.1&total#=5.812286
```

where the # symbol is replaced with an integer number to identify the sample.

6.2.2 dbread.php

For this website it was also important to keep the design simple. This website can provide data in three different ways, as defined by an argument passed to the server when loading the website. The newest 500 entries in the database is given if no argument is passed to the server. Arguments that can be passed to the server can either request a specified amount of entries after a certain date and time, or request a specified amount of entries which falls after a certain record ID.

The data returned by this website is in comma separated value (CSV) format. It is advantageous to use CSV format, since it is easy to interpret by a user and also compatible with other software. An optional argument that can be passed to the server can specify if the timestamps of the data returned should be converted to Unix timestamps, as it might be easier to work with. An Unix timestamp represents the number of seconds that has

passed since the Unix epoch, 1970-01-01 00:00:00 [60]. It has the disadvantage that it is not easily read by humans, but it is easier to perform mathematical operations on a Unix timestamp.

An example of the data returned is as follows:

```
timestamp,usec,x,y,z,total,flag
2014-01-29 13:48:59.888,888000,-0.02103,-0.035695,0.014072,0.043754,5
```

6.3 Web interface for viewing data

The Highcharts API was used to implement a live graph. An example was expanded to be able to read data out of the database. For this a query to `dbread.php` was added with the necessary parameters. The data could then be used to plot a graph. A live and historic graphing website was implemented, where the main difference is that the live graph periodically updates its data with a timer. The historic graph may refer to second-average or minute-average data in order to reduce the amount of data that had to be transferred. A screenshot of this graph is shown in Figure 6.1.

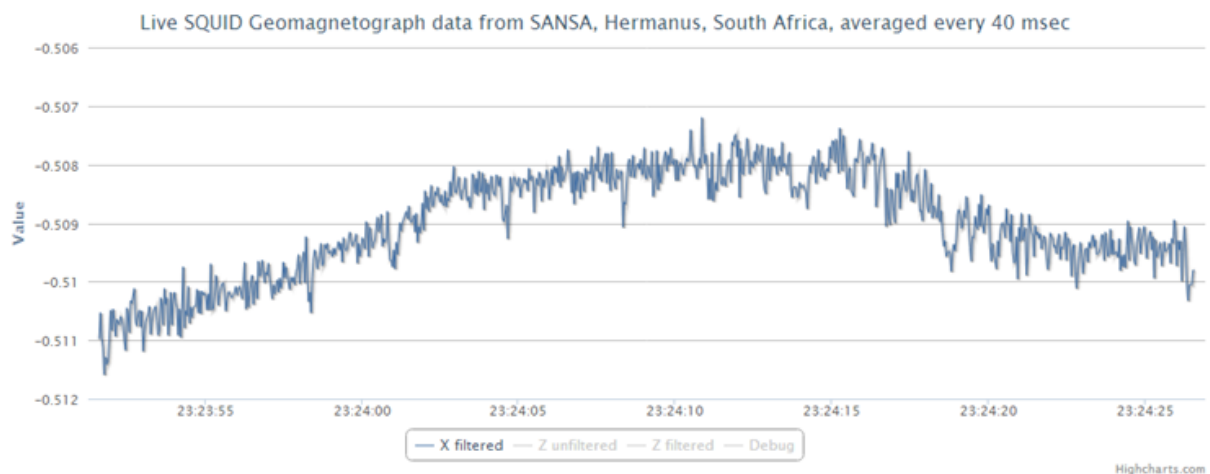


Figure 6.1: Screenshot of live graph implementation.

6.4 Preprocessing

Preprocessing the data will be advantageous for data analysis and viewing, as it can enable quick analysis of specific statistics over extended periods. If a specific parameter

is required, it could be searched for in preprocessed data rather than downloading geomagnetic data and processing it locally. For example, averaged data can be used to plot data of extended periods. Preprocessed data can be used to identify signatures of certain phenomena in the geomagnetic field. Certain phenomena can be identified by looking at variations with specific periods, so band pass filtered data and Discrete Fourier Transforms can be made specifically for those and is discussed in sections 6.4.3 and 6.4.2. Automated analysis and report making is also possible during or after preprocessing.

6.4.1 Averaging to reduce data (Downsampling)

Averaging data is useful for several reasons:

- It reduces the number of samples required to plot a graph of the data recorded over an extended period. This is useful to reduce the bandwidth required to send data of an extended period.
- Noise can be reduced by averaging, which is useful for visualising faint, slow variations.
- Sometimes high frequency variations is undesired or not required. High frequency variations can be removed by averaging.

6.4.2 Discrete Fourier Transforms (DFTs)

Using a Fourier transform is an easy way to determine which sinusoidal periodic signals are present in the measured data. Efficient algorithms are available to produce discrete Fourier transforms, and it can quickly process large amounts of data. Having pre-made discrete Fourier transforms can reduce the time required to analyse data, and can help to avoid transferring a large amount of data. Automated analysis can also be implemented on discrete Fourier transforms.

Adapting resolution

The discrete Fourier transform gives data in a fixed frequency interval. It is typically more desired to have a better frequency resolution at low frequencies. A more accurate frequency resolution helps to determine the period of the specific variation more accurately and also enables more individual sinusoidal variations to be distinguished. However, the amount of data required for a more accurate frequency resolution increases with the accuracy. This can cause a single discrete Fourier transform to require a large amount

of storage space. The data can be reduced by decreasing the frequency resolution as frequency increases, since less accuracy is required with higher frequency.

When adapting resolution of a discrete Fourier transform, it is often desirable to maintain the correct amplitudes for the frequencies calculated. Averaging the data will affect the calculated amplitudes, so it may be desirable only to use the maximum value measured in a range of frequencies when adapting the resolution. The accuracy required at higher frequencies must also be considered.

6.4.3 Band pass filtered data

To identify specific phenomena in geomagnetic variations, it is useful to determine whether any signal variations are present in a specified frequency range. This data can be obtained by preprocessing recorded signals with a band-pass filter.

6.5 Data integrity

To ensure that there are no errors introduced in the data while transmitting it over the internet, it is necessary to check that it is still intact. It is also necessary to check the continuity of the recorded data to ensure that the data acquisition is done correctly. Any erratic values or missing data points may appear as false disturbances, and could also make the results of a Discrete Fourier Transform invalid. Several methods can be used to do this, each with some disadvantages. The size of the dataset requires careful consideration of these disadvantages.

6.5.1 Sample by sample

The easiest method to find discontinuities in a dataset is to check if the timestamp of each data point follows on the previous data point. Since the sample rate is constant, there should be a constant offset in time between each data point. This can be verified easily, however checking each sample on a dataset is not practical when the dataset becomes very large. It is still practical if verification is done when data is received at the server. If it is found that there are data points missing, it must be logged separately. A separate marker flag with each data point will cause a large increase in the size of the dataset.

6.5.2 Verifying number of samples in dataset

A faster method of verifying continuity is to calculate what the end time of a number of samples with a specific start time and constant sample rate should be, and then verifying it. If there is one or more data points extra or missing, the end time will differ.

Finding the specific position where a missing or extra data point is could be difficult. However, with this method it is possible to modify a search algorithm to find the last valid end time in a dataset. The best search method for this is binary search, which is also one of the fastest available. Using this method, it is practical to verify the continuity of all the data available before using it.

Binary search

Binary search is also known as the half-interval search algorithm. It requires that the dataset is sorted, and also that it is in an array-addressable format. There are more than one method to execute a binary search, but for the purpose of this modification an iterative method is used, and the increment is adapted.

The algorithm is as follows: it starts at the position in the middle of the dataset, and increases / decreases the position to seek an item in the dataset. The increment by which the position will be increased / decreased by is initially set at a quarter of the size of the dataset, rounded to the upper integer.

It then iterates the following:

- Check if the item searched for is larger or smaller than the item at the current position in the dataset:
 - If it is larger, increase the current position in the dataset by the aforementioned increment.
 - If it is smaller, decrease the current position in the dataset by the aforementioned increment.
 - If it is equal, the search has ended.
- Set the increment to half its current value, rounded to the upper integer.

When the increment is 1 and the algorithm wants to half it, it means that the search has failed. An example search is illustrated in Figure 6.2.

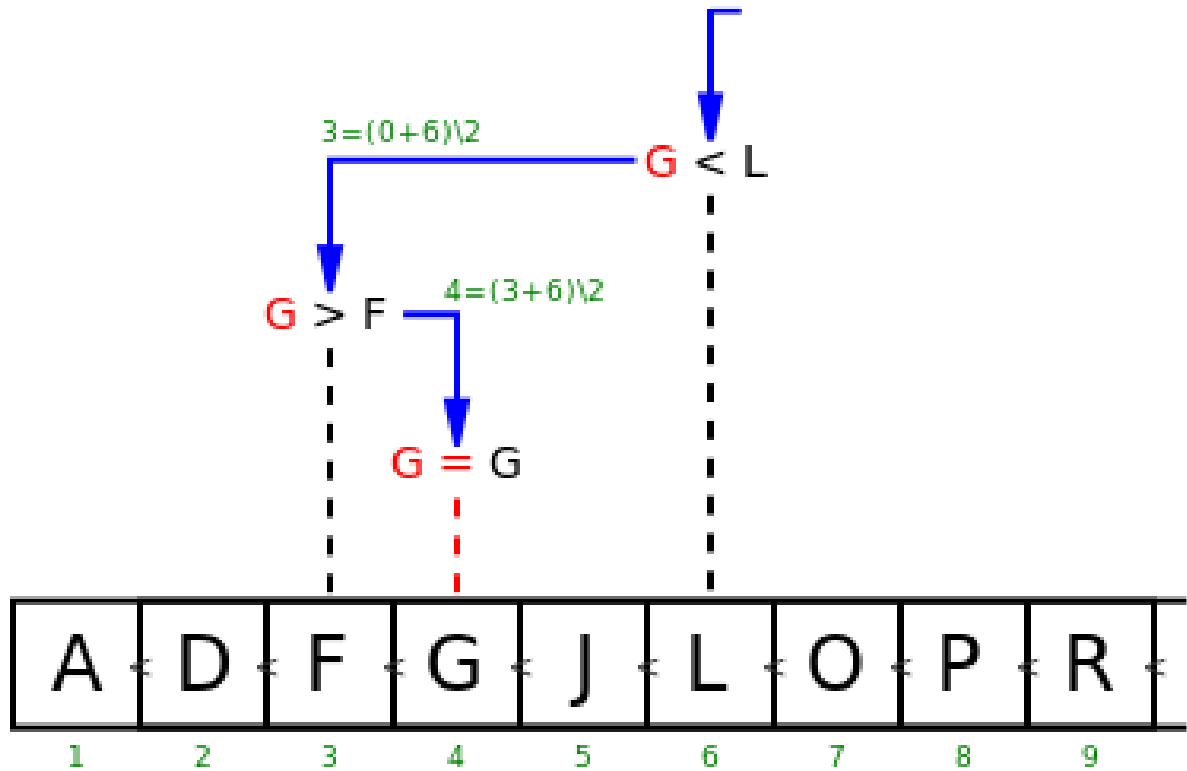


Figure 6.2: Illustration of a short binary search [16].

Adapting algorithm for finding discontinuities

To locate a discontinuity in a dataset, the binary search algorithm has to search for the point in the dataset where it stops having the correct number of samples instead of finding a specific item. Since each sample has a sequential ID number together with its timestamp, the dataset can be addressed as an array. The number of samples in a specific timespan can also be calculated by checking the ID numbers of the samples at the beginning and at the end of the timespan. To find a discontinuity, it is therefore also necessary to check if the next sample is at the correct time interval to maintain the sample rate of the dataset.

The decision step in the binary search algorithm is changed as follows:

- If the timestamp of the current item in the dataset corresponds with its position in the dataset, the discontinuity must be after the current item in the dataset.
- If the timestamp of the current item in the dataset does not correspond to its position in the dataset, the discontinuity must be before the current item in the dataset.

- If the current item is at the correct time interval and the next item is not, the search has ended.

For a dataset with 2 billion samples, the algorithm can find a discontinuity in 30 iterations, which can require up to 100 database read operations.

6.6 Reliability concerns

As mentioned earlier, the data acquisition and storage system has been developed in an earlier project and was implemented in this project. The implementation issues that arose as well as steps taken or recommendations to solve them are discussed in this section.

6.6.1 Hard drive wear

It was originally calculated that 3.942 billion timestamped three-axis samples will be recorded during a year of operation. At a sample rate of 125 Hz with uploads being performed each second, it translated to at least 31.536 million write operations by the hard drive each year. One of the hard drives used failed after about 15 million write operations. It is possible to configure the database in such a way that it would initially store data in memory and less frequently write to the hard drive. This should help to reduce server failures and hard drive wear.

Solid state drives have also become a financially viable option to store data, and do not have mechanical components that will wear out with repetitive accessing. This is also an option to increase reliability of the system.

6.6.2 Slow file systems

When installing Ubuntu Linux on the server, a choice can be made between several file systems that are available to use on the hard drives. Many of these are journalling file systems, which have a double write feature. To increase reliability, it first writes any changes made to a journal on a separate location on the hard drive, then to the location where it is intended to be. If, for some reason, there is an interruption during the write to the journal, it will leave the actual data that needed the change unchanged. If there is an interruption during the write to the actual data, it can be completed from the information that can be obtained in the journal. This reduces the chance for data corruption during power failures or other interruptions.

Journalling file systems are a default option with Ubuntu Linux at the moment, and has shown to take much more time to write a new entry into the database used. Any addition of data to the database took 1.3-1.8 s with the Ext4 file system. The Ext2 file system would take 0.1 s or less for such an operation. The slow entry rate would be acceptable if the database was only used for archiving, but to allow live viewing and preprocessing of data, it is necessary to use a faster file system.

As mentioned above, solid state drives have become financially viable and could also be considered if one of the aforementioned file systems is desired.

6.6.3 Incomplete data transmissions

Due to problematic internet connections, incomplete data is sometimes received by the server. This created a requirement to check if data is complete before accepting the transmission and storing the data. By doing this, the majority of data discontinuities can be avoided. The best way for this application to verify if the data is complete is to use a hashing algorithm.

Hashing

Hashing refers to using a scrambling operation performed on a set of data to create a hash key. This hash key is typically given as a hexadecimal number of specific length, which depends on the hashing algorithm used. The hash key of a specific set of data will always be the same, even if calculated on different computers. Hashing algorithms will produce hash keys that differ greatly if different datasets are used, even if there are only small differences in the datasets. Several different hashing algorithms are available, of which some have very fast and efficient implementations. The MD5 hashing algorithm was used for this implementation.

Implementing hashing to verify data transmissions

To resolve the problem of incomplete data transmissions, the transmission has been provided with a hash key of the transmitted data. The hash key is to be verified at the receiver by recalculating it from the data received. A message will then be sent back to the sender to indicate if the data was received correctly or not. If the hash key does not match the one received, a failure message is sent as a reply to have the data retransmitted.

Chapter 7

System Tests

7.1 Database size

A table with 10 800 000 records in the database would correspond with the amount of data recorded in a full day of operation. After some tests it was determined that the actual size required for the recorded data of a full day is 394 MB, which is higher than the 288.39 MB expected in Table 6.2. The storage required for one year's data at the aforementioned rate is about 140.8 GB. The reason for this is indexing. MySQL indexes data to make searching inside a table faster, which has proven to be of benefit for this project.

During 2013 and 2014, about 3.9 billion three-axis timestamped samples were recorded. The total size of this data has also been larger than expected. The database grew to about 290 GB, which is again larger than expected from the adapted prediction above. About 800 MB of storage is required per day.

It is suspected that the unexpected growth is due to the size of the database itself. Multiple databases can be created to alleviate this problem.

7.2 Spectrum comparison between ± 1 V and ± 10 V sampling

The range in which the data acquisition unit used in this project can measure voltage can be adjusted in several steps between ranges of ± 10 V to ± 0.1 V. 18 bits of resolution would still be possible in each of these ranges. To determine if this would improve the noise floor of the instrument, data was recorded for a period at the ± 10 V and ± 1 V

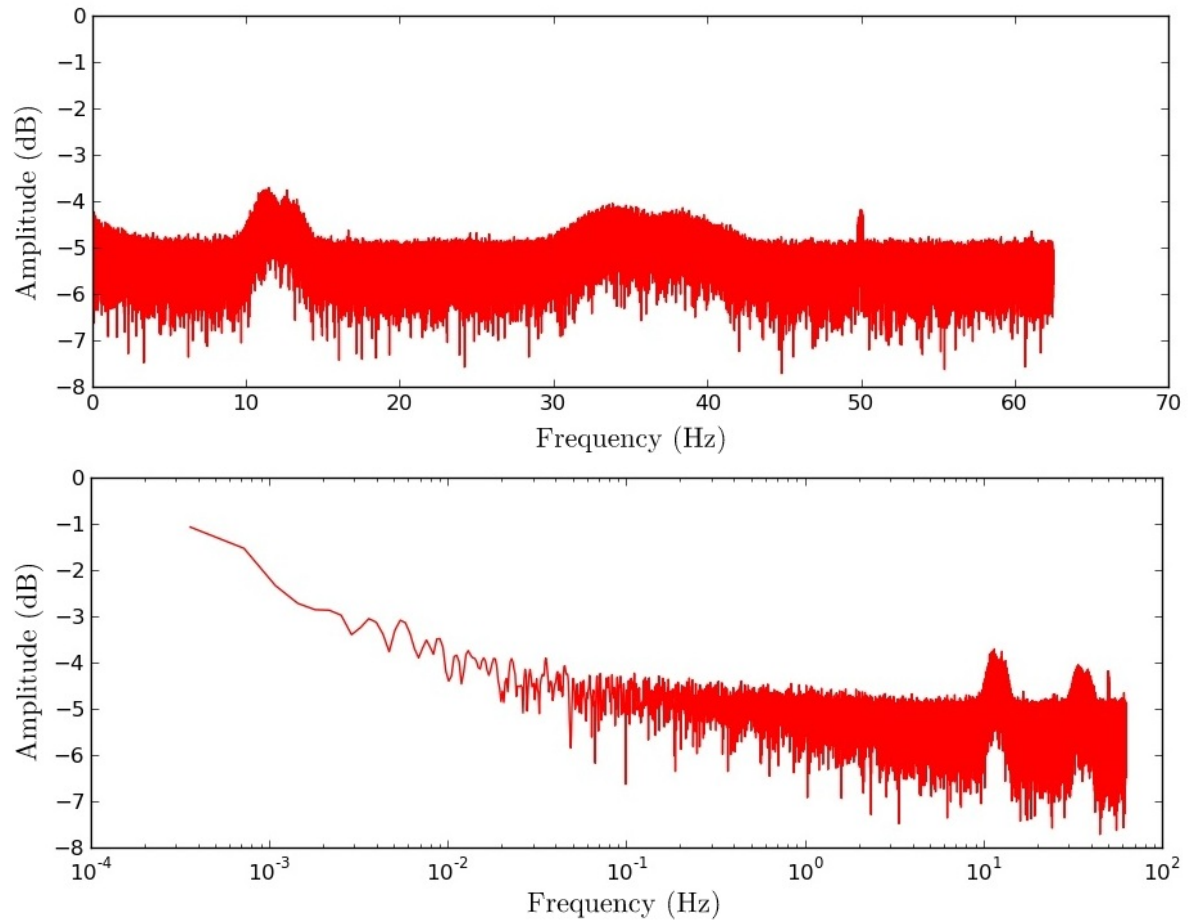


Figure 7.1: Spectrum of a 45 minute period of the X-axis SQUID at ± 1 V sampling, with linear (top) and logarithmic (bottom) frequency axes.

voltage ranges. Frequency spectra of each of these recordings are shown in Figures 7.1, 7.2, 7.3, and 7.4. It was noted that the noise floor is not notably affected by the voltage range used with the current configuration of the SQUID magnetometers.

7.3 Power Spectra

As part of taking all noise sources into account, it is necessary to check the noise levels of the data acquisition unit itself. These noise levels were measured by connecting the measurement pins of the data acquisition unit to its ground. Analysis can be done by either looking at the amplitude of the noise signal recorded, or by looking at the power spectrum of the recorded noise signal.

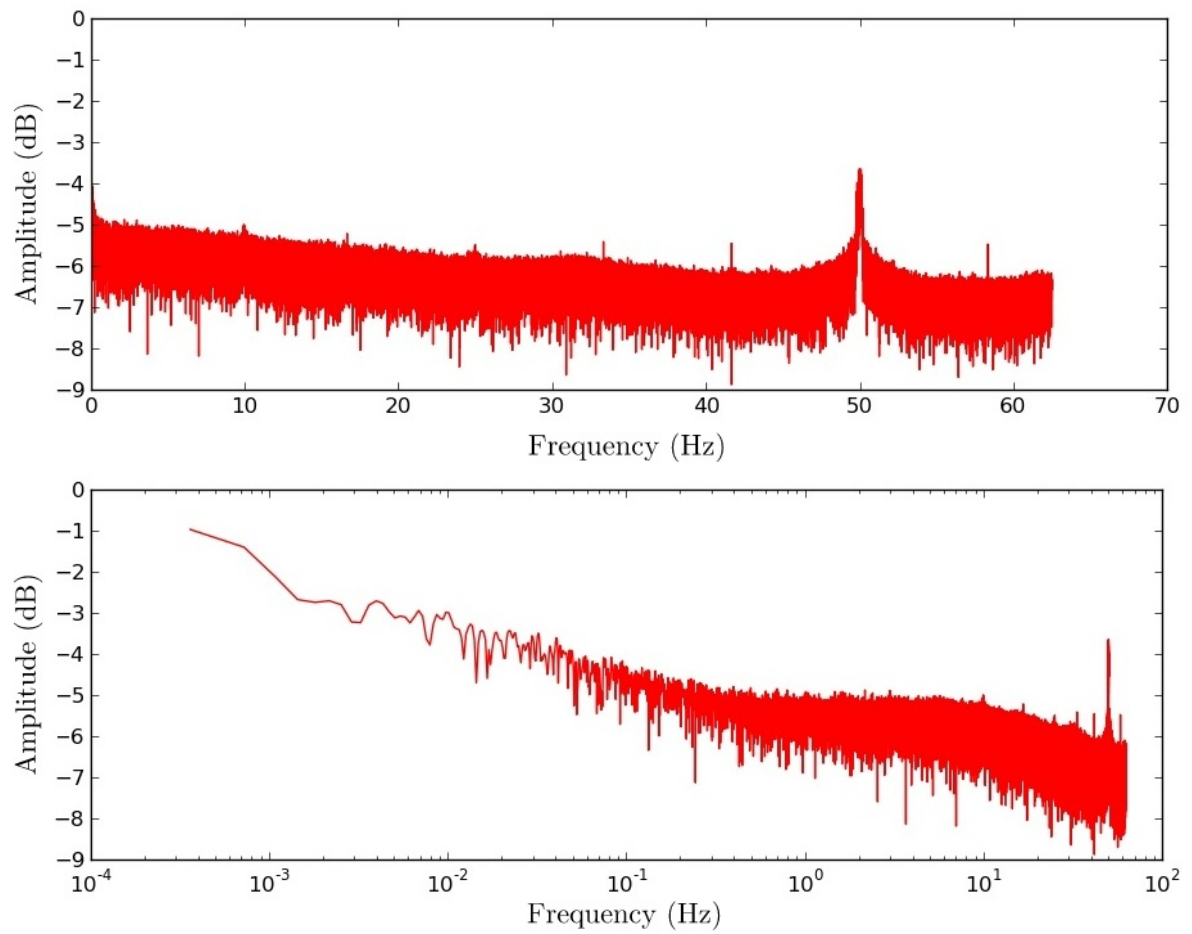


Figure 7.2: Spectrum of a 45 minute period of the Z-axis SQUID at ± 1 V sampling, with linear (top) and logarithmic (bottom) frequency axes.

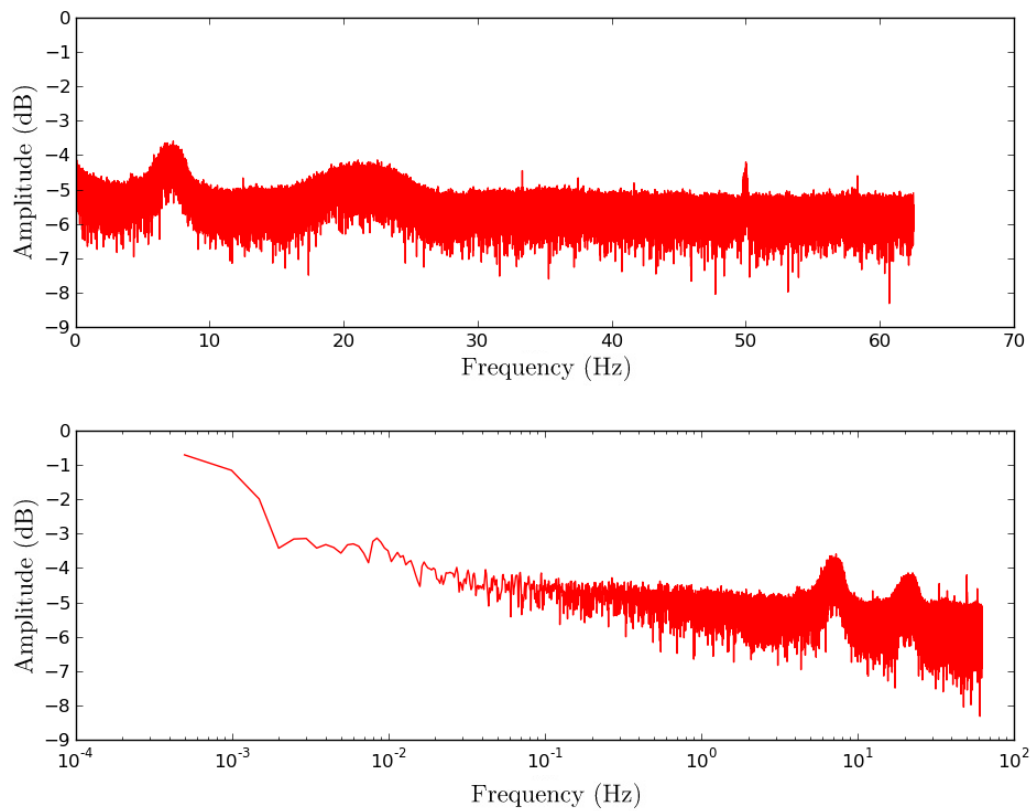


Figure 7.3: Spectrum of a 45 minute period of the X-axis SQUID at ± 10 V sampling, with linear (top) and logarithmic (bottom) frequency axes.

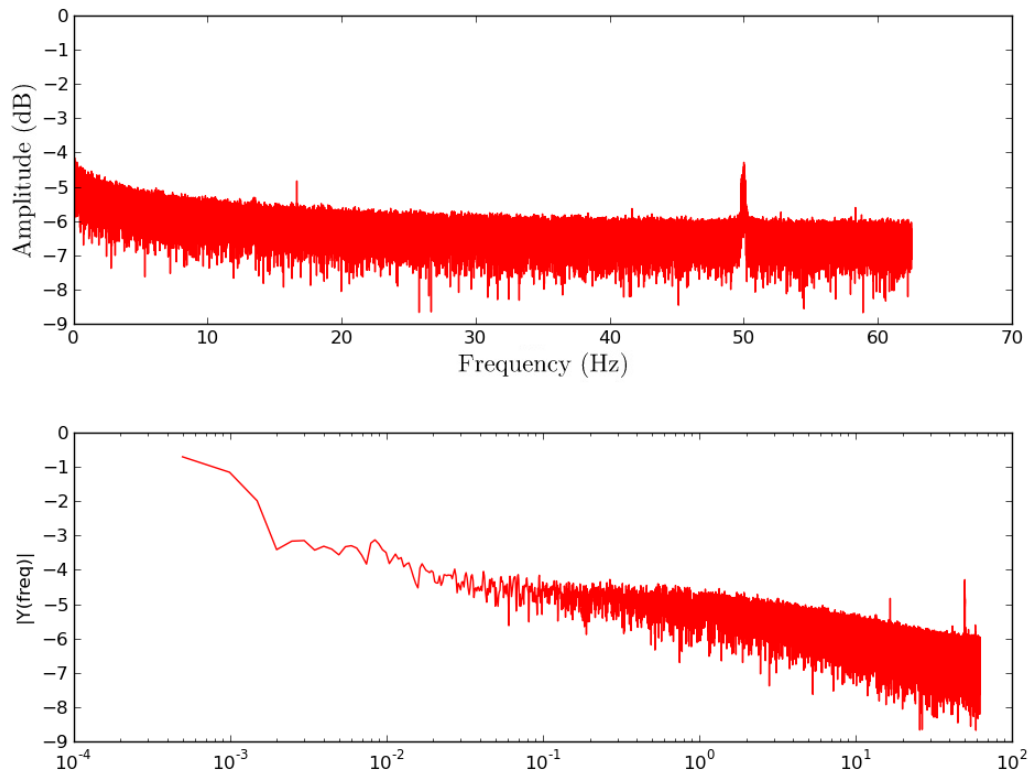


Figure 7.4: Spectrum of a 45 minute period of the Z-axis SQUID at ± 10 V sampling, with linear (top) and logarithmic (bottom) frequency axes.

7.3.1 Zero signal power spectrum

This power spectrum reveals something interesting. The oscillogram in Figure 7.5 gives an impression of gaussian noise, however the power spectrum in Figure 7.6 shows that there are specific frequencies present, with their own harmonics. These frequencies could originate from switching power supplies, but could also be caused by external sources or sources inside the data acquisition unit itself. However, it does seem that these specific frequencies are outside the band of interest. These could be filtered out digitally to lower the noise floor, if the signal is recorded at a high enough frequency.

If it is not possible to record at a high enough frequency for digital filtering, the highest noise peak will determine the maximum sensitivity of the device. This noise peak may cause an image frequency, but the amplitude will still be the same as the original frequency.

7.3.2 Zero signal power spectrum with internal filter

The data acquisition unit possesses an internal low pass filter with a cut-off frequency at 40 kHz. This filter can be switched on separately. This filter has some benefits and some

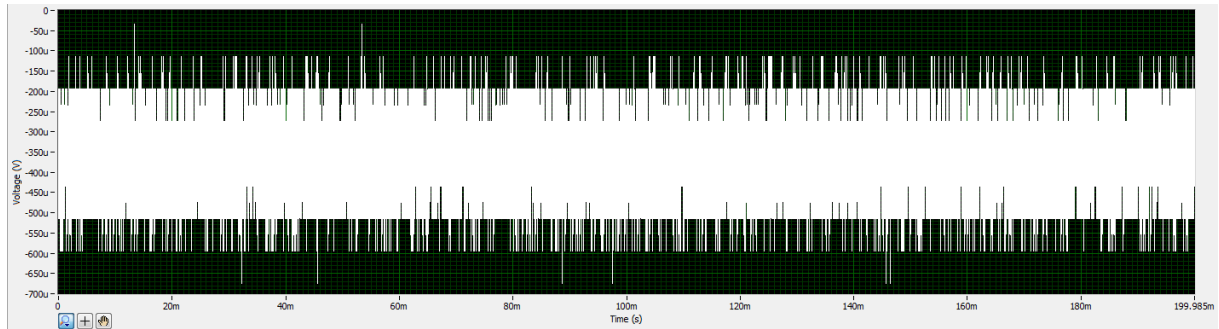


Figure 7.5: Oscilloscope of a differential channel on the data acquisition unit at 500kHz sample rate.

disadvantages. The most significant disadvantage is that another signal delay that must be taken into account, which also does not necessarily possess a constant group delay as discussed in Section 5.2.

Comparing the spectra of Figures 7.6 and 7.7, some differences are notable: The white noise floor is slightly lower by about 1 dB, and the strongest noise peaks are also attenuated, which improves the maximum unfiltered sensitivity by about 4 dB. It also introduces some new harmonics, however they are not stronger than the original harmonics.

7.3.3 SQUID magnetometer power spectrum

Power spectra of unfiltered squid channels were measured in January 2013, using a short evaluation version of National Instruments' LabView software. The initial SQUID magnetometers were both oriented in the Z direction. The corresponding power spectral density plots are in Figures 7.8, 7.9, 7.10 and 7.11.

Deductions from these measurements are as follow:

- The 5 Hz, 20 Hz, 30 Hz, 40 Hz and 60 Hz components in Figure 7.8 was not present in the second spectrum measurement of the channel in Figure 7.10, and may have been caused by a specific event. The origin is not clear.
- In Figures 7.8 and 7.9 it can be seen that the bias reversal frequency of the SQUIDs at about 128 kHz is a prominent component of the output signal of both SQUID magnetometers. There is also a strong component at about 105 kHz, which may also originate from the SQUID bias electronics or more specifically, the PFL-100 programmable feedback loops. It is not present in the measurement of the noise floor of the DAQ in Figure 7.6.

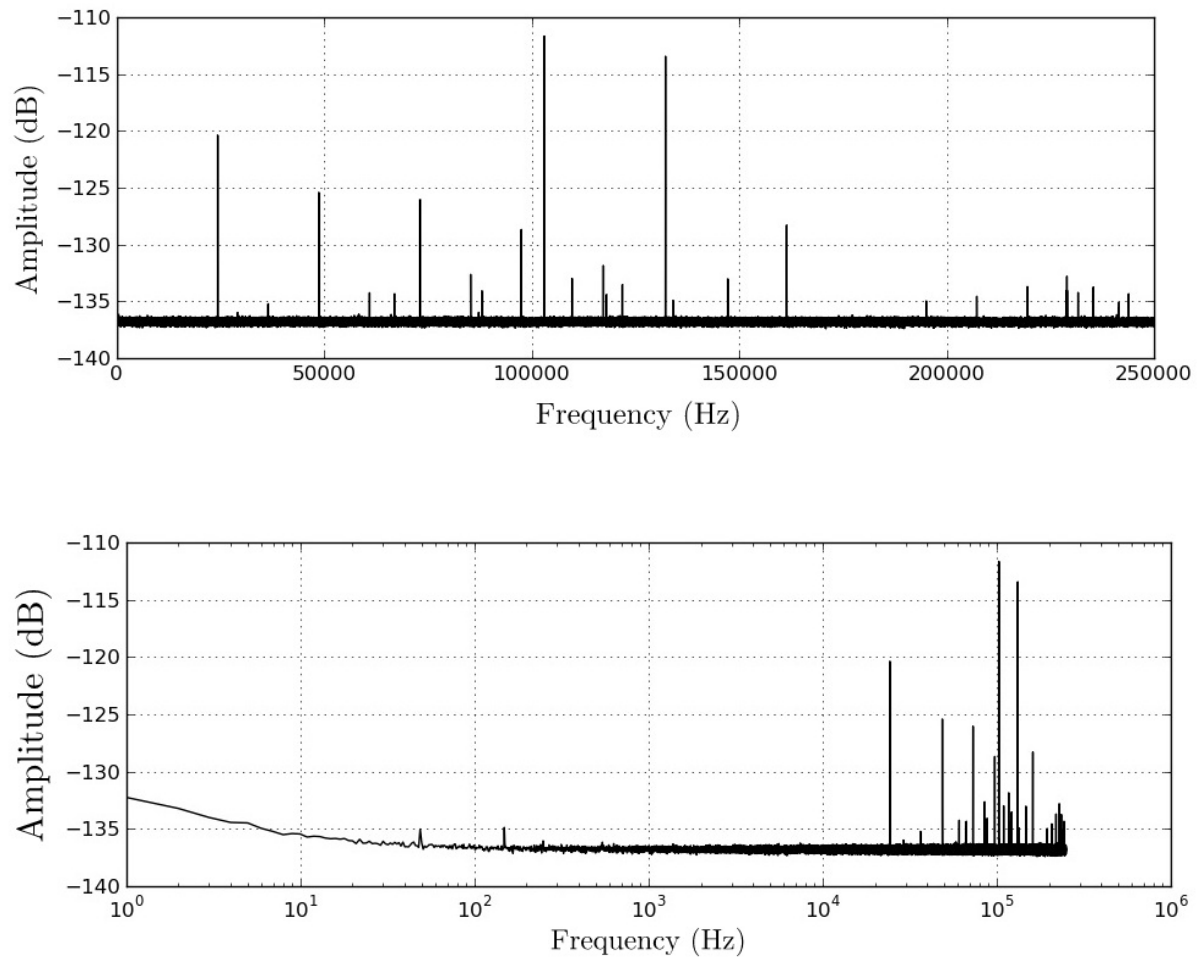


Figure 7.6: Power spectral density of a differential channel on the data acquisition unit, with linear (top) and logarithmic (bottom) frequency.

- The 50 Hz component of AC electricity, as well as several harmonics thereof, are present in the output signals. Other measurements at SANSa determined that a ground return current might be present in the soil of the premises.

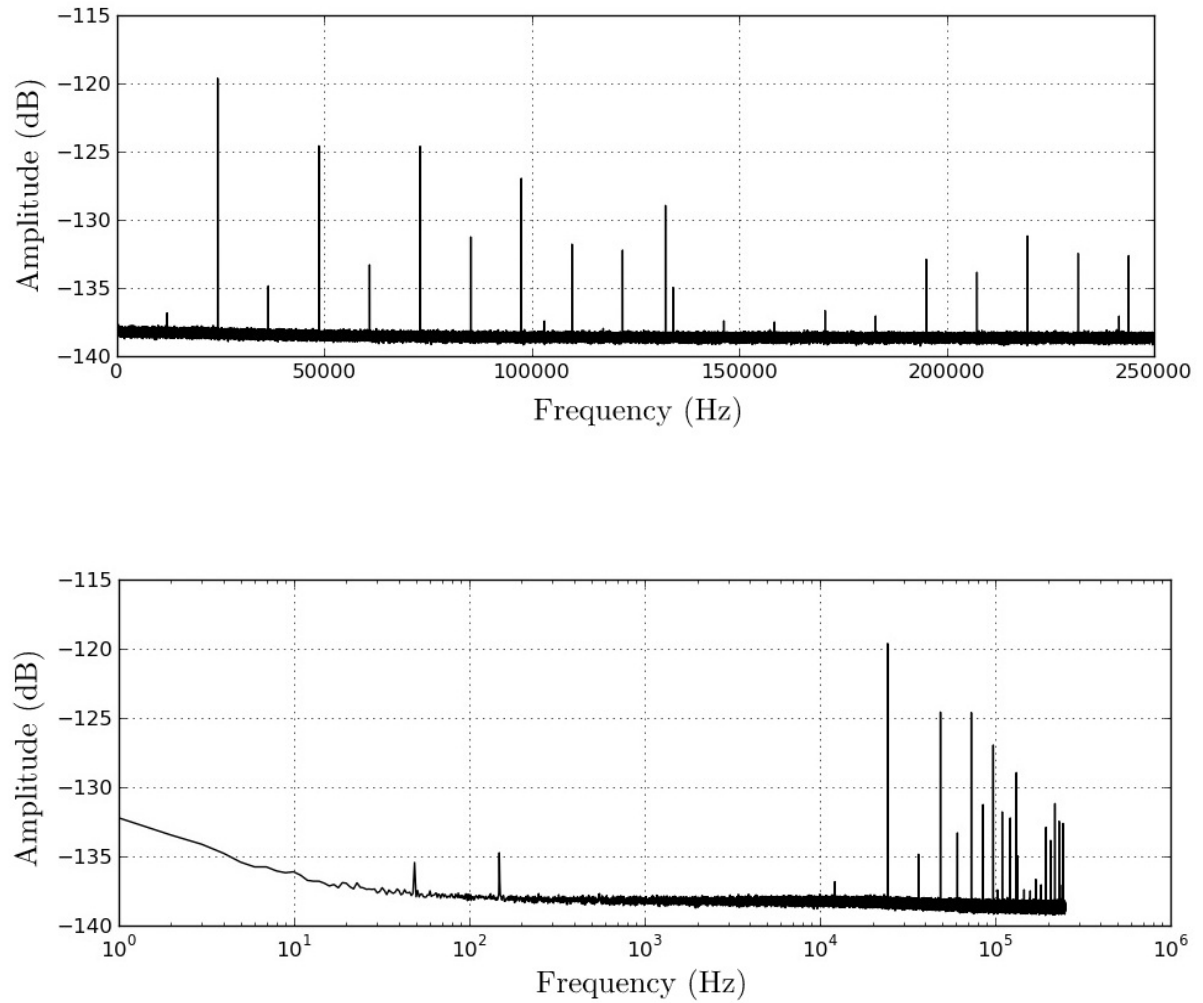


Figure 7.7: Power spectral density of a differential channel on the data acquisition unit, with the internal 40 kHz filter switched on.

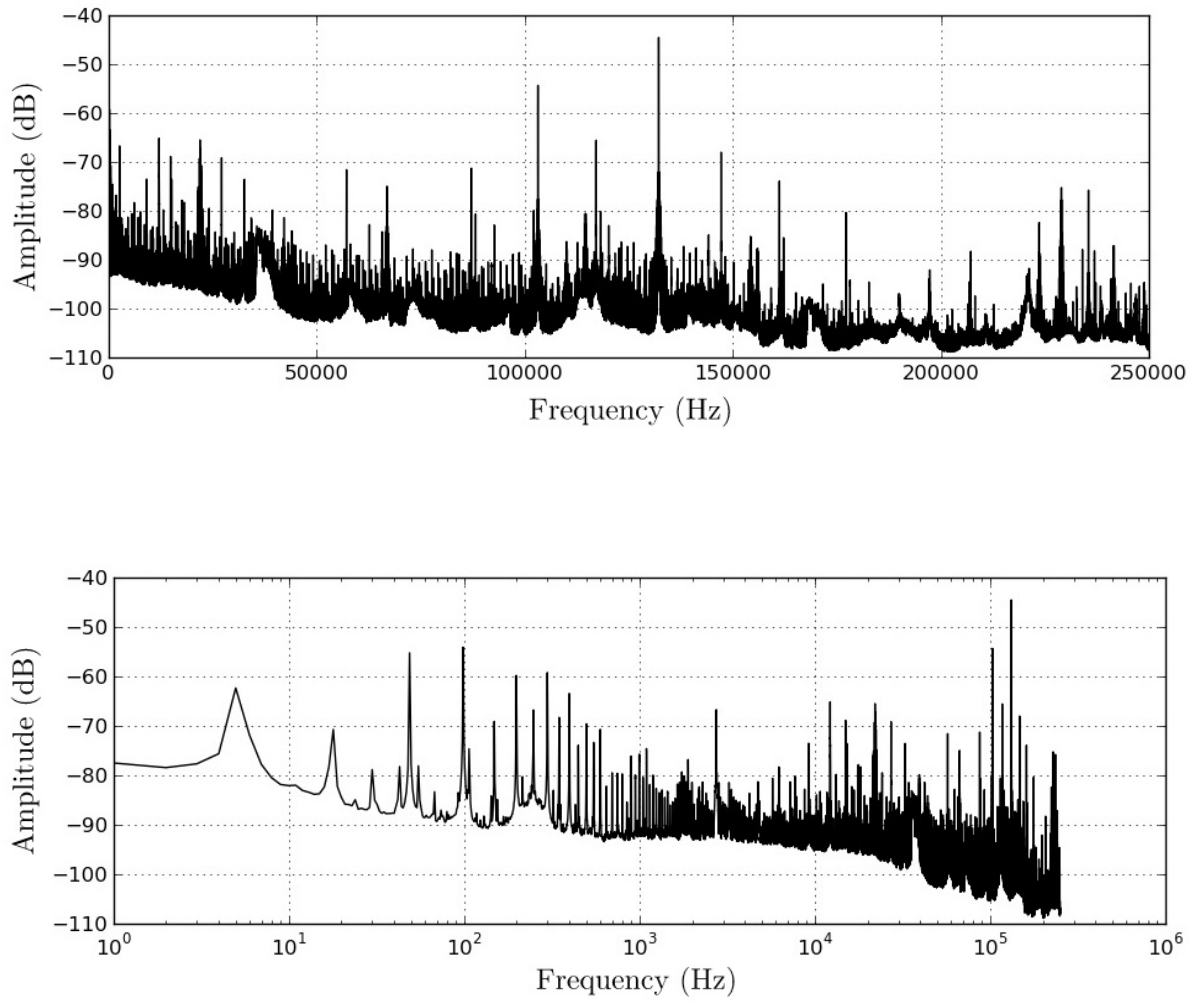


Figure 7.8: Power spectral density of channel 1 M2700 SQUID magnetometer, with linear (top) and logarithmic (bottom) frequency axes.

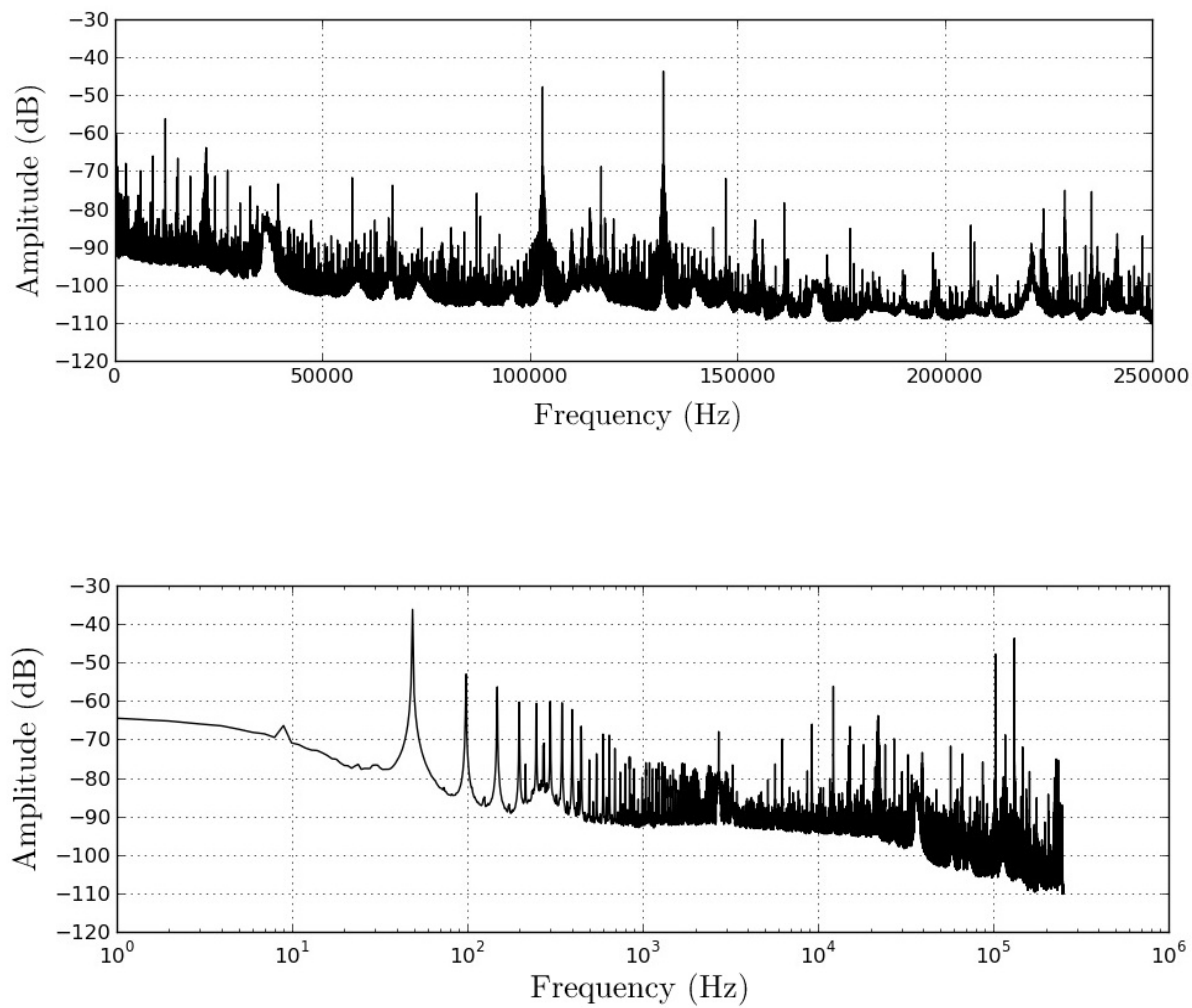


Figure 7.9: Power spectral density of channel 2 M2700 SQUID magnetometer, with linear (top) and logarithmic (bottom) frequency axes.

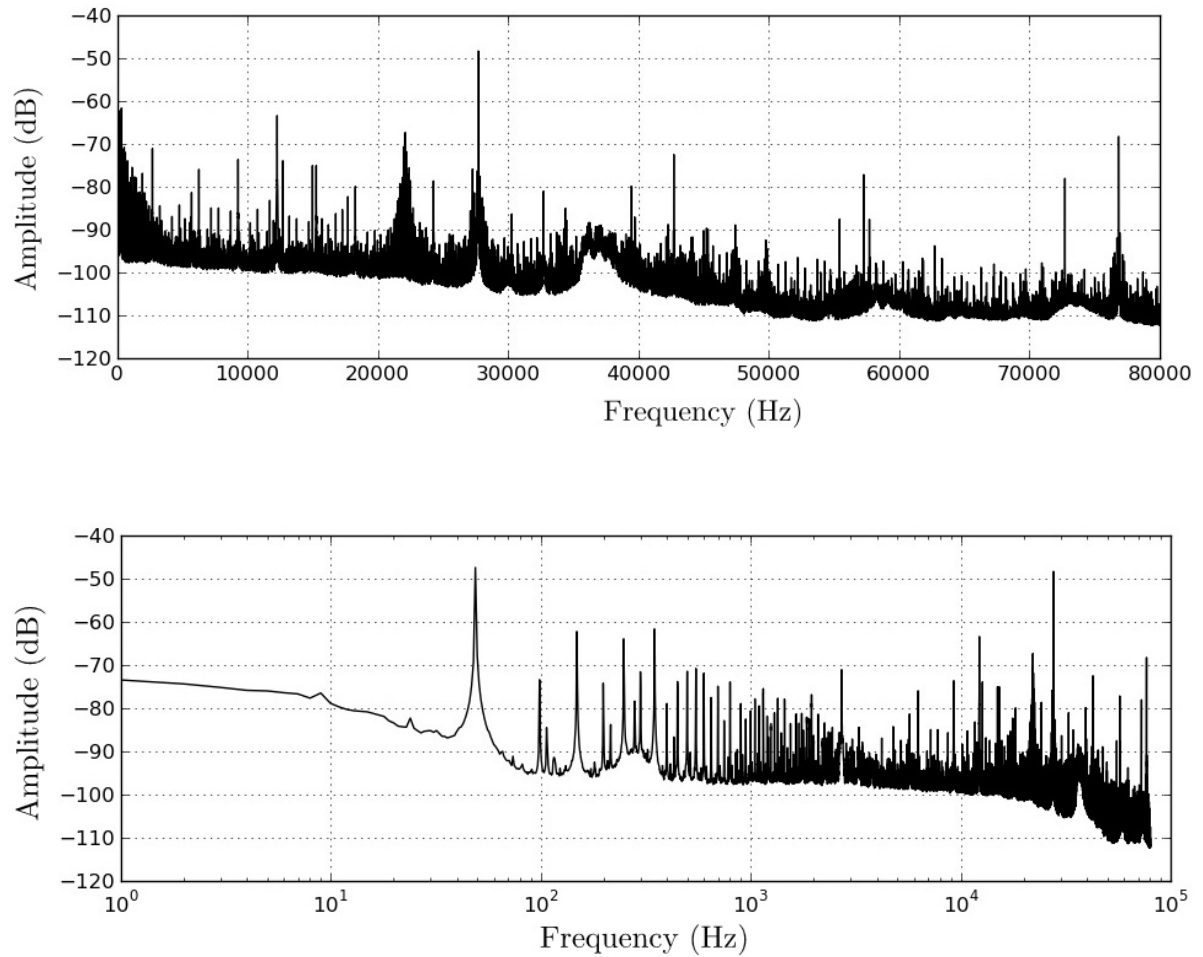


Figure 7.10: Power spectral density of channel 1 M2700 SQUID magnetometer, with linear (top) and logarithmic (bottom) frequency axes. Measured simultaneously with spectrum in Figure 7.11.

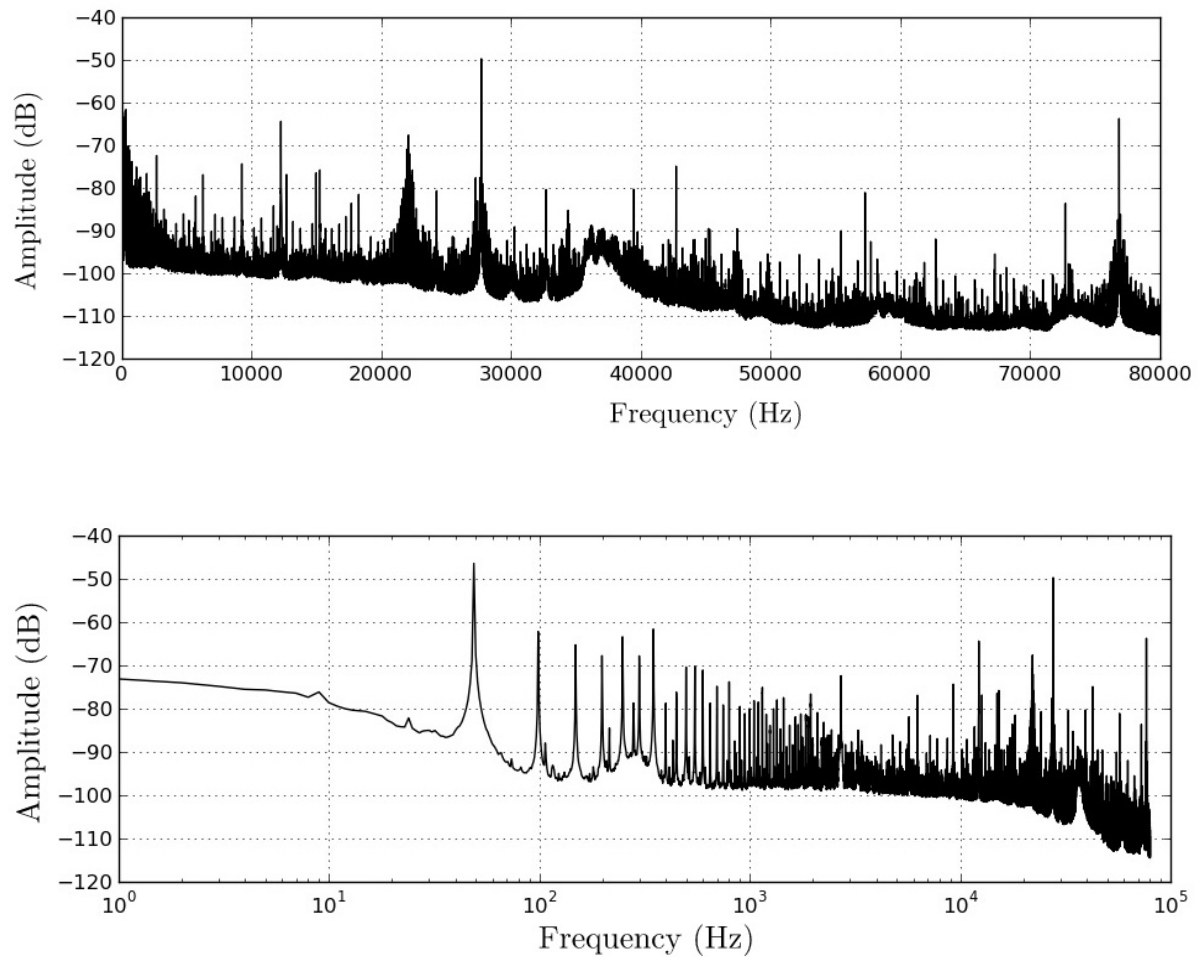


Figure 7.11: Power spectral density of channel 2 M2700 SQUID magnetometer, with linear (top) and logarithmic (bottom) frequency axes. Measured simultaneously with spectrum in Figure 7.10.

Chapter 8

Conclusions

The unshielded SQUID geomagnetometer has proved to be a very complex device, in concept and in implementation. However, a working model of a more replicatable SQUID geomagnetometer system has been produced, and a valuable base of knowledge and expertise has been gained. Multiple conclusions are possible from the different components of the system, and will be discussed separately.

8.1 Results of software-interrupt based precision-timed data acquisition system

This project has confirmed that it is possible to do GPS-timestamped data acquisition without using expensive GPS-synchronised and accurately clocked equipment. By using a novel method to put timing information into simultaneously sampled signals, it was possible give accurately timed data without using a real time clock implementation. This can theoretically be more accurate than real-time clock implementations, but still has to be verified.

After more than a year of testing and painstaking incremental improvements, the software could function reliably for several weeks at a time until refills of liquid nitrogen were required. Several technical difficulties arose from uncommon events, as discussed in 5.5.

The data acquisition unit that is used for this project is over-specified, but the extra capabilities has proved to be advantageous for this project. Recording data on the extra channels available has helped with some of the hardware debugging for this project, and is now available to record data from other sensors. It was also determined that some of the control aspects of operating the specific SQUID magnetometers present at SANSA

Space Science could be automated, such as resetting the SQUIDs when the limits of its dynamic range were reached.

However, this system should only be viewed as a proof of concept, as many improvements are still possible, particularly in the total sample rate of the system.

8.2 Results of the implementation of a robust data-storage and post-processing system

A database has been developed and successfully implemented to store the large amounts of data recorded. Novel procedures to confirm continuity of large amounts of data was also successfully implemented. This system was eventually successful at receiving data from SANSA Space Science for several months without interruption. About 290 GB of data was stored, and was analysed in other projects [43], [61].

This system has proved to work well with very large amounts of data - several hundred gigabytes - without noticeable decrease in performance. Data access was not delayed by the size of the database, however transfer times has been a difficulty due to file systems and difficulties with internet connection. It was also highlighted that server hardware reliability was a concern.

8.3 Recommendations

There are several aspects of the unshielded SQUID geomagnetometer that can be improved, each with varying degrees of usefulness. The time and resources required to implement these may have to be considered during implementation.

8.3.1 Data capture software

The implementation of the software was done with a programming environment and toolset which allows easy testing of proposed features, but is not processor efficient or optimal for reliability. Much higher sample rates are possible, and data can also be preprocessed.

It is recommended that the data capture software is rewritten using a faster programming language. The NI-DAQmx API provides libraries for ANSI C, which would likely be the best option. Less overhead processing is required by ANSI C, which will enable sample rates above 10 kHz, while still maintaining accurate GPS-timestamping. This will

make it possible to do oversampling, which can increase the accuracy of the measurements overall. High resolution DFTs and digital filtering would also be an option.

8.3.2 Preprocessing of data at the web server

Data analysing can be aided by having preprocessed data available. A detailed analysis to determine which kinds of preprocessing will be of benefit is recommended. It can also be considered if data should be processed on demand or if data should be preprocessed and then stored. Machine learning algorithms could also be considered: it could be used as an attempt to identify whether certain geological events have signatures in the geomagnetic field. Other statistical analysis methods or bundled packages could also be considered.

8.3.3 World Data System

The World Data System is an international group which provides data services for interdisciplinary scientific data, particularly for astronomical and geophysical data. Some assistance as well as accreditation, storage and access to data are provided. This can be advantageous for publicity, accessibility and analysing of the geomagnetic data. However, it is not recommended to have it as the primary storage for all the data, to maintain some customisability of the data storage system.

8.3.4 Server stability: automatic shut down on UPS

When considering stability over very long terms, it may be necessary to consider what will happen during an extended power failure. In the current implementation the server is not using a journalling file system, which may make it more vulnerable to data corruption when power to the server is lost. A feature can be implemented which monitors the UPS, and can then facilitate an automatic shut down if there is an extended power failure.

8.3.5 Mobile SQUID geomagnetometer

If a mount bracket can be made to mount SQUID probes directly on a dewar as it is done at LSBB, a mobile SQUID geomagnetometer system could be possible. With some modifications, the entire system, including a laptop to record data, can be powered from batteries. Cables can be used to ensure enough distance between control equipment and the SQUID magnetometers. Setting up this system in an open field far from towns and power lines may yield results with very low interference.

8.3.6 Using a well for measurements

In densely populated areas where it is impossible to avoid electromagnetic interference, a well may be sunk deep enough into the ground to achieve enough separation from sources of electromagnetic noise. If all the equipment required to operate the SQUIDs can be attached to the dewar with only the necessary cables coming to the surface, measurements can be performed from the surface. The data acquisition equipment could also be mounted to the dewar. Fibre optic extensions may be considered for the USB and the GPS trigger signals. However, the latencies caused by these extensions may be of note and should be measured.

Bibliography

- [1] J. Clarke and A. I. Braginski, eds., *The SQUID Handbook, Volume 1: Fundamentals and Technology of SQUIDs and SQUID Systems*. Wiley-VCH Verlag GmbH & Co. KGaA, 2004.
- [2] “Superconductors Model 1000 Kit Resistance vs Temperature & Persistent Current in a Ring.” Futurescience, Inc. <http://www.futurescience.com/manual/sc1000.html>, 1998.
- [3] T. P. Orlando and K. A. Delin, *Foundations of Applied Superconductivity*. Addison-Wesley Publishing Company, 1991.
- [4] “File:Hall Effect Measurement Setup for Electrons.png.” Wikimedia Commons. Online: http://commons.wikimedia.org/wiki/File:Hall_Effect_Measurement_Setup_for_Electrons.png, 2009.
- [5] E. Lochner, “Magnetic field measurements taken at laboratoire souterrain à bas bruit (lsbb) in rustrel, france, during june 2012.” South African National Space Agency, DOC 6036-0001-706-A1, July 2012.
- [6] S. Gaffet *et al.*, “Simultaneous seismic and magnetic measurements in the Low-Noise Underground Laboratory (LSBB) of Rustrel, France, during the 2001 January 26 Indian earthquake,” *Geophysical Journal International*, 155, 981990, 2003.
- [7] A. T. Kilian, *Magnetic Sensing Network for Space Weather and Terrestrial Phenomena using Superconducting Quantum Interference Devices: Progress Report*. Stellenbosch University, 2011.
- [8] T. J. Phiri, “Correlation between SQUID and Fluxgate Magnetometer Data for Geomagnetic Storms,” Master’s thesis, Stellenbosch University, 2013.
- [9] M. Garton *et al.*, “PNI White Paper: Local Magnetic Distortion Effects on 3-Axis Compassing.” PNI Sensor Corporation, Online: <http://www.pnicorp.com/technology/files/magnetic-distortion-explanation-and-testing>, 2009.

- [10] *Aviation Maintenance Technician Handbook*. Federal Aviation Administration, Oklahoma City, Oklahoma, 2011.
- [11] J. R. Moser, “Low-frequency low-impedance electromagnetic shielding,” *IEEE Transactions on Electromagnetic Compatibility*, 1988.
- [12] “LEA-6 Data Sheet.” u-blox AG, Thalwil, Switzerland, 2010.
- [13] “File:AliasingSines.svg.” Wikimedia Commons. Online: <http://commons.wikimedia.org/wiki/File:AliasingSines.svg>, 2009.
- [14] A. B. Williams, *Active Filter Design*. Artech House Inc., 1975.
- [15] P. Horowitz and W. Hill, *The art of electronics, second edition*. Cambridge University Press, Cambridge, United Kingdom, 1989.
- [16] “File:Binary search into array.svg.” Wikimedia Commons. Online: http://commons.wikimedia.org/wiki/File:Binary_search_into_array.svg, 2012.
- [17] “Kephren Data Logger.” S. A. R. L. Agecodagis, Rieux Volvestre, France, 2007.
- [18] “[SQUID]=[Superconducting QUantum Interference Device] with [Shielding QUalified for Ionosphere Detection].” EMMAH, Online: <https://www4.paca.inra.fr/emmah/Les-moyens/Sites-experimentaux/Fontaine-de-Vaucluse-LSBB/SQUID-2#>, 2011.
- [19] “D74 & DP74 Series Fixed Frequency 4-Pole Filters.” Frequency Devices, Inc. Online: <http://www.freqdev.com/products/filters/d74.html>, 2014.
- [20] G. Waysand *et al.*, “Seismo-ionosphere detection by underground SQUID in low-noise environment in LSBB-Rustrel, France,” *The European Physical Journal Applied Physics*, 47, 12705, 2009.
- [21] “GPS-based Timing Considerations with u-blox 6 GPS receivers Application Note.” u-blox AG, Thalwil, Switzerland, April 2011.
- [22] “NMEA 0183 Interface Standard.” Robosoft, Online: <http://robosoft.info/en/technologies/knowledgebase/nmea0183>, 2009.
- [23] “High-Accuracy M Series Multifunction DAQ for USB - 18-Bit, up to 625kS/s, up to 32 Analog Inputs.” National Instruments, Online: <http://sine.ni.com/app/doc/p/id/ds-24/lang/en>, May 2011.
- [24] “MySQL 5.6 Reference Manual: 10.2 Numeric Types.” Oracle Corporation, Online: <http://dev.mysql.com/doc/refman/5.6/en/numeric-types.html>, October 2011.

- [25] “MySQL 5.6 Reference Manual: 10.3.1 The DATETIME, DATE, and TIMESTAMP Types.” Oracle Corporation, Online: <http://dev.mysql.com/doc/refman/5.6/en/datetime.htm>, October 2011.
- [26] “MySQL 5.6 Reference Manual: 10.5 Data Type Storage Requirements.” Oracle Corporation, Online: <http://dev.mysql.co./doc/refman/5.6/en/storage-requirements.html>, October 2011.
- [27] “MySQL Field Types.” SciBit, Online: https://help.scibit.com/mascom/masconMySQL_Field_types.html, 2011.
- [28] J. Marfaing *et al.*, “Global observation of 24 November 2006 Pc5 pulsations by single mid-latitude underground [SQUID]² system,” *Annales Geophysicae*, 29, 19771984, 2011.
- [29] J. Kawai *et al.*, “Three Axis SQUID Magnetometer for Low-Frequency Geophysical Applications,” *IEEE Transactions on Magnetics*, vol. 35, pp. 3974–3976, September 1999.
- [30] J. Kawai *et al.*, “Geomagnetic field measurement using LTS-SQUID magnetometers and its evaluation,” *Conductivity Anomaly*, pp. 91–95, 2013.
- [31] Y. Katori *et al.*, “High Temperature Superconductor Based SQUID (HTS-SQUID) Magnetometer System for Super-sensitive Observation of Geomagnetic Field Changes,” *Conductivity Anomaly*, pp. 70–73, 2013.
- [32] J. Clarke and A. I. Braginski, eds., *The SQUID Handbook, Volume 2: Applications of SQUIDS and SQUID Systems*. Wiley-VCH Verlag GmbH & Co. KGaA, 2004.
- [33] D. van Delft and P. Kes, “The discovery of superconductivity,” *Physics Today*, vol. 38, pp. 38 – 43, September 2010.
- [34] B. S. Deaver and W. M. Fairbank, “Experimental evidence for quantized flux in superconducting cylinders,” *Physical Review Letters*, vol. 7, pp. 51–52, 1961.
- [35] S.-M. Kang and Y. Leblebici, eds., *CMOS Digital Integrated Circuits, 3rd edition*. New York: McGraw Hill, 2003.
- [36] P. Ripka, ed., *Magnetic Sensors and Magnetometers*. Artech House, Norwood, Massachusetts, USA, 2001.
- [37] “AK09912 3-axis Electronic Compass.” Asahi Kasei Microdevices Corporation, Online: <http://www.akm.com/akm/en/file/datasheet/AK09912.pdf>, 2014.

- [38] I. K. Kominis *et al.*, “A subfemtotesla multichannel atomic magnetometer,” *Nature*, vol. 422, pp. 596–599, April 2003.
- [39] “Magnetometry with numerical SQUIDs.” LSBB, Online: <http://lsbb.oca.eu/spip.php?rubrique153>, 2009.
- [40] G. Waysand *et al.*, “First characterization of the ultra-shielded chamber in the low-noise underground laboratory (LSBB) of Rustrel-Pays d’Apt,” *Nuclear Instruments and Methods in Physics Research A* 444, 336-339, 2000.
- [41] C. Bordes *et al.*, “Evidence of the theoretically predicted seismo-magnetic conversion,” *Geophysical Journal International*, vol. 174, no. 2, pp. 489–504, 2008.
- [42] M. S. Reisch, “Coping with the helium shortage,” *Chemical & Engineering News*, vol. 91, pp. 18–19, February 2013.
- [43] T. K. Matladi, “Correlation between SQUID and Fluxgate Magnetometer Data-sets for Geomagnetic Storms: Hermanus,” Master’s thesis, Stellenbosch University, 2013.
- [44] H. Ott, *Noise Reduction Techniques in Electronic Systems, Second Edition*. John Wiley and Sons, Inc., 1988.
- [45] G. Giusi, *High-Sensitivity Instrumentation for Low Frequency Noise Measurements*. PhD thesis, University of Messina, 2005.
- [46] STAR Cryoelectronics, LLC., Santa Fe, New Mexico, *pcSQUID Users Manual*, 2001.
- [47] “MACS Active Cancellation System.” Herzan LLC, Online: <http://www.herzan.com/products/electromagnetic-interference-isolation/active-emi-cancellation.html>, 2014.
- [48] “Active magnetic shielding (field cancellation).” EMF Services LLC, Online: <http://www.emfservices.com/afcs.htm>, 2014.
- [49] “Magnetic field cancelling systems.” Spicer Consulting Limited, Online: <http://www.spicerconsulting.com/fieldcancelling.htm>, 2008.
- [50] L. J. J. van Vuuren, *GPS-Timestamped Online Measurement System*. Stellenbosch University, 2011.
- [51] F. C. B. B. Brandenburg, “A Comparison of Scheduling Latency in Linux, PRE-EMPT RT, and LITMUSRT,” *OSPERT 2013*, p. 20, 2013.
- [52] “Context switches.” Microsoft Technet, Online: <http://technet.microsoft.com/en-us/library/cc938613.aspx>, 2014.

- [53] “System benchmarks.” Anandtech Inc., Online: <http://www.anandtech.com/show/7532/asus-maximus-vi-impact-review-rog-and-miniitx/5>, 2013.
- [54] J. A. Lichter, “Crystals and oscillators.” Online: <http://www.nelfc.com/pdf/pdfapp/9113.pdf>.
- [55] “Timing standard definition: UTC, GPS, LORAN and TAI.” IPSES S.r.l., Online: <http://ipses.com/prod/timing/UTC-GPS.php?language=en>, 2011.
- [56] “Oven Controlled Crystal Oscillator, AOCJY5 Series.” Abracon Corporation, Rancho Santa Margarita, California, USA, 2011.
- [57] “OCXO’s.” Suntsu Frequency Control, Inc., Online: http://www.suntsuinc.com/Products_OCXO.aspx, 2010.
- [58] T. Straumann, “Open source real time operating systems overview,” *Particle Accelerator Conferences Proceedings*, no. 8, pp. 235–237, 2001.
- [59] “NI-DAQmx Software Services Feature Gallery.” National Instruments, Online: <http://www.ni.com/white-paper/5612/en/>, 2014.
- [60] “PHP strtotime() Function.” w3schools.com, Online: http://www.w3schools.com/php/func_date_strtotime.asp, 2011.
- [61] C. Kwisanga, *Correlation Between SQUID Measurements at Hermanus and LSBB Data Sets for Near-Earth Environment and Seismic Events: PhD Project Proposal*. Stellenbosch University, 2013.